3D Modelling of a Net and Design of a Flexible Mounting Rod

Master's Thesis

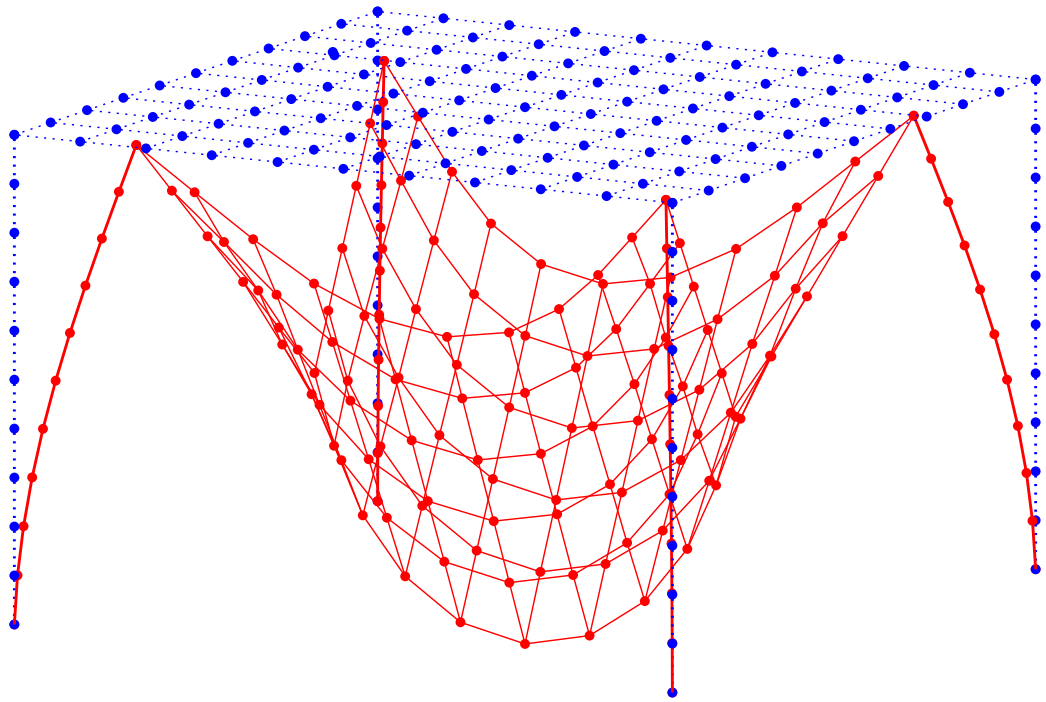

1st June 2016

4th Semester - Design of Mechanical Systems

AALBORG UNIVERSITY
STUDENT REPORT

Group 1.126A

Jonas Støttrup Marciniak & Daniel Jacobi Knutzen

Abstract

Dette speciale omhandler et system bestående af et net monteret på fleksible stænger, som udspænder nettet. På basis af net-stang systemet programmeres en model og der udføres et redesign af stangen.

Modellen af net-stang systemet er programmeret, så den kan løse den geometriske ulinearitet, der kommer ved store flytninger i nettet. Løsningsmetoden er baseret på det totale elastiske potentials minimum, som har vist sig at være en meget robust løsningsmetode. Modellen konfigureres ved at angive nettets størrelse og placering af stænger. Der kan påføres kræfter og randbetingelser på nettet og stænger, hvilket gør det muligt at opstille mange typer af problemer. Stængerne kan diskretiseres i et ønsket antal sektioner, hvilket muliggør, at opførelsen af stængerne kan ændres til specifikke formål. Modellen tillader brug af ulineære stivheder for både net og stænger. Modellen er skrevet i MATLAB og bruger den indbyggede gradientbaserede optimieringsrutine *fmincon* til løse systemet med flytninger som design variabel. Løsningen kan plottes, hvor både startkonfigurationen og den deformerede konfiguration vises.

Til projektet er der udleveret et net og nogle stænger. For at kunne simulere det udleverede net og stænger i modellen, er stivhederne bestemt eksperimentelt. Modellen er efterfølgende blevet valideret ved sammenligning med et fysisk system. Sammenligningen viste, at fordi knuderne i nettet ikke er modelleret i net-stang modellen, er der en afvigelse mellem model og virkelighed. Disse er ikke blevet medtaget i modellen, da opførsel er meget kompleks.

Redesignet indledes med en morfologisk analyse, for at belyse stangens funktionaliteter og udvælge et koncept for redesignet. Projektet begrænser sig til at forbedre stangens udbøjningsegenskaber, da energien i net-stang systemet ønskes reduceret ved store deformationer. Dette opnåes ved at give stangen en ulineær stivhed. Den ulineær stivhed opnåes ved at ændre tværsnittet fra solidt til hult. Herved vil stangen ovalisere ved bøjning og på et tidspunkt kollapse. Designprincippet har udgangspunkt i Brazier effekten.

Ud fra konceptet defineres et nyt design af stangen, hvor yderdiameteren af midtersektionen forstørres og fastholdes, og tykkelsen bestemmes i et parameterstudie. Parameterstudiet udføres i simuleringsprogrammet ANSYS. Tykkelsen af tværsnittet undersøges ved simuleringer for at opnå den ønskede stivhedskarakteristik. På baggrund af sammenligning af stivhedskarakteristikker fra geometrisk ulineære analyser vælges en tykkelse på 5 mm.

En prototype er blevet produceret med en tykkelse på 6 mm. Tykkelsen er 6 mm i stedet for 5 mm pga. en fejl ved data behandling, som blev opdaget efter prototypen var produceret. Prototypen er testet og viste tydelig ovalisering af tværsnittet som forventet. Prototypen er brugt til at vise at den brugte designmetode virker, ved at sammenligne

med simulationer ved en tykkelse på 6 mm. Simuleringerne er i god overensstemmelse med opførelsen af prototypen med antagelser og fremstillingskvalitet taget i betragtning.

Det lykkedes i projektet af opstille en model af net-stang systemet, som kan modellere det udlverede system tilfredstillende. Modellen kan forbedres ved at medtage knuderne i nettet i modelleringen. Det lykkedes også at nå frem til et redesign, der kan reducere energien i net-stang system ved store deformationer. Test af prototypen viste overenstemmelse med simuleringerne af redesignet, hvilket validerer designmetoden.

AALBORG UNIVERSITY
STUDENT REPORT

Study Board of Industry and Global Business Development
Fibigerstraede 16
DK – 9220 Aalborg East
Phone +45 99 40 93 09
lft@m-tech.aau.dk
www.en.ses.aau.dk

Title: 3D Modelling of a Net and Design of a Flexible Mounting Rod

Study: Design of Mechanical Systems

Semester: 4th Semester

Semester title: Master's Thesis

Project period: 1/2-2016 to 1/6-2016

ECTS-points: 30

Supervisor: Jørgen Asbøl Kepler

Project group: 1.126A

Jonas Støttrup Marciniak

Daniel Jacobi Knutzen

Prints: 3

Pages: 60

Appendix: 9 (A-I)

Synopsis
A system consisting of a net and rods has been provided. The project seeks to establish a model of a net suspended by flexible rods and to develop a redesign of the flexible rods.
The model of the net-rod system is programmed to solve the geometrical non-linearity, caused by large displacements of the net. The problem is solved using a gradient based optimisation routine which minimises the total elastic potential.
The stiffnesses of the net and rod are determined experimentally, in order to implement the provided net and rod in the model. The model is validated through a comparison with a physical system. The knots in the net are not modelled in the net-rod model which lead to some deviation, but otherwise there was coherence.
A concept for the redesign is found in a morphological analysis. The redesign reduces the energy in the net-rod system by introducing a non-linear stiffness behaviour in bending. The non-linear behaviour in bending is achieved by ovalisation of a tubular cross section. The thickness of the tubelar cross section is determined through a parameter study performed in ANSYS. The study showed a thickness of 5 mm provided the desired behaviour.
A prototype has been made with a thickness of 6 mm. The prototype was tested and the desired collapsible behaviour was achieved as the simulations predicted. The redesign of the rod has reduced the energy in the net-rod system as intended.

By signing this document each group member declares equal participation and responsibility for the contents of this report.

Preface

This report documents a master's thesis done at 4th semester on the master's program Design of Mechanical Systems at Aalborg University. The project is done in collaboration with a company whose name is not mentioned due to a non-disclosure agreement. Sensitive information provided by the company is removed from the published report.

Software

The following software has been essential in the making of this project:

- ANSYS Mechanical APDL 17.0
- GIMP 2
- Inkscape
- LaTeX
- MATLAB 2015b
- Microsoft Excel 2007
- SolidWorks 2015

Reader's Guide

Units used in this report follow the SI unit system.

Source Reference in this report follows the Harvard method characterised by (author surname, year of publication). An alphabetic bibliography can be found at the back of the report at page 61.

Figures and Tables are stated as chapter number followed by figure or table number. A caption is placed above tables and underneath figures. The figures/tables are of own production unless a source reference is present in the caption.

Nomenclature is located in the beginning of the report after the table of contents and is sorted alphabetically by variables.

Appendix is represented by letters (A,B, ... ,), and is located at the end of the report. A CD is attached to the back cover of the report. The CD content can be found in appendix A.

Contents

Nomenclature

Symbol	Description	Unit
A	Area	[m^2]
$[A]$	Inequality coefficient matrix	[-]
α	Step size	[-]
$\{b\}$	Inequality value vector	[-]
$[C]$	Equality coefficient matrix	[-]
$d, \{d\}$	Displacement	[m]
	Search direction	[-]
$\{e\}$	Equality value vector	[-]
Δ	Elongation	[m]
E	Modulus of elasticity	[Pa]
f	Cost function	[-]
$F, \{F\}$	Force	[N]
$[\tilde{H}]$	Approximation of the Hessian	[-]
i	Iterator	[-]
I	Moment of inertia	[m^4]
j	Iterator	[-]
k	Stiffness	[N/m]
	Iterator	[-]
k_{Net}	Tensile stiffness of the net	[N/m]
$k_{Rod,t}$	Tensile stiffness of the rod	[N/m]
$k_{Rod,\theta}$	Bending stiffness of the rod	[Nm]
$[K_L]$	Displacement stiffness matrix	[N/m]
l	Length	[m]
L	Length	[m]
M	Moment	[Nm]
$[M]$	Gradient inequality coefficient matrix	[-]
n_i	Node number i	[-]
$[N]$	Gradient equality coefficient matrix	[-]
Π	The total elastic potential	[J]
P_{cr}	Critical buckling load	[N]
s	Wall spacing	[m]
r	Radius	[m]
θ	Angle of deflection	[rad]
t	Thickness	[m]
U	Elastic energy	[J]
$\{u\}$	Equality constraint value	[-]
$\{v\}$	Inequality constraint value	[-]
W	Work	[J]
$x, y, z, \{x\}, \{y\}, \{z\}$	Coordinate	[m]

1 Introduction

This project concerns a net mounted on flexible rods as illustrated in figure 1.1. The purpose of the rods is to suspend the net above a surface and ensure the net is stretched out. In addition the rods are flexible to allow large deflections thereby avoiding large loads in the system.

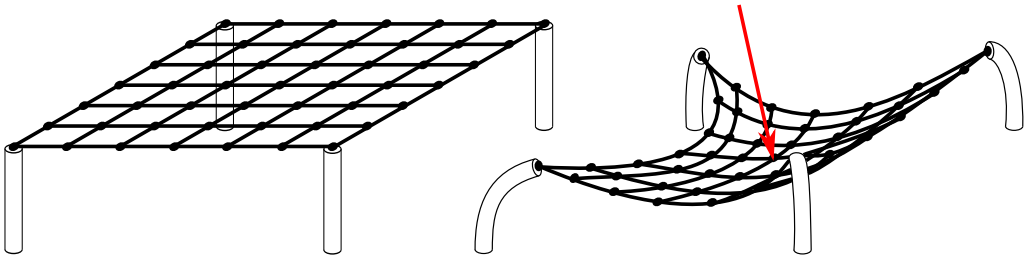

Figure 1.1: Net mounted on flexible rods before and after deformation.

A net and some flexible rods have been provided for the project as a starting point. The net is described in section 1.1 and the flexible rod in section 1.2. The project seeks to add new features to the rod, through a redesign, in order to improve the performance of the system. A model of the provided net-rod system is to be established in MATLAB to benchmark the performance of the net-rod system before and after the redesign.

1.1 Description of the Net

A piece of the provided net is shown in figure 1.2. The net is made of high strength thermoplastic fibers.The fibers are braided into rope which are knotted together to form a net with a mesh size of about 4 cm (distance from knot to knot). The knot type used to form

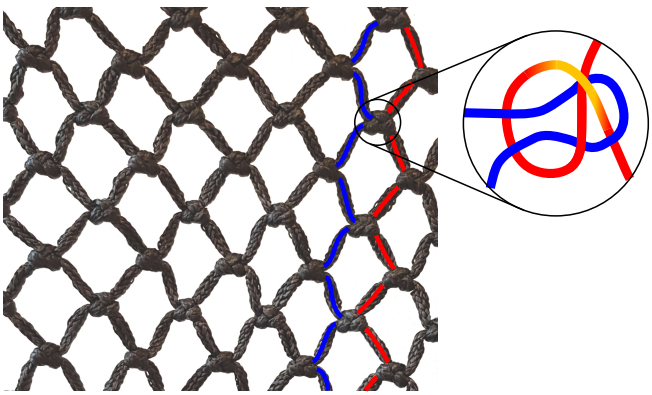

Figure 1.2: The path of two strings is shown with a red and blue line. The flag knot is shown in the circle.

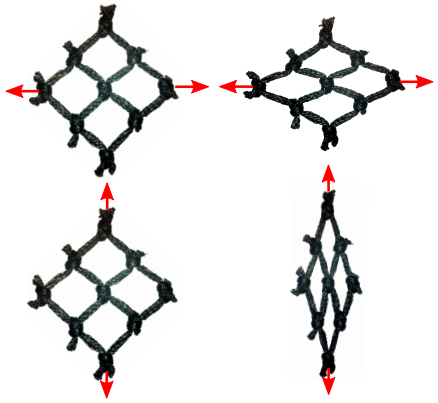

Figure 1.3: Deformation characteristics of the net.

the mesh is a flag knot. In figure 1.2 the path of two strings is shown with a red and blue line, and the way the flag knot is tied is enlarged in the circle.

It is observed that the knots affect the deformation characteristic of the net significantly. This is clearly seen in figure 1.3 where a piece of net is pulled in two directions, in turn, perpendicular to each other. The change in distance between the two knots pulled are:

$$\Delta_H = 127 \text{ mm} - 106 \text{ mm} = 21 \text{ mm} \tag{1.1}$$

$$\Delta_V = 142 \text{ mm} - 106 \text{ mm} = 36 \text{ mm} \tag{1.2}$$

Where Δ_H is the elongation from the horisontal case and Δ_V is the elongation from the vertical case w.r.t figure 1.3. The elongation in the horisontal direction is 42 % smaller than the vertical direction. This show that the knots has a significant influence on the behaviour of the net.

1.2 Description of the Rod

The provided rod with mounting cup and locking pin is seen in figure 1.4. The rod is made of a thermoset elastomer and the mounting cup and pin are made of steel. To mount the rod on a surface, the mounting cup is first bolted to the surface using a Ø10 slotted hole in the bottom. The rod is then inserted and locked into place using the locking pin which fits through matching holes in the rod and mounting cup. To mount the net, the rod has a M10 steel thread insert in the top. The small square with a hole which extrudes from the top of the rod is used to connect rods if needed.

Figure 1.4: The rod, mounting cup and locking pin.

1.3 Task Statement

The introduction provided a description of the components which this project concerns. The goal of this project is formulated as a task statement and reads:

> *Write a program to model the mechanical behaviour of a net mounted on flexible rods. Analyse the provided rods and develop a new design which improves upon the functionality of the rod.*

2 | Net-Rod Model

In this chapter the net-rod model is described. The purpose of the model is to predict the behaviour of a net-rod system. The model is programmed in MATLAB and consists of multiple scripts and functions. Following an overview of the program is given in section 2.1 succeeded by a description of the modelling in section 2.2 and the programming in section 2.3 to 2.6.

2.1 Program Overview

In general the program establishes a net and rod system and determines the deformation caused by applied forces or prescribed displacements. The main script *NetRodModel* can be divided into four parts: Input, pre-processor, solver and post-processor. These parts are shown in figure 2.1.

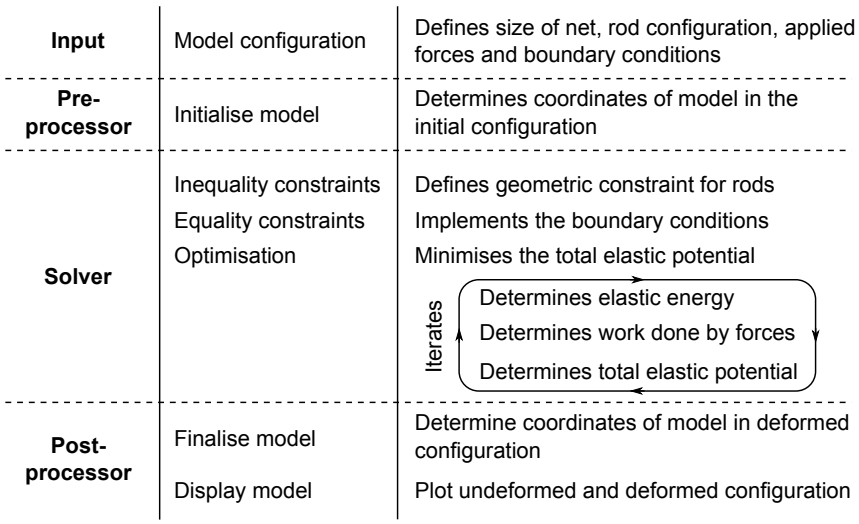

Figure 2.1: Structure of the program.

In the input section the user can configure the model by adjusting the size of the net, rod positions, rod discretisation, boundary conditions and applied forces. The pre-processor section determines the coordinates of the model in the initial configuration. In the solver an optimisation routine is performed which minimises the total elastic potential to solve the model. The post-processing section determines the deformed configuration and plots it alongside the undeformed configuration in true scale.

The program consists of many functions and not all the processes in the program are shown in figure 2.1. All the functions are documented in MATLAB. By writing *help FunctionName* in the command window a description of the function is displayed.

2.2 Modelling

The modelling of the net-rod system is illustrated in figure 2.2. The net is modelled with springs connected at nodes where the knots would have been. The size of the net is specified by the number of horisontal and vertical nodes (HxV) and the node distance. This enables modelling of any rectangular net.

The knots are not modelled which is a rough simplification when modelling the provided net, but not necessarily for other type of nets. The severity of the simplification depends on the knot geometry, knot size and knot distance. For the provided net the simplification will results in noticeable discrepancies, but the effort to model the knots was deemed to costly for the increased accuracy.

The rod is modelled as regular springs and torsional springs in segments. The number of segments in the rod is controlled by a discretisation parameter. This enables a more realistic modelling of the rod and better representation of the geometrical non-linearity. Each segment can be given a unique stiffness, but at default the stiffnesses are equal. The bottom node of the rod is always fixed, but the rods can be positioned at any node in the net, and by defining net size of a single node (1x1), a rod can be modelled alone. The net can also be modelled alone by not defining any rod positions, but then some boundary conditions must be applied.

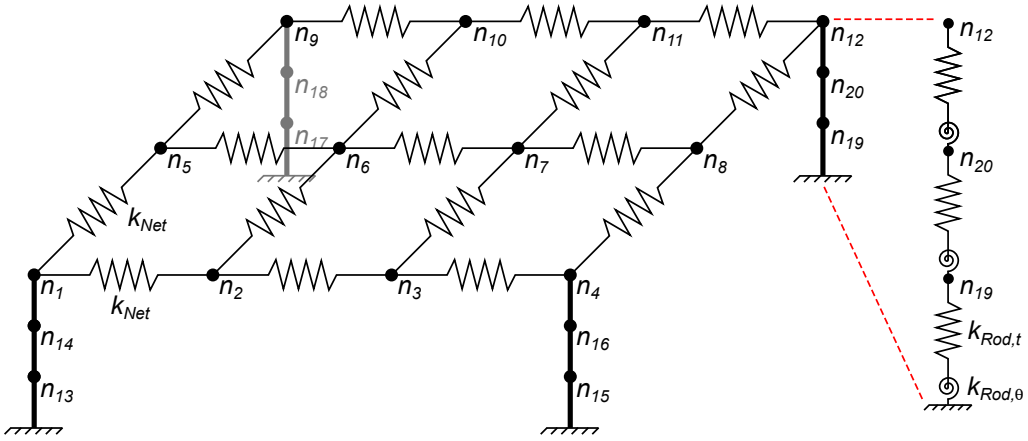

Figure 2.2: Illustration of the 4x3 net model and with a rod in each corner. The rods have a discretisation of three. Node numbering is also shown.

Each node provide three degrees of freedom (DoF) i.e. displacement in the x-, y- and z-direction. Each node can be assigned boundary conditions (prescribed displacements) and forces.

2.2.1 Stiffnesses of the Model

The net-rod model uses three different stiffnesses: The tensile stiffness of net, the tensile stiffness of the rod and the bending stiffness of the rod. The stiffnesses of the provided net and rod are determined in chapter 3. The tensile stiffness of the net is constant regardless of the configuration of the net. The stiffnesses of the rod on the other hand are affected by the discretisation. In section 3.2 and 3.3 the tensile and bending stiffnesses of the rod are determined, but these only applies for a undiscretised rod (one segment). When the rod is discretised the stiffness needs to be adjusted. The adjustment of the stiffnesses of the rod is described in the following.

Tensile Stiffness of the Rod

In order to determine how the tensile stiffness of the rod should be adjusted, the cases in figure 2.3 are examined. In figure 2.3a a model of the tensile stiffness of a undiscretised rod and is shown and in figure 2.3b a rod with a discretisation of two.

(a) Undiscretisatised. **(b)** Discretisation of two.

Figure 2.3: Modelling of the tensile stiffness with and without discretisation.

The two spring systems are applied with the same load and has to result in the same total displacement. Since the stiffnesses in figure 2.3b are equal, then the displacements must also be equal, $x_2 = x_3$. In order to result in the same total displacement as in figure 2.3a the displacements x_2 and x_3 must be half of x_1 and the stiffness k_2 must be twice the size of k_1. This is also reflected in equation (2.1)(Rao and Fah, 2011, s. cover) for tensile stiffness. $E\,A$ is unchanged when the rod is discretised and only the length L changes.

$$k_t = \frac{E\,A}{L} \tag{2.1}$$

When the rod has a discretisation of two the length is half the original length resulting in twice the original stiffness. The adjustment of the tensile stiffness in the net-rod model is therefore done by multiplying the tensile stiffness with the discretisation.

Bending Stiffness of the Rod

For the bending stiffness the adjustment is not as simple. When the rod is discretised the boundary conditions of the segments are different from an undiscretised rod. The stiffness used for the undiscretised rod is derived from a cantilever beam with a load at the end as seen in figure 2.4. When the rod is discretised the segments have the boundary conditions of a section of the cantilever beam in figure 2.4.

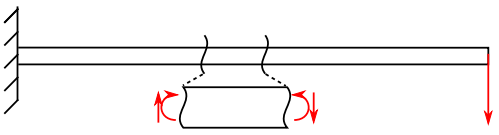

Figure 2.4: A cantilever beam with a load at the end and an enlarged section from the beam.

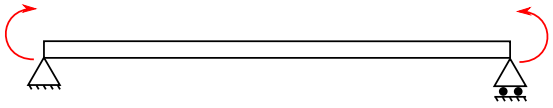

Figure 2.5: A simply supported beam with pure moment applied.

The bending stiffness of a undiscretised rod (a cantilever beam) is given by equation (2.2)(Rao and Fah, 2011, s. cover) w.r.t angles.

$$k_\theta = \frac{3\,E\,I}{L} \tag{2.2}$$

In order to determine how the stiffness of a discretised rod must be adjusted, an equation for the stiffness is derived. As a simplification the shear forces are neglected in the derivation and a simply supported beam subjected to pure moment is considered. Under the assumption of small displacements and rotations, the angle of the deflection of a simply supported beam under pure bending is:

$$\theta = \frac{M\,L}{E\,I} \tag{2.3}$$

Inserting $M = k_\theta \, \theta$ into equation (2.3) and isolating the stiffness k_θ the equation is derived:

$$k_\theta = \frac{E \, I}{L} \tag{2.4}$$

It is apparent that beside the adjustment w.r.t the length (as with the tensile stiffness) the difference between the bending stiffness of an undiscretised and a discretised rod is a factor of three. However it should be noticed that in order for the assumption of pure moment to be true the discretisation needs to be fine.

2.2.2 Assumptions

During the programming of the model some assumptions have been made in order to make simplifications:

- The net is modelled with springs of equal length and stiffness.
- The net has no rotational stiffness in the nodes.
- The net springs cannot bend i.e. only rigid body rotation and elongation are allowed.
- The knots of the net are not modelled.
- The rod is modelled in discrete segments of regular and torsional springs of equal length.
- The discrete rod segments cannot bend i.e. only rigid body rotation and elongation are allowed.

2.3 Input

The first part of the program defines the inputs for the model. The inputs are located in two script: *NetRodModel* and *Input*. *NetRodModel* contains the model configuration inputs. *Input* is loaded in *NetRodModel* and contains dimensions and stiffnesses of the net and the rod. The inputs for the model are described in the following itemisation.

Model Configuration

- *NetSize:* Vector defining the size of the net by specifying number of horisontal and vertical nodes.
- *RodPos*: Vector defining the position of the rods.
- *RodDis*: Scalar defining the discretisation of the rods.
- *Fx, Fy, Fz:* Matrices defining the nodal forces in the x-, y- and z-direction.
- *BCx, BCy, BCz*: Matrices defining the boundary conditions.

Component Constants

- *NodeDist*: Defines the distance between the nodes.
- *RodLength*: Defines the length of the rods.
- *kNet*: Defines the tensile stiffness of the net (springs).
- *ktRod*: Defines the tensile/compressive stiffness of the rods.
- *kbRod*: Defines the bending stiffness of the rods.
- *K*: Vector which collects *kNet*, *ktRod* and *kbRod*.

2.4 Pre-Processor

Once the input is read the program initialises the model and assembles the force vector. The initialisation is done by defining the coordinates of all the nodes of the net (knots), the coordinates of the end points of the springs (strings) and the coordinates of the rods. The functions which generate the coordinates are *NodeCoordinates*, *SpringCoordinates* and *RodCoordinates*. From the coordinates the initial configuration is made as seen in figure 2.6.

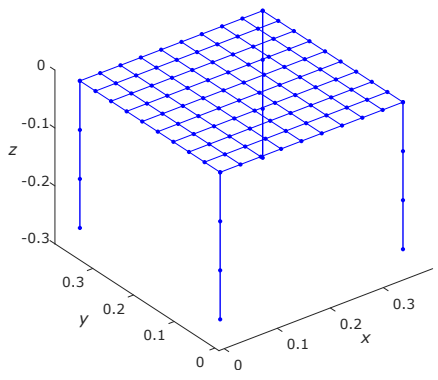

Figure 2.6: Initial configuration.

The force vector is assembled from the three matrices defined in the input section by the function *ForceVector*. The forces are defined in matrices in order to make it more user friendly. Each of the force matrices consist of two rows. In the first row the user defines the nodes the forces should be applied to and in the next row the magnitude of the force in sequence with the nodes.

2.5 Solver

The majority of the programming lies in the solver. But before taking a look at how the solver is programmed, the non-linearity of the model and the solution methods are described.

2.5.1 Non-Linearity

Although the model is made of simple springs the solution is not straight forward to obtain. This is due to geometrical non-linearity of the model. In figure 2.7 a node and four springs are modelled. A force is applied to the node causing the springs to deform. In order to determine the displacement of the node the stiffness of the node needs to be determined. The stiffness contribution of k_1 and k_2 are both constant but the contribution of k_3 and k_4 are dependent on the node displacement. k_3 and k_4's dependency of the displacement makes the problem non-linear and therefore unsuited for solving using methods assuming linearity.

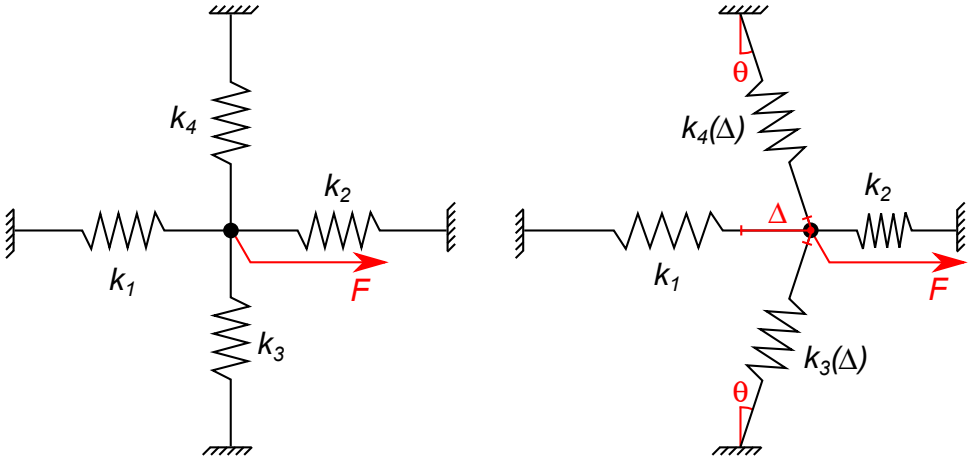

Figure 2.7: Model non-linearity.

By assuming small displacements and rotations the geometrical non-linearity can be avoided and results in a linear system, since the stiffness contributions from k_3 and k_4 can be neglected. But since large displacements and rotations are implicit, whenever deformations take place out of the plane of a generalised membrane without bending stiffness, this is not an option. In addition the net has no compressive stiffness, which has to be reflected in the model.

2.5.2 Solution Method

In order to solve the system, two general approaches have been investigated. Force equilibrium and the principle of stationary potential energy.

At first the force equilibrium approach was investigated. The force equilibrium approach iterated a linear system where the stiffness was updated in each iteration until equilibrium is reached. The force equilibrium approach lead to multiple complications and dead ends due to difficulty handling the non-linearity. The different algorithms investigated can be found in appendix B.

Using the principle of stationary potential energy proved superior resulting in simpler code

and robust solutions. The approach used is a minimisation of the total elastic potential. The total elastic potential for a linear elastic system is defined as:

$$\Pi = U - W \tag{2.5}$$

$$U = \frac{1}{2} \sum k_i \, \Delta_i^2 + \frac{1}{2} \sum k_j \, \theta_j^2 \tag{2.6}$$

$$W = \{F\} \bullet \{d\} \tag{2.7}$$

Where U is the elastic energy stored in the springs, k is stiffnesses, Δ_i is elongations, θ_j is rotations, d_i is displacements and W is the work done by the applied forces. In the next section the programming of this solver is described.

2.5.3 Optimisation

To solve the model the minimum of the total elastic potential needs to be found. This is an optimisation problem and can be formulates as:

$$\begin{aligned} \underset{\{d\}}{\text{minimise}} \quad & \Pi(\{d\}) \\ \text{subject to} \quad & [A]\,\{d\} \leq \{b\} \\ & [C]\,\{d\} = \{e\} \end{aligned} \tag{2.8}$$

For the optimisation the integrated MATLAB function *fmincon* is used. *fmincon* is a constrained gradient based optimisation routine. For this optimisation problem the following options are used.

- *LargeScale = off*: This defines the optimisation as a medium scale problem. The difference between the large and medium scale is that medium scale creates full matrices and large scale stores sparse matrices.
- *Algorithm = SQP*: This selects the optimisation algorithm SQP, an abbreviation of Sequential Quadratic Programming.

The chosen algorithm SQP is described in the following section in general terms (MathWorks, 2016).

Sequential Quadratic Programming

As with most gradient based algorithms the SQP method is based on the following iterative form:

$$\{x\}^{(k+1)} = \{x\}^{(k)} + \{\Delta x\}^{(k)} \tag{2.9}$$

$$\{\Delta x\}^{(k)} = \alpha_k \{d\}^{(k)} \tag{2.10}$$

Where $\{x\}$ is the design variable, $\{\Delta x\}$ is the design update, k is the iteration number, $\{d\}^{(k)}$ is the search direction and α_k is the step size. The SQP method determines the search direction through a Quadratic Programming (QP) subproblem. The QP subproblem is a quadratic approximation of the Lagrangian function and is generally formulated as:

$$\begin{aligned} \underset{\{d\}}{\text{minimise}} \quad & \{\bigtriangledown f(\{x\}^{(k)})\}^T \{d\} + \frac{1}{2} \{d\}^T [\tilde{H}]_{(k)} \{d\} \\ \text{subject to} \quad & [N]^T \{d\} = \{u\} \\ & [M]^T \{d\} \leq \{v\} \end{aligned} \tag{2.11}$$

The solution to the QP subproblem is the search direction, $\{d\}$. Beside the search direction the step size, α_k, also needs to be determined which can be done with a line search method.

The gradients for QP subproblem (2.11) can be determined either analytically or by using a finite difference approximation. The net-rod model uses the default option in *fmincon* which is a forward finite difference approximation, to determine the gradient. The forward finite difference approximation can be defined as:

$$\frac{\partial f(\{x\})}{\partial x_i} = \frac{f(\{x\} + \Delta x_i) - f(\{x\})}{\Delta x_i} \tag{2.12}$$

At each iteration the SQP method determines a Quasi-Newton approximation of the Hessian, $\tilde{H}$. The approximation is based on the gradients and is calculated using the BFGS (Broydon-Fletcher-Goldfarb-Shanno) method(MathWorks, 2016)(Arora, 2011).

Constraints

The optimisation is constrained using inequality and equality constraints. The inequality constraints are used to prevent the rods from deflecting further than the z-coordinate of their bottom node. The top node, which the rod and net share, is constrained in the z-direction so it cannot go lower than the length of the rod. This ensures the rods does not deflect through "the surface". The inequality constraints are defined by the function *InequalityConstraints* which generates inequality constraints in the format used in *fmincon*.

The equality constraints are used to apply the boundary conditions. The boundary conditions can also be used to define prescribed displacements. The equality constraints are defined by the function *EqualityConstraints* which generates equality constraints in the format used in *fmincon*. If a prescribed displacement is defined then the displacement is added to the initial guess by the function *InitialGuess* to improve performance. Otherwise the initial guess is the initial configuration.

Objective Function

The objective function for the optimisation is *TotalElasticPotential*. It calculates the total elastic potential as a function of the displacements. *TotalElasticPotential* contain multiple other functions in order to calculate the total elastic potential. The flow of *TotalElasticPotential* is shown in the following enumeration.

1. The coordinates of the displaced system is determined by *DispNodeCoordinates*, *SpringCoordinates* and *DispRodCoordinates* using the vector $\{d\}$.
2. The elongation of the net and rods are determined by *SpringElongation* and *RodElongation* using the displaced coordinates.
3. The rotation of the rods are determined by *RodRotation* using the displaced coordinates.
4. From the elongations and rotations the elastic energy of the net and rods is determined in *ElasticEnergy*. The energy for compressed springs are set to zero thereby enforcing that springs have no compressive stiffness.
5. The work done by the forces are determined by the dot product of the force vector $\{F\}$ and displacement vector $\{d\}$.
6. Finally the total elastic potential is determined as in equation (2.5).

2.5.4 Convergence

The time it takes to perform the optimisation is determined by three general factors: Model size, computational power and optimisation settings. The first two points are self explanatory, but the influence of the settings are important too. The following settings are used to control the optimisation runtime:

- *MaxIter*: Maximum number of iterations.
- *MaxFunEvals*: Maximum number of function evaluations.
- *TolX*: Termination tolerance for the step size.
- *TolFun*: Termination tolerance for function value.

The convergence tolerance is dictated by *TolFun*. It determines the change in function value (Π) and if the difference is below the defined tolerance then the optimisation is converged. Since the size of Π is dependent on the size of the model the convergence tolerance is also dependent on the size of the model. This means that a single *TolFun* cannot be determined. If the optimisation routine is terminated before the convergence tolerance is reached, then it may be due to reaching *TolX*, *MaxIter* or *MaxFunEvals*.

When using the principle of stationary potential energy on a system which is elastic (no energy is lost during deformation) and conservative (the work is independent of the path) then the minimum will be the global minimum (Lund and Lindgaard, 2014). This also applies to the net-rod model when all of the net is in tension. The cases where it do not apply are when the net is in compression. Since the energy contributed from compression of the net is not used, the net takes on any arbitrary configurations. This results in infinitely many local minima where the configuration of the DoF's in tension are equal but those in compression are arbitrary.

2.6 Post-Processor

Once the optimisation has found a solution the program does a final determination of the coordinates, using the functions *DispNodeCoordinates*, *SpringCoordinates* and *DispRodCoordinates*. A plotting function *PlotNet3D* plots the undeformed and the deformed models as seen in figure 2.8. To show off the capabilities of the net-rod model a number of configurations are shown in figure 2.9 to 2.12. All plots are in true scale.

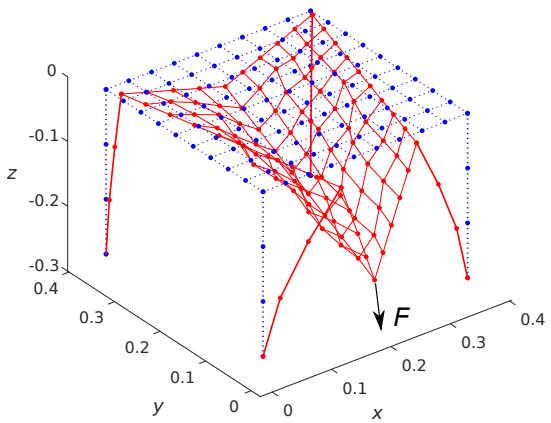

Figure 2.8: Plot of a 10x10 net with a rod in each corner. The blue dashed model is the initial configuration and the red model is the deformed configuration.

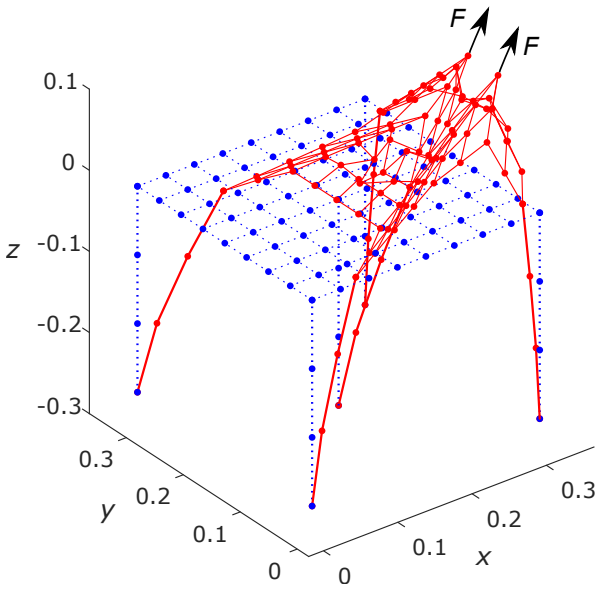

Figure 2.9: 9x9 net with a rod in each corner and one in the center. Two nodes are pulled in the x- and z-direction.

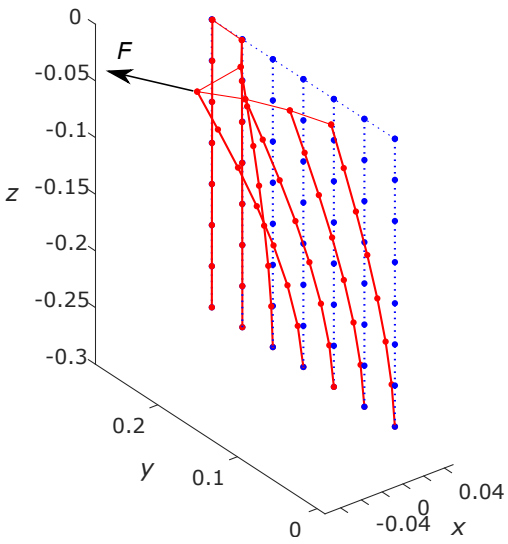

Figure 2.10: 1x7 net with a rod in each node. The middle node is loaded in the $x-$ and y-direction.

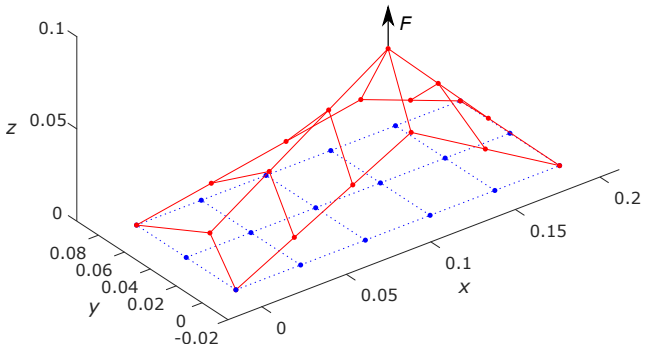

Figure 2.11: 6x3 net fixed in the corner using boundary conditions. A nodes are pulled in the z-direction.

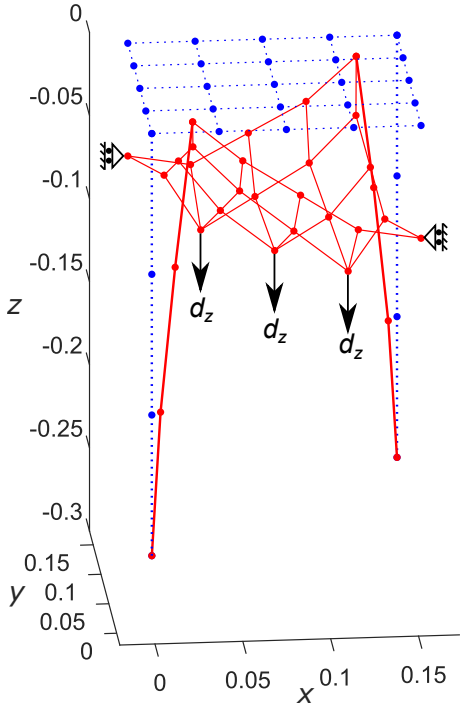

Figure 2.12: 5x5 net with a rod in two diagonal corners. Three central nodes on the other diagonal are displaced in the z-direction.

3 Determination of Stiffnesses

This chapter investigate and determine the tensile stiffness of the net and the tensile and bending stiffness of the rod. The stiffnesses are needed for the net-rod model. The modulus of elasticity is unknown for both items, which means the stiffnesses cannot be calculated. Because of this the stiffnesses are determined experimentally.

3.1 Stiffness of the Net

The experimental determination of the stiffness of the net required several attempts before a reliable method was developed. This process is documented in section 3.1.1. The journal of the final experiment is located in appendix C. Following the results of the experiment are presented in section 3.1.2 and the stiffness determined in section 3.1.3.

3.1.1 Setup for the Experiment

All experiments were conducted on a Zwick Z100/TL3S tensile testing machine. A total of twelve measurements of the net were made, but only the final four measurements are used. Three different setups, five different types of specimens and two measuring techniques were used. In the following the selection of setup, specimen and measuring technique is explained.

Setup The three setups used are shown in figure 3.1. In the first setup the knots of the specimen were clamped using serrated wedges as shown in figure 3.1a. But the clamping force was insufficient to hold on to the knots.

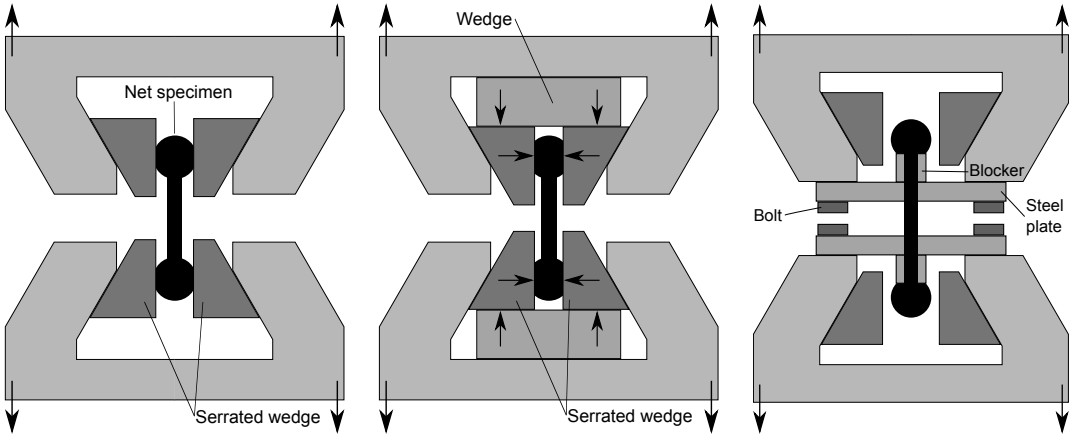

(a) First setup. **(b)** Second setup. **(c)** Third setup.

Figure 3.1: Setups for the experiments.

The second setup also used the serrated wedges, but two extra wedges were added to push the serrated wedges closer together. This is illustrated in figure 3.1b. Again the clamping force did not manage to hold the specimens in place.

In the third and final setup instead of using the serrated wedges, the end knots was blocked by fixtures which was held in place by steel plates. The steel plates were bolted in place as seen in figure 3.1c. This proved to be the best way of securing the specimen.

Specimen The specimens tested are shown in figure 3.2. The first specimen used, marked 1 in figure 3.2, was chosen since the stiffness of the net from knot to knot was wanted. The force-displacement curve should then supply the stiffness directly from the slope of the curve when measuring the total displacement. This was used in the first and second setup.

Figure 3.2: The five specimens.

The second specimen (a string with four knots) was tested to investigate the influence of the knots. Initially the knot was thought to have slipped from the wedges, but later inspection revealed that one of the knots had been untied as seen in figure 3.2.

The third, fourth and fifth specimen was tested in the final setup. This setup demanded a longer specimen in order to be mounted, so the third specimen had to have five knots. This was the first time the untying of a knot was noticed. In order to prevent the untying of the knots, the fourth specimen consisted of a net where only the ends were cut loose to allow mounting. Again a knot was untied, this time at the end of the specimen.

The fifth specimen was unraveled from the net and not cut as the other specimens. This was done in order to mount an extensometer and reduce the number of knots to be untied (only one in each end). The fifth specimen was used for the final four measurements, which was used to determine the tensile stiffness of the net.

Measuring Technique In the first and second setup and with specimen 1 to 4, the elongation was measured using the total displacement of the Zwick crossheads. The results were inconsistent even with identical specimens. The solution was to use an extensometer. This had not been done because of lack of space due to the knots. The fifth specimen was long enough to have room for the extensometer since no knots were interfering.

3.1.2 Results

The results from the final measurements are seen in figure 3.3. The force in each test is increased until the end knots are untied. The last part of each curve show the event of a knot being untied.

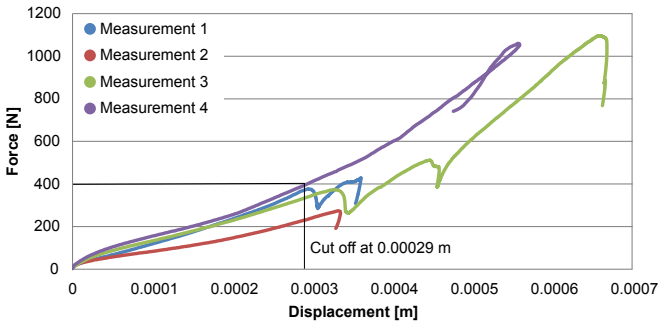

Figure 3.3: Results from the final measurements. The used part are below the cut off line at 0.00029 m.

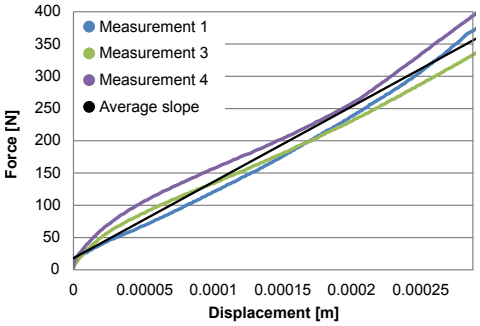

Figure 3.4: The used linear part of the results and an average slope (black line).

It is clear in figure 3.3 that not all of the data is usable. Since the net is modelled with a linear stiffness the curves are cut off at 0.00029 m to acquire the linear part. The linear parts are seen in figure 3.4. The second measurements (the red line in figure 3.3) is removed as a outlier due to the large difference in slope. It is suspected that the difference is due to a damaged specimen. For each measurement a linear trend line is fitted through the data points of the curves in figure 3.4. The slopes of the trend lines are listed in table 3.1. An average of the slopes is found to be $1.16 \cdot 10^6 \frac{\text{N}}{\text{m}}$ which is the black curve in figure 3.4.

Table 3.1: Slopes of the linear trend lines.

Measurement	Slope [N/m]
1	$1.20 \cdot 10^6$
3	$1.05 \cdot 10^6$
4	$1.23 \cdot 10^6$
Average	$1.16 \cdot 10^6$

3.1.3 Determining the Stiffness of the Net

The stiffness needed for the net-rod model is the stiffness from one knot to another knot. But as described in section 2.2 the knots of the net are not included in the model, only the strings. As an approximation the stiffness is determined for a string with the same length as the distance between two knots. This distance is measured to $l = 0.0383$ m. The stiffness of a string with the length of $l_m = 0.0195$ m (the measuring distance of the extensometer) was determined in section 3.1.2 as $k_m = 1.16 \cdot 10^6 \frac{\text{N}}{\text{m}}$. The stiffness of the net is determined as follows (Rao and Fah, 2011, s. cover):

$$k_{Net} = \frac{EA}{l} \Rightarrow EA = k_{Net} l \qquad k_m = \frac{EA}{l_m} \Rightarrow EA = k_m l_m \tag{3.1}$$

$$k_{Net} l = k_m l_m \Rightarrow k_{Net} = \frac{k_m l_m}{l} \tag{3.2}$$

$$k_{Net} = \frac{1.16 \cdot 10^6 \frac{\text{N}}{\text{m}} \cdot 0.0195 \text{ m}}{0.0383 \text{ m}} = 590601 \frac{\text{N}}{\text{m}} \approx 5.91 \cdot 10^5 \frac{\text{N}}{\text{m}} \tag{3.3}$$

3.2 Tensile Stiffness of the Rod

The experiment performed to determine the tensile stiffness of the rod is documented in a journal in appendix D. In the following the setup for the experiment is briefly described, the results are presented and the stiffness is determined.

3.2.1 Setup for the Experiment

The setup for the experiment is seen in figure 3.5. The rod is mounted in a Zwick Z100/TL3S tensile testing machine using the mounting cup and locking pin in the bottom and the thread in the top. Both ends are bolted to the steel plates. Since the base of the mounting cup is angled the rod is bend a little in order to be mounted in the top. The bend is assessed to have insignificant effect on the results. The displacements are measured using two methods. The total displacement measured by the Zwick and the displacements of two marked points (see figure 3.5) on the rod captured by a camera.

Figure 3.5: The setup for the determination of the tensile stiffness of the rod.

3.2.2 Results

The results of the experiment generated using the Zwick are seen in figure 3.6. The rod was elongated 5 mm (First measurement), 7.5 mm (second and third measurement) and 10 mm (fourth measurement). A preload of 100 N was chosen to align and tension the components. The curves in figure 3.6 show only a slight deviation between the four measurements. This is likely due to relaxation. It is also important to notice the slope decreases with the increased load (softening). This show that the elastomer has a non-linear material behavior, specifically it softens.

Since the rod is modelled with a linear tensile stiffness the curves are cut off at 1000 N to acquire an approximately linear part. The linear parts of the curves are seen in figure 3.7. Trend lines are fitted through the four curves to acquire the slopes which are collected in table 3.2. The average of the slopes is determined to be $3.25 \cdot 10^5 \frac{\text{N}}{\text{m}}$.

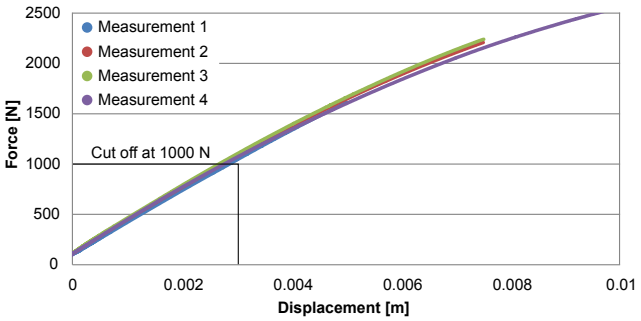

Figure 3.6: Results from the experiment. The used part are below the cut off line at 1000 N.

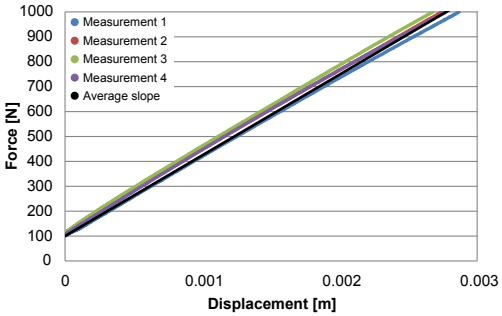

Figure 3.7: The used linear part of the results and an average slope (black line).

Table 3.2: Linear trend lines.

Measurement	Slope
1	$3.17 \cdot 10^5$
2	$3.25 \cdot 10^5$
3	$3.32 \cdot 10^5$
4	$3.24 \cdot 10^5$
Average	$3.25 \cdot 10^5$

Beside the force-displacement curves supplied by the Zwick a camera recorded the displacements. Using two frames, one before loading and one after, the change in distance between the two points is determined. Knowing this, the initial distance between the points and the thickness of the rod where the points are, the strain, stress and finally the modulus of elasticity is determined. The calculated values are collected in table 3.3.

Table 3.3: Estimated values of modulus of elasticity.

Measurement	Force [N]	Stress [MPa]	L [m]	Δ [m]	Strain [%]	E [MPa]
1	1612.97	1.42	0.0500	0.0013	2.54	56.02
2	2207.90	1.95	0.0505	0.0017	3.36	58.01
3	2239.56	1.97	0.0506	0.0018	3.62	54.58
4	2562.08	2.26	0.0509	0.0021	4.19	53.91

The initial distance between the two points is 0.05 m and the cross sectional area where the points are located is $A = 0.0011$ m^2. The average modulus of elasticity is estimated to $E_{ave} = 55.63$ MPa.

3.2.3 Determining the Tensile Stiffness of the Rod

Although a tensile stiffness has been determined in the section 3.2.2, it is first compared with a calculation of the tensile stiffness based on the modulus of elasticity also determined in section 3.2.2. To do this a expression for the tensile stiffness of the rod is derived.

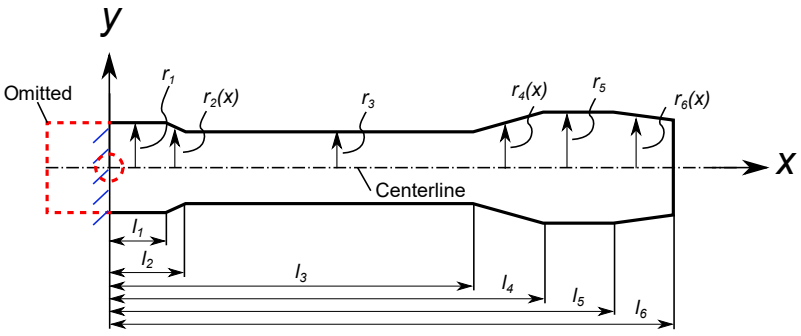

Figure 3.8: Radius, lengths and simplification of the flexible rod.

The tensile stiffness of a prismatic beam is determined using the modulus of elasticity and the geometry as evident from equation (3.4)(Rao and Fah, 2011, s. cover).

$$k_t = \frac{E\,A}{l} = \frac{E}{\frac{l}{A}} \tag{3.4}$$

The rod is non-prismatic consisting of three cylinders and three tapered cylinders with the lengths, l_i, and radii, $r_i(x)$, as seen in figure 3.8. This means equation (3.4) needs to be modified to take non-prismatic geometry into account. To account for the non-prismatic geometry piecewise integration over the length is used.

$$\frac{l_i}{A_i(x)} = \frac{l_i}{\pi r_i(x)^2} = \int_{l_{i-1}}^{l_i} \frac{1}{\pi r_i(x)^2}\,dx \tag{3.5}$$

Using the expression in equation (3.5) and summing each of the parts of the rod and inserting it in (3.4) the final equation is derived. $l_0 = 0$ m.

$$k_{Rod,t} = \frac{E\pi}{\sum_{i=1}^{6} \int_{l_{i-1}}^{l_i} \frac{1}{r_i(x)^2} dx} \tag{3.6}$$

Using equation (3.6) and the average modulus of elasticity $E_{ave} = 55.63$ MPa the calculated tensile stiffness is $k_{Rod,t2} = 2.88 \cdot 10^5 \frac{\mathrm{N}}{\mathrm{m}}$. The calculated stiffness is 11.4 % below the measured stiffness which is $k_{Rod,t1} = 3.25 \cdot 10^5 \frac{\mathrm{N}}{\mathrm{m}}$.

The difference between the two stiffnesses has two reasons. The first is the accuracy of $k_{Rod,t2}$ which is based on post-processing of the images taken by a camera and the maximum force from the Zwick. The post-processing of the images is very sensitive and subjective, meaning two different people may get different results.

The other reason has to do with non-linearity of the curves which is observed in figure 3.6. $k_{Rod,t1}$ is based on the part of the curves below 1000 N where the curve is nearly linear and where the slope is largest. $k_{Rod,t2}$ is only based on the start and the end of the measurements, meaning it is the same as the secant slope of the curves in figure 3.6. Due to the decreasing slope this will clearly result in a lower stiffness. If a linear trend line is fit to the entirety of the four measurement and the average is taken the result is $2.89 \cdot 10^5 \frac{\mathrm{N}}{\mathrm{m}}$ which is nearly identical to $k_{Rod,t2}$.

The measured stiffness $k_{Rod,t} = 3.25 \cdot 10^5 \frac{\mathrm{N}}{\mathrm{m}}$ is chosen for the model, since the rod is expected to be loaded mostly in bending and only a small amount of tension. With only a small amount of tension in the rod, it will move around in the low end of the force-displacement curve as used for determining the stiffness.

3.3 Bending Stiffness of the Rod

The experiment performed to determine the bending stiffness of the rod is documented in a journal in appendix E. In the following the setup for the experiment is briefly described, the results are presented and the stiffness is determined.

3.3.1 Setup for the Experiment

The setup for the experiment is seen in figure 3.9. A steel fixture has been fabricated for the experiment to mount the rod on a steel beam. Instead of using a locking pin to secure the rod, it is clamped in the fixture. Using threaded bars and nuts the fixture is clamped to the steel beam. The rod is mounted on a vertical surface in order to use weights to load the rod.

Figure 3.9: Setup for determining the bending stiffness

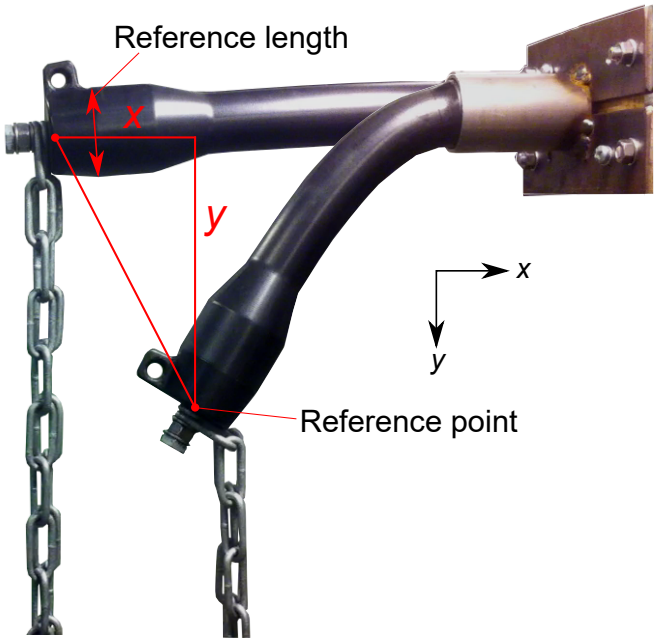

Figure 3.10: Illustration of the method used for determining the displacement of the rod.

The experiment is recorded by a camera in order to determine the displacements by image post-processing. The tip of the rod is used as a reference point and the diameter of the cylindrical part of the rod head is the reference length, as seen in figure 3.10. The reference length is used to determine the meter per pixel ratio.

3.3.2 Results

The result of the experiment is seen in figure 3.11 and 3.12 for the x- and y-displacements respectively. Eight weights were applied in the sequence; 2, 3, 5, 10.3, 15.3, 20, 30.3 and 50 kg.

The x-displacement is not used to determine the bending stiffness, but has been measured to determine the full deflection behavior of the rod. The y-displacement or deflection is used to determine the bending stiffness. Since a linear bending stiffness is used in the

net-rod model, the non-linear part of the curve in figure 3.12 is cut away. The stiffening seen is geometrical non-linearity due to the rod being in tension as well as bending. The cut removes the two last loads (30.3 and 50 kg). A trend line is fitted trough the remaining points resulting in the black line seen in figure 3.12. The slope of the line is $k_b = 1436.8 \frac{\text{N}}{\text{m}}$.

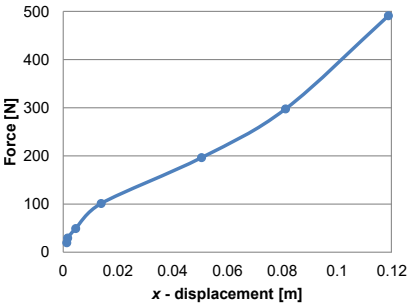

Figure 3.11: The force-displacement curve for the x-direction.

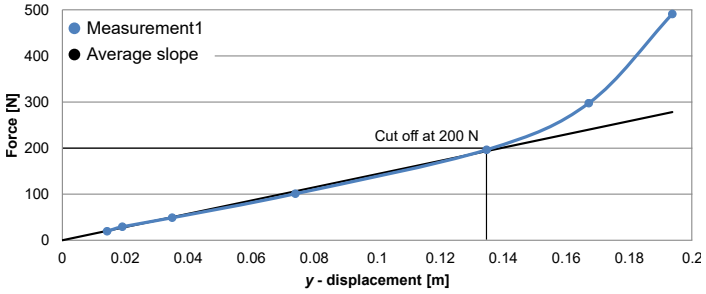

Figure 3.12: The force-displacement curve for the y-direction. The black line is a linear trend line of the linear part.

3.3.3 Determining the Bending Stiffness of the Rod

The slope determined in section 3.3.2 is the linear bending stiffness of the rod w.r.t displacement. In the net-rod model it is the angle of deflection which is used to describe the deflection of the rod. Because of this the linear bending stiffness k_b needs to be converted into a linear torsion stiffness k_θ, to relate applied load to angular deflection. The relation between the two stiffnesses is determined by equating the elastic energy of the two stiffness types.

$$\frac{1}{2} k_\theta \, \theta^2 = \frac{1}{2} k_b \, x^2 \tag{3.7}$$

The relation between the angle and displacement is seen to the left in equation (3.8). By assuming small rotations the relation can be simplified as seen in equation (3.8).

$$x = sin(\theta) \, l \qquad \Rightarrow \qquad x = \theta \, l \tag{3.8}$$

Inserting equation (3.8) in equation (3.7) yields the relation between the two stiffnesses.

$$\frac{1}{2} k_\theta \, \theta^2 = \frac{1}{2} k_b \, (\theta \, l)^2 \tag{3.9}$$

$$\Downarrow$$

$$k_\theta = k_b \, l^2 \tag{3.10}$$

The stiffness for the net-rod model is determined using the length of the rod, $l = 0.254$ m (distance from the fixation to the tip).

$$k_{Rod,\theta} = k_b \, l^2 = 1436.8 \, \frac{\text{N}}{\text{m}} \cdot (0.254 \text{ m})^2 = 92.7 \text{ Nm} \tag{3.11}$$

4 Validation of the Net-Rod Model

The purpose of this chapter is to validate the net-rod model described in chapter 2 configured with the stiffnesses determined in chapter 3. The validation is done in two steps. First the modelling of the rod is validated against the experiments used to determine the stiffnesses. Afterwards a model comprising of multiple rods and a net will be validated up against a similar physical system.

4.1 Rod Modelling

The validation of the rod modelling is done by comparing the deflection of the model with the measured deflection from the experiment described in section 3.3. First the results of a model of a undiscretised rod is considered. The comparison is seen in figure 4.1 where the blue curve is from the experiemnt and the magenta curve is from the model of the undiscretised rod. The three first points are nearly coincident with the experiment, but the next three points have a bit smaller deflection and the last point is nearly coincident. In section 3.2 it was evident that the rod displayed non-linear material behaviour by softening with increased load. This could explain the way the deviation gets larger as the load increases, with an exception of the last point.

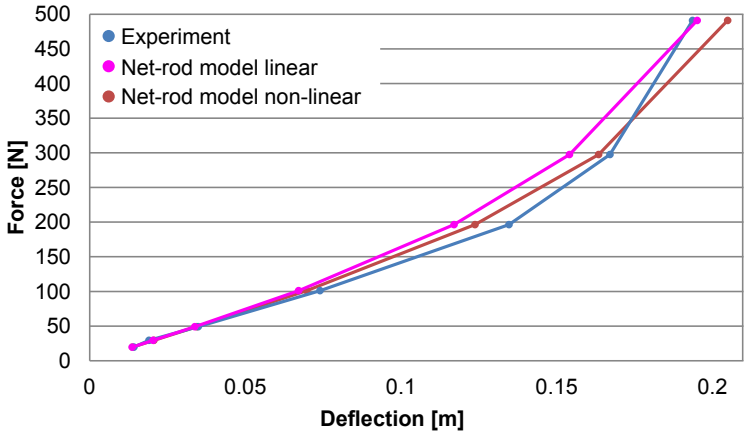

Figure 4.1: Comparison of the deflection of a undiscretised rod and experiment.

4.1.1 Non-Linear Stiffness

In order to improve the modelling of the rod a linear softening term is added to the bending stiffness to account for the material non-linearity. The non-linear stiffness is expressed in equation (4.1).

$$k_{Rod,\theta} = 92.7Nm - (9Nm)\,\theta \tag{4.1}$$

The non-linear terms is determined by fitting the model to the experiment. The model with the non-linear stiffness is the red curve in figure 4.1. In order to measure the improvement of the model, the sum of squares is calculated. The linear stiffness model deviates by $5.33 \cdot 10^{-4}$ while the non-linear stiffness model improves with $2.83 \cdot 10^{-4}$. In general the non-linear stiffness is closer than the linear, but at the expense of the last point which is no longer coincident with the experiment. The non-linear stiffness will be used since a generally more precise model is achieved.

4.1.2 Discretisation

Next the effect of increasing the discretisation is examined. To limited the amount of data three discretsations are used: Three, five and ten. The deflection curves of the different discretisations is seen in figure 4.2.

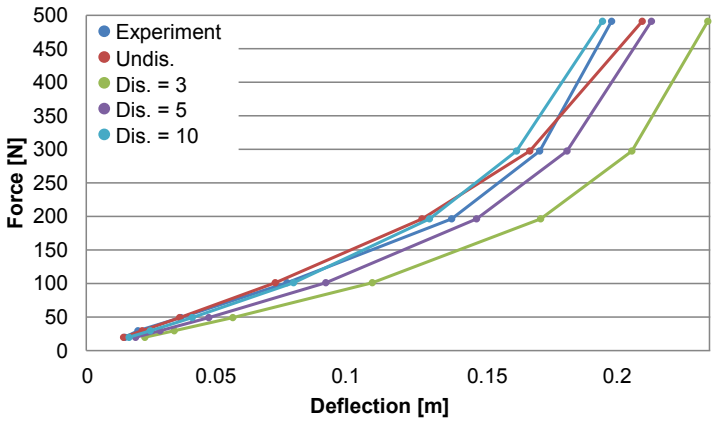

Figure 4.2: Comparison of the deflections of models of different discretisations and experiment.

From the curves large deviations in the deflections are clearly observed. The sum of squares are $5.33 \cdot 10^{-3}$, $7.95 \cdot 10^{-4}$ and $1.98 \cdot 10^{-4}$ for the discretisation of three, five and ten respectively. The largest deviation is produced by the model with a discretisation of three. The two other discretisations are closer to the experiment with the discretisation of ten being closets. The discretised rods seem to follow the shape of the curve of the experiment better than the undiscretised model.

The deviations observed may be due to the assumption stated in section 2.2.1 that the factor of three (adjustment factor for discretised rod compared to undiscretised rods) only applies when the discretisation is fine. At a low discretisations the boundary conditions are something between the two cases shown in figure 2.4 and 2.5 with associated equations (2.2) and (2.4).

4.1.3 Scaling

To compensate for violation of the assumption the factor of three is scaled with the discretisation. In theory the scaling starts at 1 for a undiscretised rod and then approach $\frac{1}{3}$ as the discretisation is refined. The scaling is determined for each discretisation by fitting the model to the curve form the experiment. The sum of squares is used to determine the best scaling value for each discretisation. This has resulted in the scaling curve seen in figure 4.3. It should be noticed that the curve in figure 4.3 does not converge to $\frac{1}{3}$ as expected. The reason to this is that the scaling was done by fitting the model to the experiment, thereby compensating for more than just the boundary condition assumption. Using the scaling the model produces the curves seen in figure 4.4. The sum of squares are $1.41 \cdot 10^{-4}$,

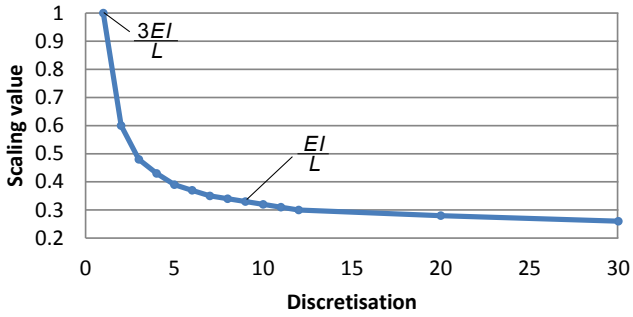

Figure 4.3: The scaling of the factor of three.

$1.01 \cdot 10^{-4}$ and $1.49 \cdot 10^{-4}$ for the discretisation of three, five and ten respectively.

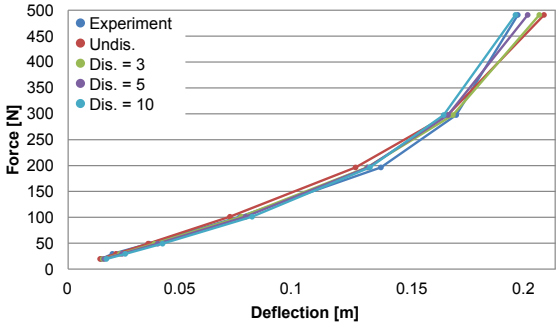

Figure 4.4: Comparison of the deflections of models of different discretisations, with scaling, and experiment.

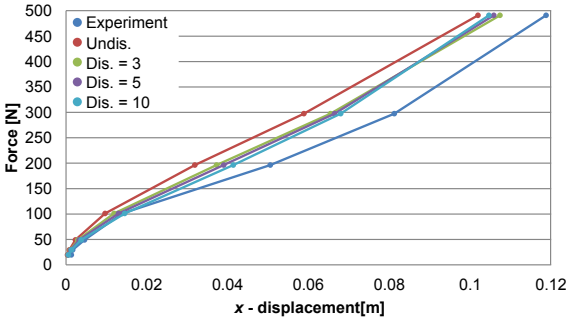

Figure 4.5: Comparison of the x-displacement of models of different discretisations, with scaling, and experiment.

It should be noted that the lowest sum of squares was achieved with a discretisation of five, outperforming the discretisation of ten. But if the x-displacement, which is seen in figure 4.5, is taken into account the total deviation is smallest for the discretisation of ten. The total sum of squares for the discretisation of ten is $6.10 \cdot 10^{-4}$ while for the discretisation of five it is $6.23 \cdot 10^{-4}$. Considering figure 4.5 it is seen that the deviation is larger in the x-direction than the y-direction (the deflection), which is because the scaling was fitted to the y-direction and not the x-direction. The y-direction was prioritised over the x-direction since y-direction directly relates to the bending stiffness. If the fitting of the stiffness was done w.r.t. x-direction the system would need to be more compliant.

The reasons for the remaining deviation in the rod model are assumed to be combination of several factors. Through the modelling there have been assumed small angles of rotation, which have been violated in some configurations and there are the uncertainties in the measurements to which the model is fitted. When using the non-linear bending stiffness and the fitted scaling the modelling of the rods is assessed to be capable of representing the behaviour of the rod thereby validating the modelling of the rod.

4.2 Physical System

The physical system for the validation consists of a net with 7x7 knots and four rods, one in each corner of the net. The remaining net is used for the validation which has limited the size of the system. The setup for the physical system is described in section 4.2.1 and the results are presented in 4.2.2. A journal of the experiment can be found in appendix F.

4.2.1 Setup

The experimental setup is seen in figure 4.6. The rods are mounted on a board of MDF using mounting cups and bolts. The net is secured on top of the rods using bolts, large washers and the thread in the rods. The setup is mounted vertically using flat steel bars bend around a concrete wall. The loads are applied to the lower center knot using a hook, chain and weights. Two cameras are placed in front and beside the setup to capture the x-, y- and z-displacements. Each rod and the knot where the load is applied are marked with a dot which is used to capture the displacements. The origins of the local coordinate systems coincide with the marked dots as seen in figure 4.6a and 4.6b.

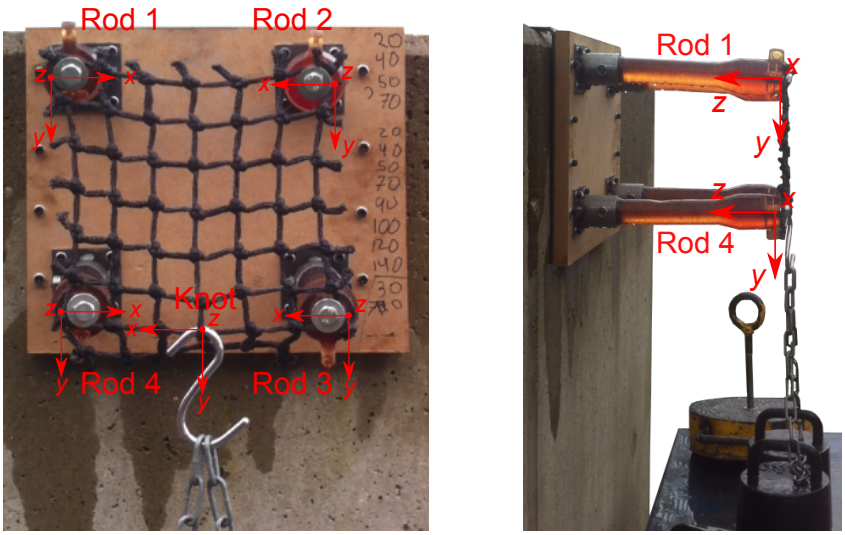

(a) Front view. **(b)** Side view.

Figure 4.6: Setup of the physical system.

4.2.2 Results

The physical system has been loaded with three different weights in the sequence; 40, 70 and 100 kg. The physical system with loads applied is seen in figure 4.7.

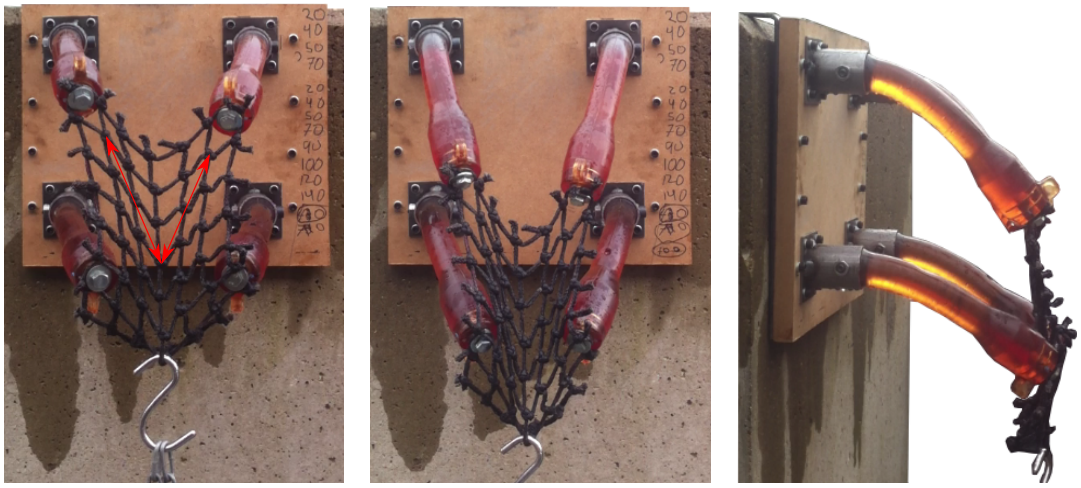

(a) Front view at 50 kg. **(b)** Front view at 100 kg. **(c)** Side view at 100 kg.

Figure 4.7: The physical system with loads applied.

The displacements w.r.t. the local coordinate systems (shown in figure 4.6) are seen in figure 4.8 to 4.11. The front camera is used to capture the x- and y-displacements and the side camera is used to capture the y- and z-displacement of rod 1 and rod 4. The y-displacement of rod 1 and rod 4 is captured twice and are found to be coincident, so the y-displacements from the side camera are omitted to reduce the number of curves in figure 4.9. The displacements of rod 1 compared to rod 2 are not the same though the load is

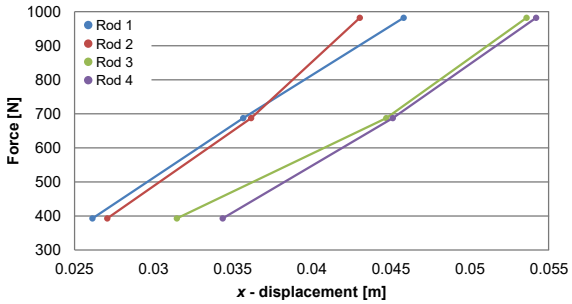

Figure 4.8: x-displacements.

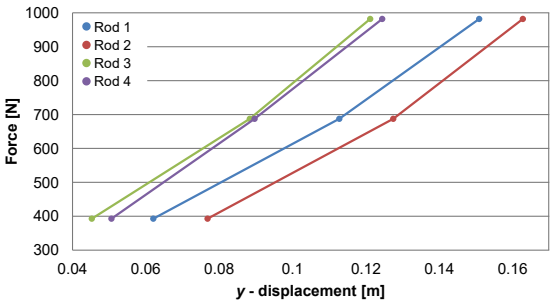

Figure 4.9: y-displacements.

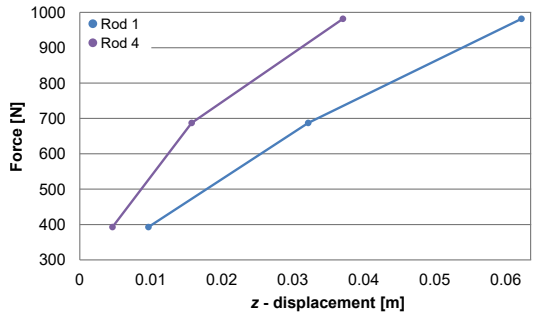

Figure 4.10: z-displacements.

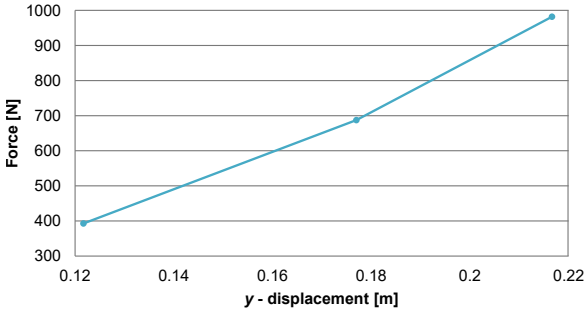

Figure 4.11: y-displacement of the knot.

applied on the vertical symmetry line. This also applies for rod 3 compared to rod 4. The vertical symmetry line is parallel and coinciding with the local y-axis of the knot in figure 4.6a. The reason for the large difference in displacements of rod 1 and 2 or 3 and 4 is due to the knots in the net. The knots make the stiffness dependent on the orientation as described back in section 1.1. Investigating the deformed configuration in figure 4.7a the left side of the net collapses more than the right side indicated by the red arrows. This shows the deformation characteristics caused by the knots.

The knots have significant influence on the behaviour of the system as explained. This influence is expected to result deviations later in the validation. The results of the physical system will be compared to the results of a identical system configured in the net-rod model in section 4.4.

4.3 Net-Rod Model

The net-rod model is configured to match the physical system described in the previous section. The stiffnesses used are determined in chapter 3 and section 4.1. The setup of the net-rod model is briefly described in section 4.3.1 and results are presented in section 4.3.2.

4.3.1 Setup

The model is configured with a net size of 7x7 knots with a knot spacing of $3.83 \cdot 10^{-2}$ m. A rod is positioned in each corner of the net and have a length of $2.54 \cdot 10^{-1}$ m, which is the distance from the top of the rod, to the top of the mounting cup as can be seen in figure 4.6b. A discretisation of ten is chosen for the rod since it showed the best overall precison in section 4.1. The model can be seen in figure 4.12. The loads are applied to the bottom center knot in the y-direction.

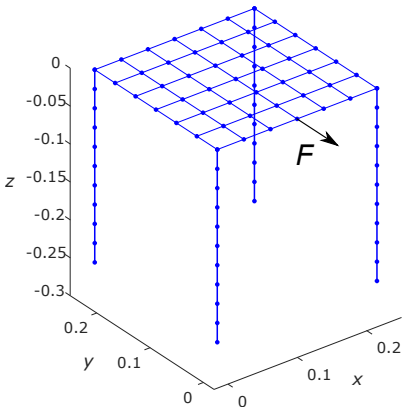

Figure 4.12: Net-rod model of the system.

4.3.2 Results

The model is applied with the same three loads as the physical system; 40, 70 and 100 kg. A plot of the deformed model can be seen in figure 4.13 and 4.14. Contrary to the physical system, symmetry is present in the model because the behaviour of the knots is not modelled. The symmetry can be observed in figure 4.15.

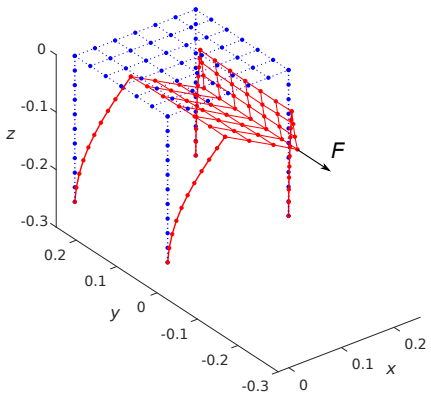

Figure 4.13: Deformed model at 40 kg.

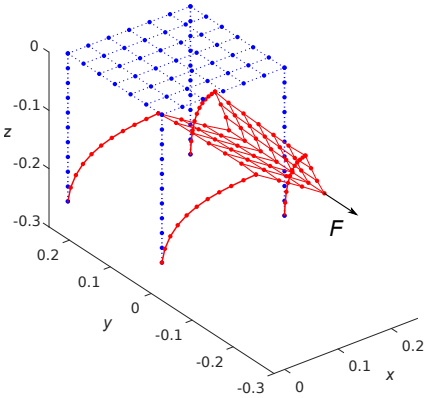

Figure 4.14: Deformed model at 100 kg.

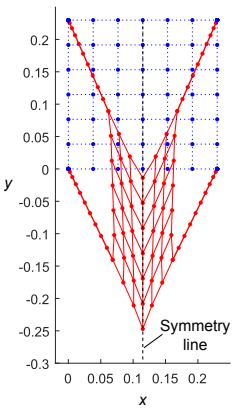

Figure 4.15: Symmetry in the model.

The displacements of the rods and the selected knot are seen in figure 4.16 to 4.19 using the local coordinates systems in figure 4.6 as reference. The displacements of rod 2 and rod 3 are not shown in the results as the displacements are the same as rod 1 and rod 4, because of symmetry. It should be noticed that the curve for rod 1 and rod 4 are coincident in figure 4.17.

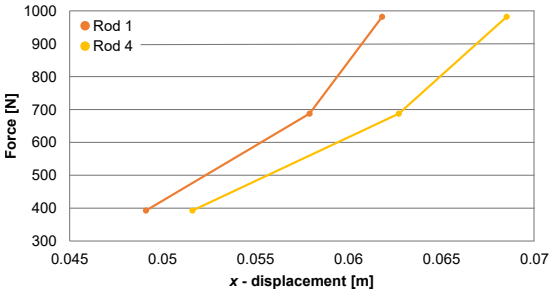

Figure 4.16: x-displacements.

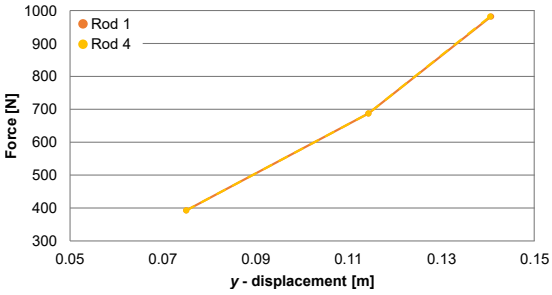

Figure 4.17: y-displacements.

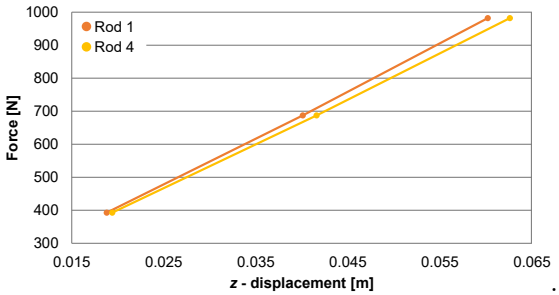

Figure 4.18: z-displacements.

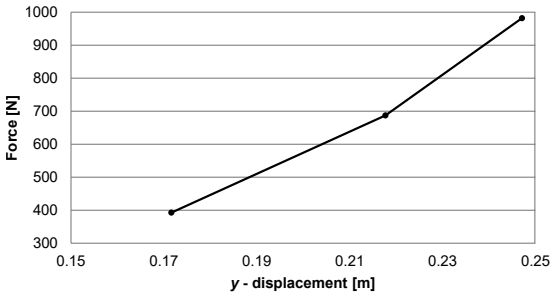

Figure 4.19: y-displacement of the knot.

4.4 Comparison

Having the results from the physical system and the net-rod model, the results can be compared in order to validate the net-rod model. The comparison of the results are shown in figure 4.20 to 4.23 where the curves label with a P is the physical system results and the curves label with M is the net-rod model results.

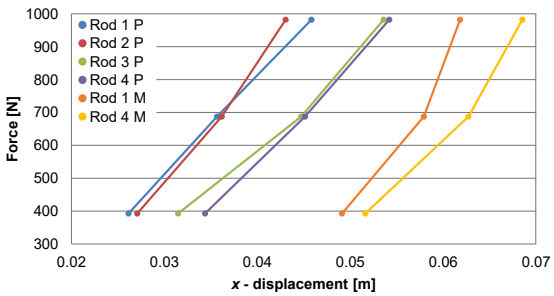

Figure 4.20: x-displacements.

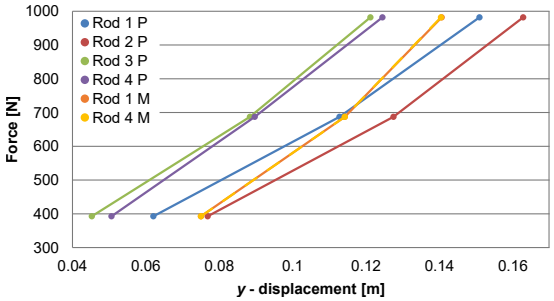

Figure 4.21: y-displacements.

In figure 4.20 there is a significant deviation. The x-displacements of the model are nearly twice the size of those of the physical system. It is suspected that it is the knots which causes the deviation. By not modelling the knots, the strings of the net have no resistance against rotation in the knots, thereby allowing the net to contract in the x-direction.

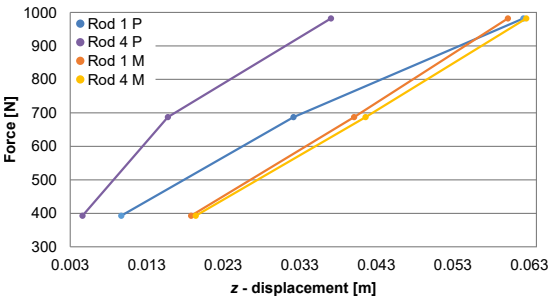

Figure 4.22: z-displacements.

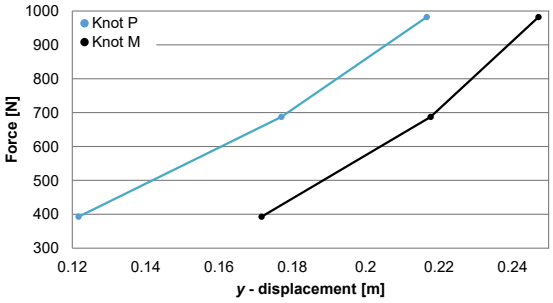

Figure 4.23: y-displacement of the knot.

In figure 4.21 the displacements are more similar. Notice that the model results are coincident. The model results are close to the results of rod 1 of the physical system. The reason for the difference in the physical results is due to the behaviour of the net, which was discussed in section 4.2.2.

In figure 4.22 the displacements of the model are a bit larger than those of the physical system. The reason the displacement of rod 4 in the physical system is smaller than rod 1 is due to the way the net was mounted. The corner knot was clamped between two washers, but by studying figure 4.7a and 4.7b it can be seen that the intended knot slips out during loading, and instead, the knot above is pulling the rod down. This results in a smaller deflection of rod 4.

The last comparison in figure 4.23 is of the knot on which the load is applied. The displacement of the model is significantly larger than the physical system. Again this is due to the knots, as was described in the discussion of the x-displacements.

From the discussion of the comparison figures it is clear that the primary source of deviation is the knots of the net. To provide a more visual comparison of the physical system and the model, the deformed net has been traced in figure 4.24.

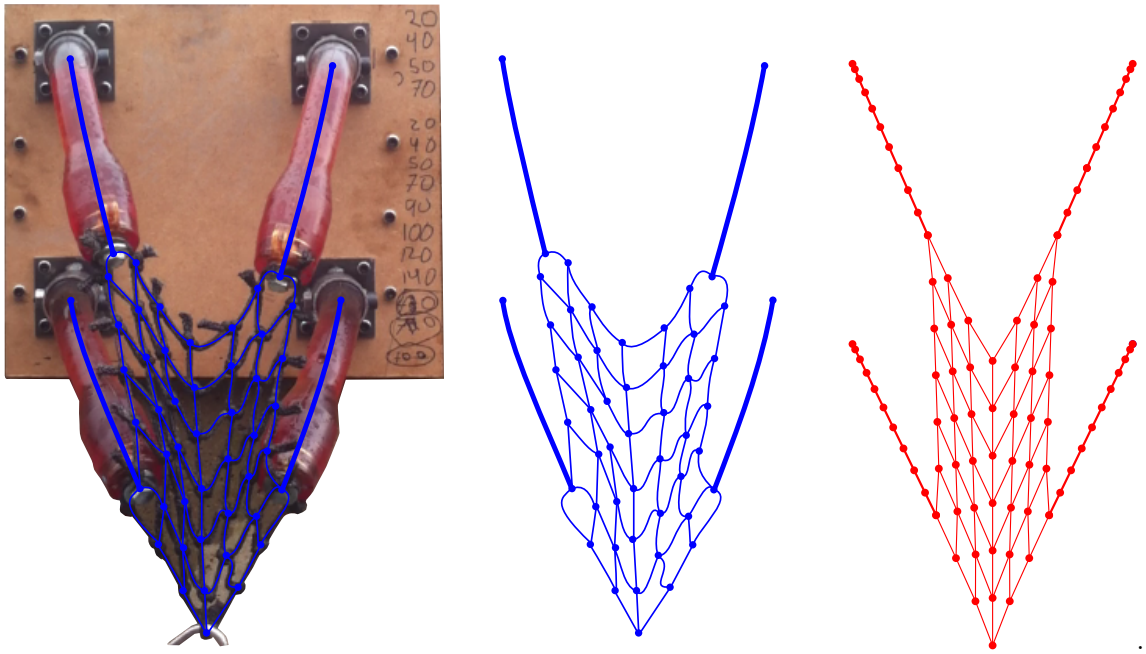

Figure 4.24: Comparison of the deformed configuration of the physical system and the model. The net is traced on the picture and copied for easier viewing of the difference in the deformations. Both deformed configurations are at 100 kg.

From the figure it is seen that there are many factors which contribute to the deviations. The rod have not been mounted directly under in the knots of the net. This necessary to apply tension to the net. Mounting the net to the rods require large pieces of the net to be wrapped around the bolts, resulting in the knot not be centered. And lastly the behaviour of the knots result in different deformations dependent on the orientation.

Taking these sources of deviation into account the overall behaviour of the model is within acceptable limits, although the are room for improvements. The validation of the model could have been improved by using another net with longer strings and smaller or different types of knots thereby reducing the influence of the knots or ideally a net made of springs could be used.

5 | Morphological Analysis

In this chapter a morphological analysis is made in order to develop a redesign of the rod. A functionality analysis of the rod is performed in section 5.1, in order to determine the basic functionalities the redesign must fulfill. The redesign is limited to focus on two of the functionalities to be improved. Solution concepts are generated in section 5.3 for the redesign and a final concept is selected in section 5.4 based on defined requirements. The selected concept forms the basis for the redesign.

5.1 Functionality Analysis

As it was described in chapter 1 the purpose of the rod is to suspend the net above a surface and reduce the loads in the net by allowing large deformations of the rod. The overall functionality of the rod can be broken into four underlying functionalities, which are marked in figure 5.1. The underlying functionalities are described in the following.

The first functionality of the rod is fixation of the net. The net is fixated on the rod using a M10 thread in the top of the rod. With a large washer and a bolt the net is clamped between the washer and the top surface of the rod. The two interfaces used are the M10 thread and the top surface of the rod.

The second functionality is allowance of large deflections. The large deflection is possible due to the flexibility of the rod which is achieved by the reduced diameter of the middle of the rod and by using a elastomer as material.

The third functionality is tensioning of the net. Even though the rod is flexible it is still stiff enough to keep the net stretched out.

The fourth functionality is mounting of the rod. The rod is mounted to a surface using a mounting cup and a locking pin. Horisontal movement is restricted by the cup while the locking pin restricts vertical movement related to figure 5.1. The cup is then bolted to the surface. The interfaces are the hole in the bottom of the rod and the surface in contact with the cup.

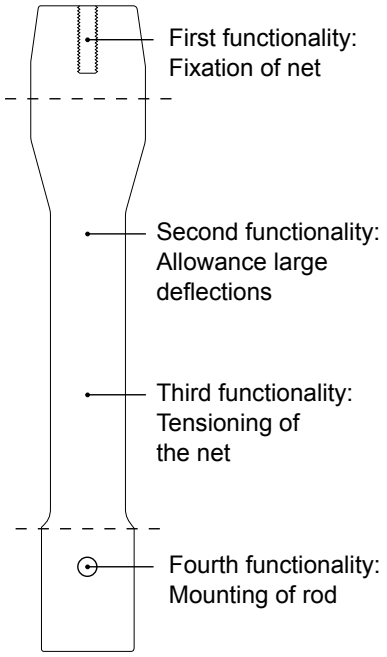

Figure 5.1: The rod with the function interfaces marked.

5.2 Limitation

In last section the functionality analysis explained the four functionalities that enables the rod to fulfill its purpose. A redesign of the rod requires that all functionalities remain fulfilled, but the way they are achieved is arbitrary. This project limits the redesign and morphology to focus on the middle section of the rod (enclosed by the dashed lines in figure 5.1), which governs two functionalities of the rod: The second and third functionality, which is allowance of large deflections and tensioning of the net.

5.3 Concept Search

This section seeks to find ways of improving the main body of the rod and its functionalities. But the two functionalities counteracts each other. In order to allow large deflection the rod needs to be flexible, but on the other hand the rod needs to be stiff to stretch out the net without deflecting significantly. The redesign shall be designed such that both functionalities are achieved without compromising each other.

This can be achieved by introducing a non-linear stiffness response to the rod. During small deflections of the rod, the stiffness of the rod should be high to keep the net in tension. But if the rod is subjected to a large deflection the stiffness should be small in order to reduce the energy absorbed by the system. A force-displacement curve of this behaviour is seen in figure 5.2. This is the behavior of which a concept is sought.

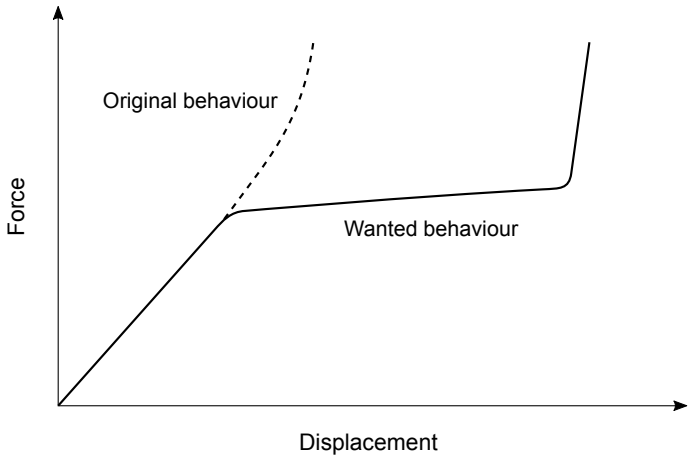

Figure 5.2: Illustration of the sought stiffness behaviour of the rod.

5.3.1 Volume of Concepts

With the wanted behaviour of the rod defined a volume of concepts is generated through brainstorming and sketching. This resulted in eight different concepts which are seen in figure 5.3 to 5.7. In the following the concepts are presented and the working principle explained.

Concept 1 The concept is seen in figure 5.3 marked 1. Instead of using a solid cross section this concept suggest a tubular cross section. By having all the material far from the center the moment of inertia is roughly kept ensuring rigidity. But at large deflections, the hollow interior allows the cross section to ovalise reducing the moment of inertia greatly, making the rod buckle.

Concept 2 The concept is seen in figure 5.3 marked 2. Instead of using a circular cross section this concept suggests a cross shaped cross section. When bending in the direction marked in figure 5.3, the cross section will at some point collapse and the rod will buckle. The stiffness is directional dependent having a larger bending stiffness along the cross and lower in between.

Concept 3 The concept is seen in figure 5.3 marked 3. This concept is inspired by a measuring tape. A thin curved rod (like a measuring tape) is surrounded by a thin flexible wall. The thin curved rod is stiff until the bending flattens the curvature of the rod and it buckles. The thin curved rod needs to be able to rotate inside the flexible wall to be aligned with the bending direction.

Concept 4 The concept is seen in figure 5.3 marked 4. The four walls of the concept is joined in "hinges" to allow rotation. The deformation of the cross section is controlled by springs inside the walls. This way the springs determine at which load the cross section should collapse and the rod should buckle.

Concept 5 The concept is seen in figure 5.4. A section of the rod is exchanged with two springs. One with high stiffness and one with low stiffness. At a certain load level the the stiffest spring disengages thereby greatly reducing the stiffness. When the load is removed the less stiff spring brings the rod back to the initial position and reengages the other spring.

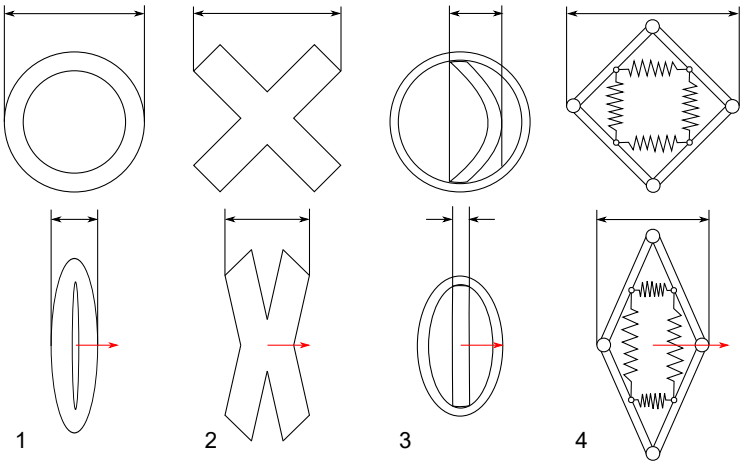

Figure 5.3: Concept 1 to 4 shown before and after deformation. The concepts use different collapsible cross sections in order to manipulate the stiffness characteristic of the rod. The red arrow shows the direction of the load.

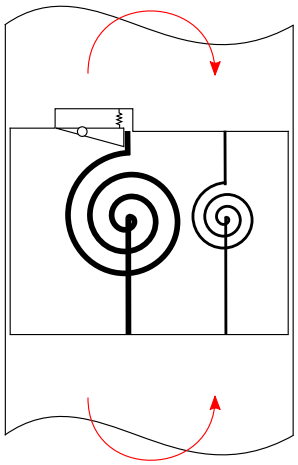

Figure 5.4: Concept 5 is a two stage spring system. The concept is illustrated using two torision springs in a two dimensional case.

Concept 6 The concept is seen in figure 5.5. This concept utilises magnets to achieve the non-linear stiffness behavior. The rod is separated into two parts which each has a strong magnet embedded. This keeps the rod together as long as the magnetic force is larger than the deflecting load. When the magnetic force is exceeded the stiffness is lost and a spring or a strong rubber keeps the two parts connected and pulls the top back when the load is released.

Concept 7 The concept is seen in figure 5.6. This concept also uses a cross shaped cross section like concept 2, but only at a small part of the rod. The rod is divided in the middle

where only the center of the cross is connected. The idea is that when subjected to a large load the crosses of each end will slide past each other resulting in a loss of stiffness.

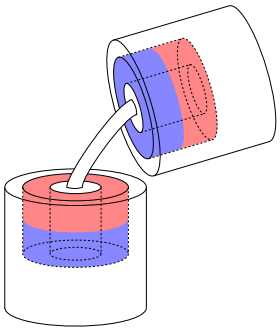

Figure 5.5: Concept 6 uses a magnetic connection.

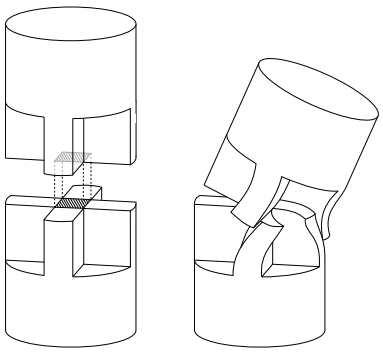

Figure 5.6: Concept 7. The two parts are connected at the marked area.

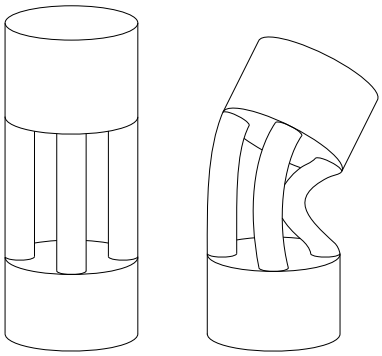

Figure 5.7: Concept 8 exhanges the solid cross section with muliple smaller rods.

Concept 8 The concept is seen in figure 5.7. A section of the rod is exchanged with multiple smaller rods. This is supposed to make the area more prone to buckling.

5.4 Selection of Concept

The volume of concepts has been presented, but before a concept can be selected for the redesign, the concepts are evaluated against defined requirements and wants. The arguments for the selection are presented afterwards.

5.4.1 Design Requirements and Wants

The design requirements are demands that the concept must fulfill, while the design wants are not necessary, but if fulfilled adds value to the concept. The design requirements and wants are:

Requirements

- **Geometry:** Only the area between the two dashed lines in figure 5.1 can be manipulated by the concepts. The diameter cannot exceed the diameter of bottom of the rod.
- **Material:** The material used for the rod cannot be changed, but inserts or other added components can be made of other materials.
- **Manufacturing:** The rod has to be cast, but not necessarily in one piece.

Wants

- **Rotational Symmetry:** By having rotational symmetry in the design, it is ensured that the behaviour is the same in all directions.
- **Same Cost:** An increase in the cost of producing a rod is not wanted.
- **Hidden Mechanism:** Hiding the mechanism which allows the non-linear behavior of the rod, will make it harder to be copied.

5.4.2 Argumentation for Choice of Concept

The concept which fulfills the requirements and wants best is concept 1, the tubular cross section. The reasoning behind this choice is presented by describing why the rest of the concepts were excluded.

Concept 2 This concept was excluded since it does not have rotational symmetry and no other advantages over concept 1.

Concept 3 It is required by the concept that the internal beam can rotate and always have the correct orientation in order to have the desired function. It is doubtful that it is possible to be effectively realised, which is why it is excluded.

Concept 4 This concept is excluded due to being overly complicated. It has the same properties as concept 2, but are achieved in a less effective way.

Concept 5 The design task required to translate the two dimensional concept into three dimensions including rotational symmetry is assessed to be unjustifiable. The eventual mechanism would be to complex and expensive to be competitive. Due to this the concept is excluded.

Concept 6 This concept can fulfill most of the requirements and wants but it looses ground in the want for same cost. The custom magnets would add to the cost of the concept, which is why the concept is excluded.

Concept 7 This concept is excluded since the buckling mechanism of this concept is unpredictable and does not have rotational symmetry.

Concept 8 This concept is similar to concept 1, with the exception being the distribution of material. But by using a number of smaller rods, instead of a solid ring, the rotational symmetry is lost and concept 1 is superior.

5.4.3 Final concept

A sketch of the final concept can be seen in figure 5.8 where a section view of the rod is shown before a load is applied and when the rod has buckled. The next step is to determine the dimensions for the redesign which is done in chapter 6.

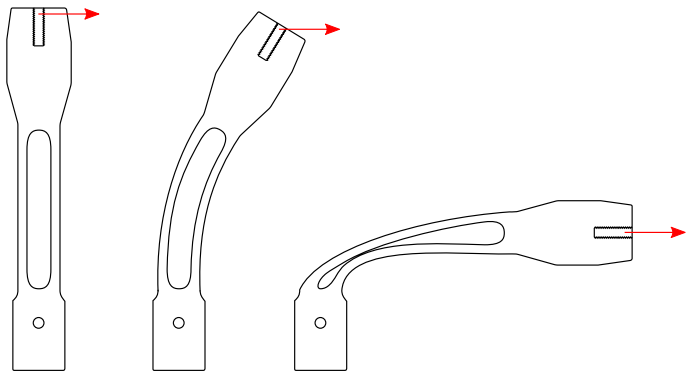

Figure 5.8: A sketch of the section view of the selected concept during deflection.

6 Redesign of the Rod

In this chapter the concept selected in section 5.4 is developed into a redesign. The principle of the concept is verified with a small experiment in section 6.1. The outer geometry of the redesign and the force at which the redesign collapses are determined in section 6.2. A model is established in ANSYS in section 6.3 and the thickness of the hollow part of the rod is adjusted to find the desired behaviour in section 6.4. The final dimensions of the redesign are presented in section 6.6.

6.1 The Brazier Effect

The concept utilises the ovalisation of the cross section to reduced the moment of inertia and initiate buckling. Ovalisation due to bending has been studied by L. G. Brazier and is called the Brazier effect.

A small experiment is performed to illustrate the Brazier effect, which is seen in figure 6.1. The bottom of a tube is fixed and a load is applied using a string attached to the top of the tube. A bottle is attached to the string and a constant flow of water is poured in. The deflection is recorded by a camera. The deflection as function of time (force) is seen

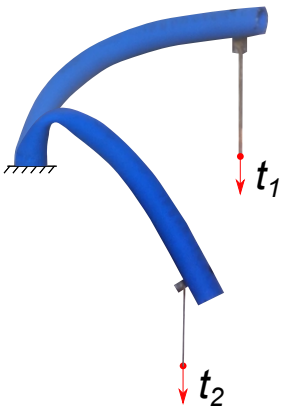

Figure 6.1: Before and after buckling.

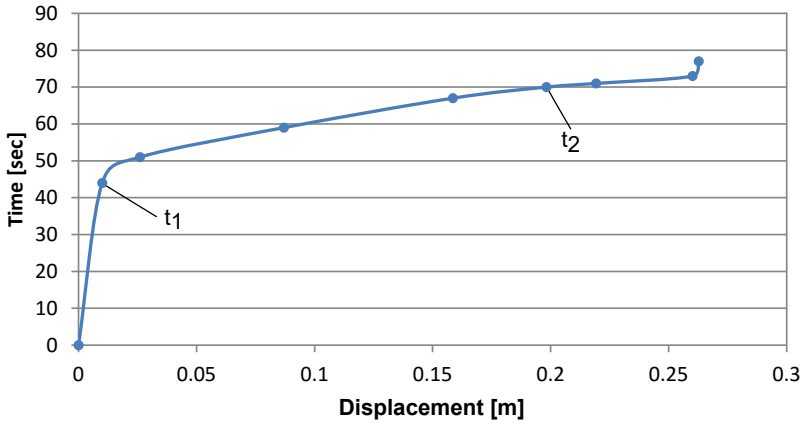

Figure 6.2: Results from the experiment.

in figure 6.2. The response of the tube in figure 6.2 is similar to the idealised behaviour in figure 5.2. The first linear part show the bending stiffness. The middle part, where the slope is decreasing, show the event of buckling i.e. reduced bending stiffness. In the last part of the curve the tube has deflected 180° and is now in tension. The slope of the last part is approaching the tension stiffness, which is why the slope increases.

The Brazier effect is explained by considering the bending stresses and the associated components. As the tube is bend, longitudinal compressive and tensile stresses are generated. Both longitudinal stresses have a component directed toward the center of the tube which tends to flatten the cross section as seen in figure 6.3 (Brøndsted and Nijssen, 2013).

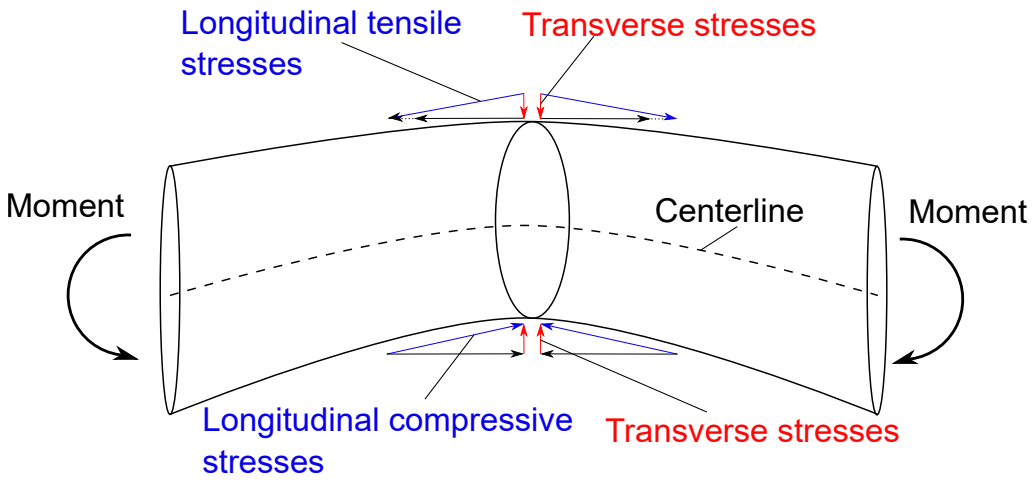

Figure 6.3: Transverse and longitudinal stresses of bend tube.

It has been shown that the concept utilises the Brazier effect to obtain non-linear stiffness behaviour and that the concept works as intended.

6.2 Design Considerations

The starting point for the redesign is to have the same bending stiffness as the original design. As material is removed from the inside of the mid section, the outer diameter has to be increased, in order to get equivalent stiffness. The outer diameter set to be equal to the bottom part i.e Ø45 as seen in figure 6.4. Equating the moment of inertia for the original design and redesign with a outer diameter of Ø45 and solving w.r.t. thickness yields a thickness of 3.66 mm. A thickness of 3.5 mm is chosen to be the starting point for a parameter study. The thickness is also chosen to be uniform through out the rod mid section of the rod.

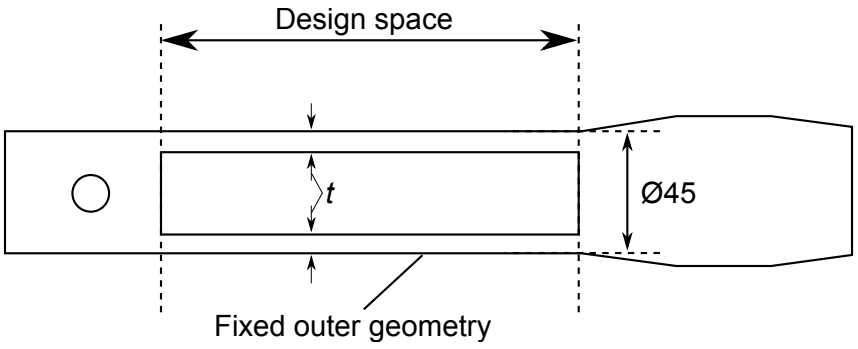

Figure 6.4: The geometry of the redesign.

The redesign needs to provide sufficient tension to the net and to allow large deflections. The buckling has to be initiated at the right time to satisfy both functionalities. It is assessed that the redesign must provide a minimal tension force of 90 N to the net. This requires the buckling to be initiated after 90 N, including a margin of safety.

6.3 Finite Element Modelling

A model of the redesign is established in ANSYS 17.0. The redesign has been studied with a shell and a solid model. The solid will be presented in this section and the shell model is documented in appendix G.

6.3.1 Model Geometry

The rod geometry and boundary conditions are seen in figure 6.5. The rod is fixed where the cup ends and the applied force is distributed to the nodes at the end as seen in figure 6.5a.

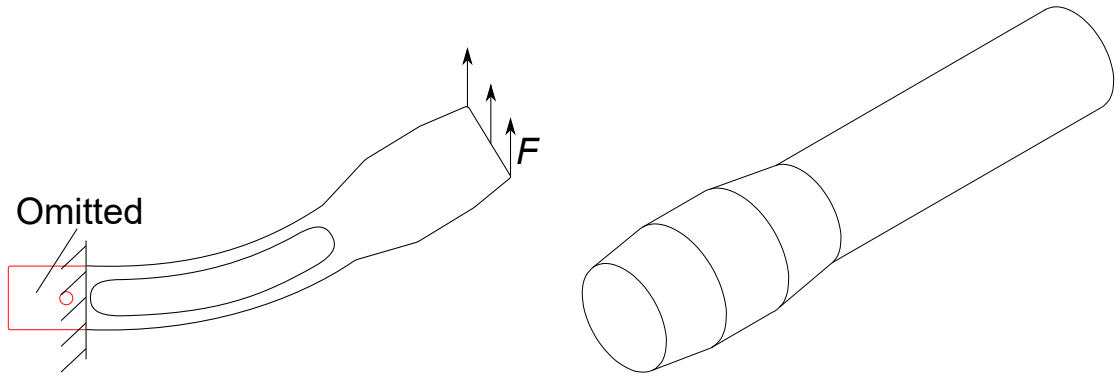

(a) The rod is fixed and the force is distributed to the nodes at the end.

(b) The geometry of the rod.

Figure 6.5: Solid model with applied forces and boundary conditions.

Material Properties

Linear material properties are used in the model. The modulus of elasticity is based on the bending stiffness determined in section 3.3.2. Using the same approach as in section 3.2.3 the modulus of elasticity is derived for a non-prismatic beam. The bending stiffness, assuming small displacements, for a prismatic beam is:

$$k_\theta = \frac{3\,E\,I}{l} \;\rightarrow\; E = \frac{k_\theta\,l}{3\,I} \tag{6.1}$$

The moment of inertia is a function of the length. Piecewise integration along the length of the beam yields:

$$\frac{l_i}{I_i(x)} = \frac{l_i}{\frac{\pi r_i(x)^4}{4}} = \int_{l_{i-1}}^{l_i} \frac{4}{\pi r_i(x)^4}\,dx \tag{6.2}$$

Using equation (6.2) in equation (6.1) and summing each part of the rod gives:

$$E = \frac{4\;k_b}{3\;\pi} \sum_{i=1}^{6} \int_{l_{i-1}}^{l_i} \frac{1}{r_i(x)^4}\,dx \tag{6.3}$$

Using equation 6.3 the modulus of elasticity is calculated to $E = 53$ MPa. The Poissons ratio has not been experimentally determined and is therefore arbitrarily chosen to $\nu = 0.3$. $\nu = 0.21$ is also tested and no difference is observed in the non-linear solution. A model, with the material properties presented, is compared to the results from the bending experiment in section 3.3.2. The model is seen in figure 6.6 and results are seen in figure 6.7. The ANSYS model with linear material properties is in good agreement with the experiment.

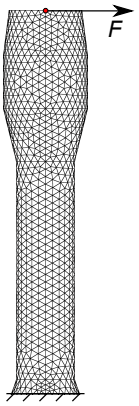

Figure 6.6: Solid model of original design.

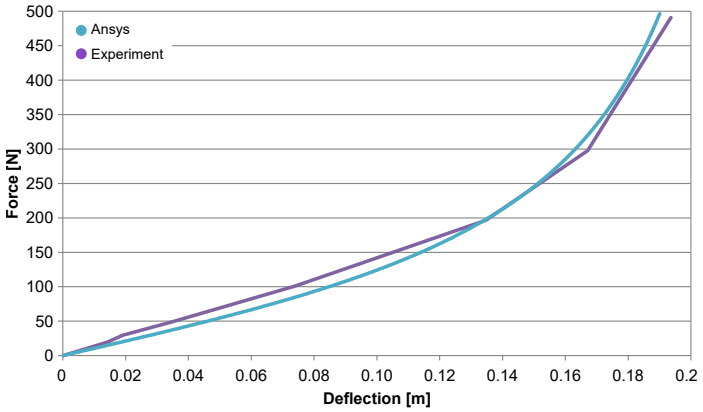

Figure 6.7: The Solid model is compared with the bending experiment.

6.3.2 Elements

The solid model meshed can be seen in figure 6.8. The element type used is the Solid186, 10 node tetrahedral. A convergence study with a global element size have been made and at an elements size of 0.01 m the model is considered appropriate. The meshed model with a global element size of 0.01 m is seen in figure 6.8.

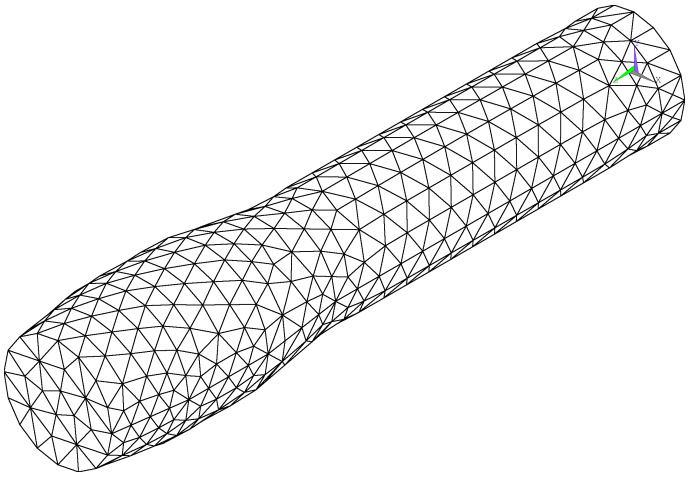

Figure 6.8: The meshed solid model with a global element size of 0.01 m.

The key options used in this model are:

KEYOPT(2) Full integration.

KEYOPT(3) Homogeneous Structural Solid (default) – nonlayered

KEYOPT(6) Use pure displacement formulation (default)

KEYOPT(8) Store data for bottom of bottom layer and top of top layer

Full integration is used to get a more accurate results than reduced integration. The rest are at default.

6.3.3 Solution Method

The functionality of the redesign is based on buckling. Buckling occurs when the structure converts stored membrane energy into bending energy without any change in applied load. This problem can approach using two methods: Linear buckling analysis or geometric non-linear analysis. The difference between these two analyses is, whether the displacement stiffness matrix $[K_L]$ is included or not. In a linear buckling analysis the displacements are assumed small and the displacement stiffness matrix is neglected. This assumption is violated for this design and therefore a geometric non-linear analysis is used.

The arc-length solver is used to generate the equilibrium path of the redesign. This solver can handle problems where limit and turning points are present as is the case for this redesign. The arc-length solver iteratively determines equilibrium points within a circular arc where both forces and displacements are incremented Cook et al. (2002).

6.4 Parameter Study of the Thickness

In section 6.2 the general redesign was defined, but to obtain the wanted behaviour the design, a parameter study of the thickness is performed.

Unfortunately due to a mistake in the data processing of the force-displacement curves, the thickness was initially determined based on wrong curves. This meant the prototype, described in chapter 8, is based on the wrong thickness. The prototype is based on curves from the shell model where symmetry has been applied. The symmetry condition was not included in the data treatment and therefore the forces used to generate the equilibriums curve are halved. This had not been observed before the prototype was made.

The shell model with wrong and corrected curves is presented and lastly the results from the solid model will be presented.

6.4.1 Shell Model

First the design process with the wrong curves is shown. Force-displacement curves for three different thicknesses are determined with the shell model as seen in figure 6.9. All analyses were carried out to the first limit point i.e. the event of buckling and some a bit beyond. As can be seen in the figures 6.9a and 6.9b the equilibrium curves stop at different displacement. This is because of divergence at that time. The results without considering symmetry are seen in figure 6.9a and with symmetry in figure 6.9b. The force in curves in figure 6.9b are multiplied by two.

The force required to tension the net is the solid red line at $F_t = 90$ N. The thicknesses investigated are: 4, 5 and 6 mm. From figure 6.9a the redesign with a thickness 6 mm meets the requirement of buckling after 90 N. The prototype which has been manufactured is based on this choice. If the prototype has been designed with the corrected curve, figure 6.9b, the thickness should have been 5 mm. The safety margin is used to compensate for simplifications and assumptions in the modelling.

The arc-length solver options for the models are: 2000 substeps, maximum arc length radius multiplier is equal to three, minimum arc length radius multiplier is equal to $1 \cdot 10^{-8}$ and 400 equilibrium iterations are defined for each substep. Increasing the number of substeps provides a more accurate and stable analysis, but the computation time increases. Allowing more equilibrium iterations helps the solver to converge but increases the compu-

tational time too. It is believed that if the number of substeps and equilibriums iterations are increased, the model would have converged.

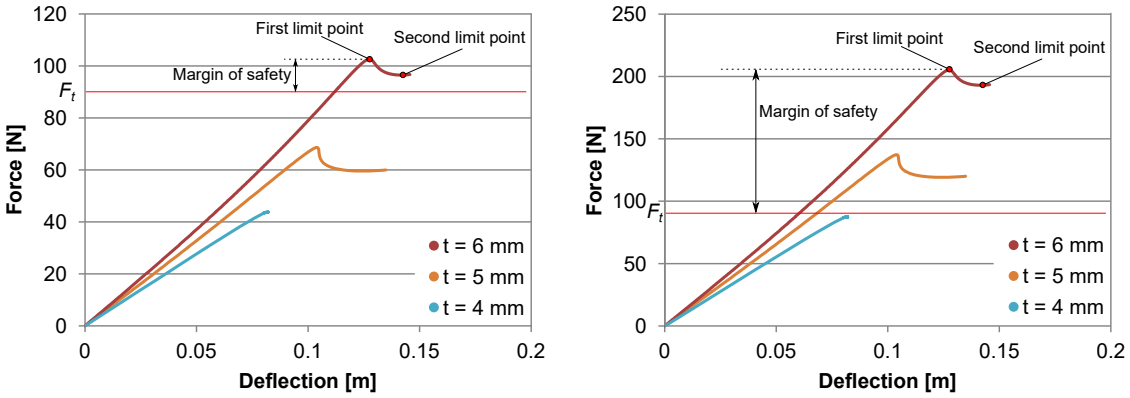

(a) Wrong curves, symmetry not included. **(b)** Corrected curves, symmetry included.

Figure 6.9: Equilibrium curves from the shell model.

6.4.2 Solid Model

The results from the parameter study with the solid model are seen in figure 6.10. This model is much more stable than the shell model and therefore a more comprehensive parameter study is performed. The parameter study showed that a thickness of 4 mm could be used with a low margin of safety. A design thickness of 5 mm is assessed to be appropriate with a larger margin of safety to include manufacturing defects and simplifications during the design process.

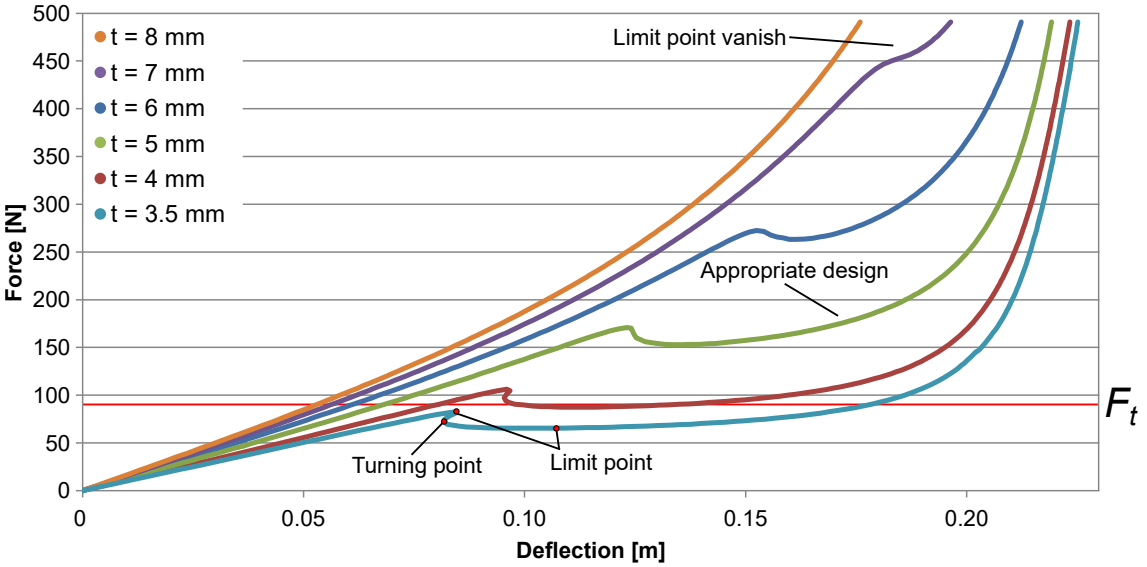

Figure 6.10: Equilibrium curves for 6 thicknesses.

For small thicknesses the limit point occurs relative early on the equilibrium curves and the distance between the first and second limit point is relatively large. A turning point is seen for a thickness of 3.5 and 4 mm. For a thickness of 3.5 and 4 mm the rod will snap no matter if forces or displacements are applied because a limit and turning point is present on the equilibrium curve. As the thickness increases the limit point occur later, the turning point disappears and the distance between the first and second limit is reduced. For a

thickness of 7 mm the limit point vanish and snapping does not occur as seen in figure 6.10.

For a thickness of 7 mm the rod will ovalise, but not buckle as in figure 5.2. For the largest thickness, 8 mm, the rod behaves like the original design for an applied load below 500 N.

The arc-length solver is used with 5000 substeps, default maximum and minimum arc length radius multipliers which is 25 and $1 \cdot 10^{-3}$.

6.4.3 Comparison

The shell and solid model are compared for a thickness of 5 and 6 mm. The equilibrium curves for both models are seen in figure 6.11. The shell model yields conservative designs compared to solid model. The shell elements are found less stable and reliable than solid

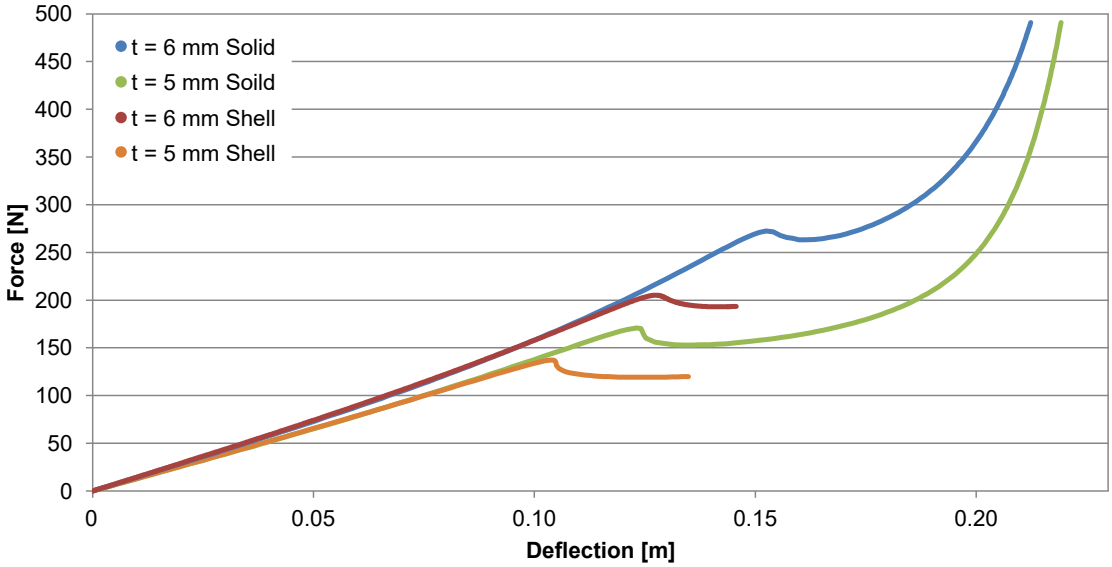

Figure 6.11: Comparison of shell and solid model.

elements. The shell elements are sensitive to problems concerning large displacements as they have locking problems such as shear and membrane locking (Cook et al., 2002). Element warnings are detected as the shell model is meshed, due to the radius to thickness ratio being above recommend value from ANSYS (ANSYS, 2013).

6.5 Imperfections

The model analysed has a perfect structure i.e. no imperfections. In the real world products have some sort of imperfections w.r.t. geometry or material. Geometry imperfection can be due to casting faults or surface roughness from the mold. These imperfections will be present in the prototype, but the size and shape of these can not be determined. The impact on the design is investigated.

When an imperfection is introduced to a structure the membrane and bending deformation becomes increasingly coupled Cook et al. (2002). This means the membrane energy will not be immediately converted to bending energy i.e the buckling will not happen instantly.

The imperfections are modelled with the mode shape from a linear buckling analysis.

The geometry is updated with the mode shape as seen in figure 6.12a. The equilibrium paths with imperfections can be seen in figure 6.13. The mode shape has a sinus shape and

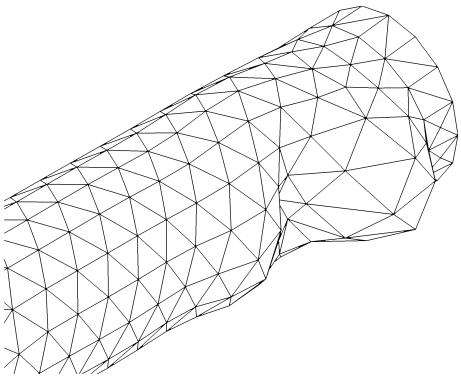

(a) Mode shape that is updated in the geometry.

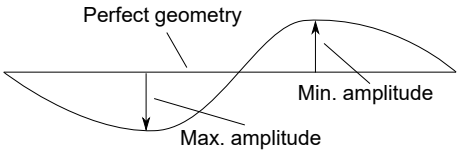

(b) Size of the imperfection referred to table 6.1.

Figure 6.12

this shape is scaled. The scaling is seen in table 6.1. The behaviour of the redesign with five different imperfections is seen in figure 6.13. The response of the redesign changes as

Table 6.1: Size of imperfections for the updated geometry where values are referred to figure 6.12b.

Imperfection	Max. amplitude [m]	Min. amplitude [m]
1	$4.65 \cdot 10^{-4}$	$3.9 \cdot 10^{-4}$
2	$9.3 \cdot 10^{-4}$	$7.8 \cdot 10^{-4}$
3	$2.8 \cdot 10^{-3}$	$2.74 \cdot 10^{-3}$
4	$4.65 \cdot 10^{-3}$	$3.9 \cdot 10^{-3}$

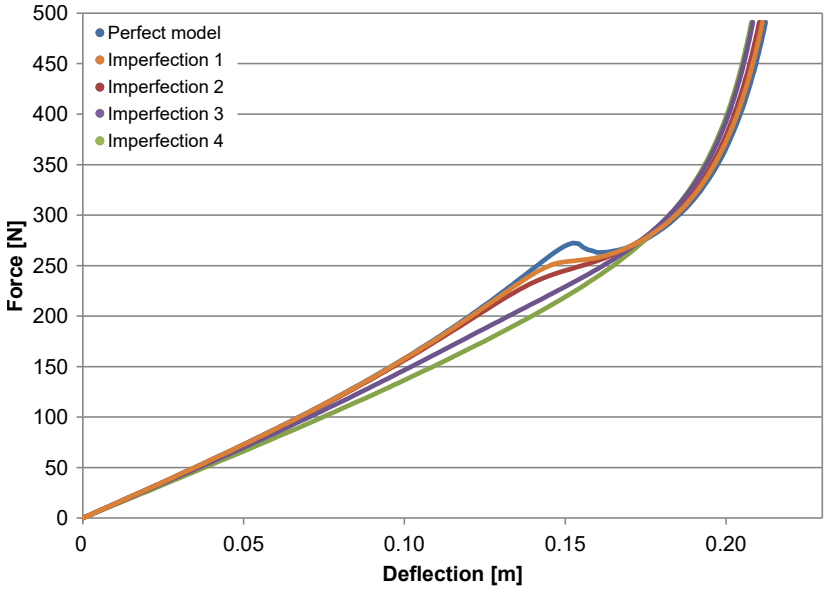

Figure 6.13: The impact of imperfections in the redesign.

the imperfection are introduced. The curves flatten as the imperfection is increased. This is because the membrane and bending deformation becomes more coupled. As seen the design is very sensitive to imperfections.

6.6 Final Dimensions of the Redesign

The dimensions of the final redesign can be seen in figure 6.14. The top and bottom of the rod are not changed, so the redesign can be directly implemented in the existing system.

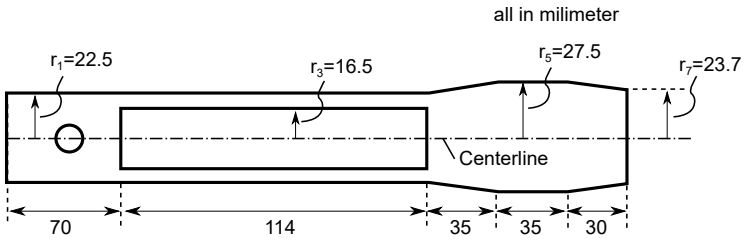

Figure 6.14: Geometry of the redesign.

The original design is compared to the redesign in figure **??**. The equilibrium curves are from the solid model. With a thickness of 5 mm the buckling is initiated as intended. The force applied to the rod is reduced by a factor of two, when the redesign has buckled as indicated by the dashed line. The deflections at the buckling load of 171 N is seen in figure 6.15.

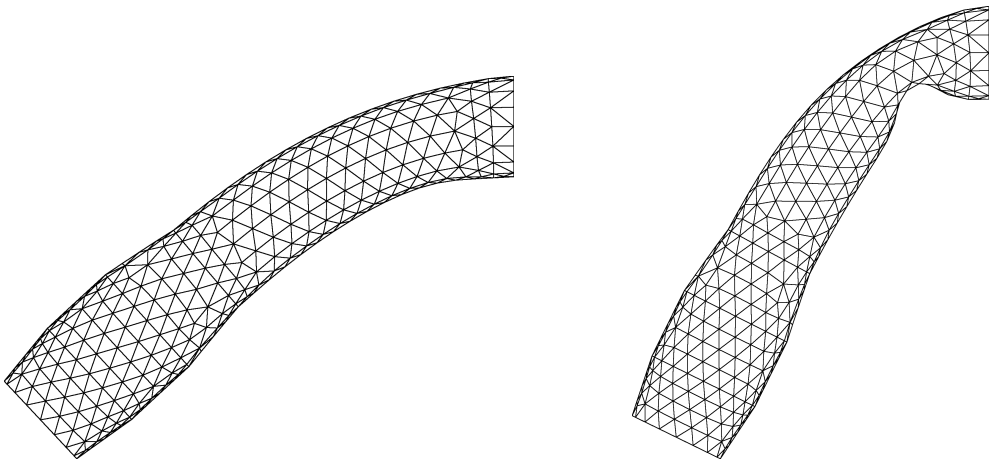

(a) Before buckling **(b)** After buckling.

Figure 6.15: The deformed geometry is shown before the first limit point is reached and past the limit point.

A linear buckling analysis have been made to show that it is unsuitable for this kind of problem as discussed in section 6.3.3. The linear analysis predicted the critical buckling load to $P_{cr} = 378.1$ N which is 121% above the limit point from a geometric non-linear analysis.

Lastly the stresses in the redesign are investigated. The Von Mises stresses divided with the tensile strength can be seen in figure 6.16. A force of 491 N is applied on the redesign. The stresses will not be investigated further but are presented to inform that certain points should be given attention before finalising the redesign. The points that need attention are shown in figure 6.16. The lowest factor of safety is located where the rod is in the compression which is point 1. The side, point 2, of the rod should be investigated as the Von Mises stress is above 1 w.r.t. factor of safety. The same applies for point 3.

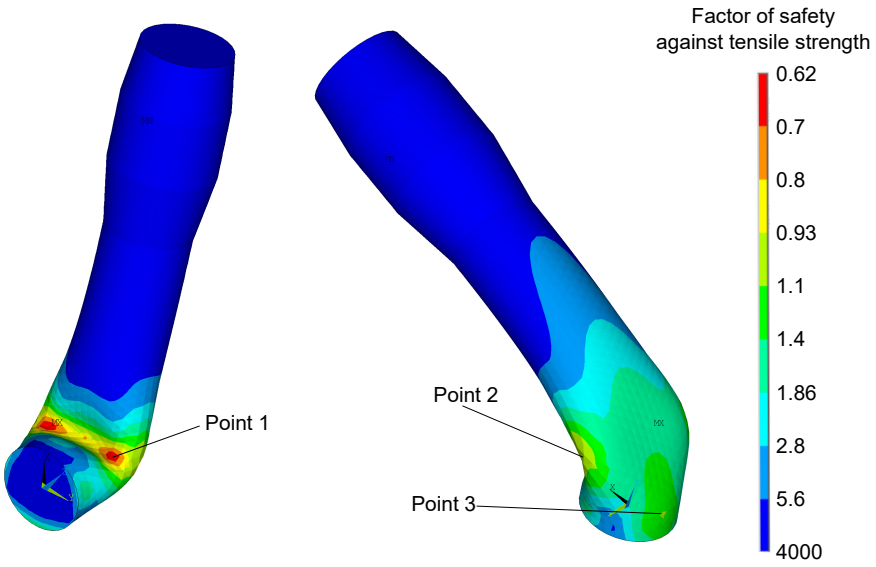

Figure 6.16: Von Mises stresses in the redesign.

7 Benchmark of the Redesign

In this chapter the redesign of the rod is benchmarked against the original design in the net-rod model. First the benchmark case is presented in section 7.1, before the implementation of the redesign in the net-rod model is documented in section 7.2. The results of the benchmark is presented in section 7.3.

7.1 Benchmark Case

The case for the benchmark is chosen to reflect a possible load scenario and to show the effect of the redesign on a system. The benchmark case is illustrated in figure 7.1. The case is studied for two configurations; applied force and prescribed displacement. A load of 1200 N is applied to the net in the y-direction. The displacement is prescribed in the same direction with a magnitude of 0.36 m. The magnitudes of the load and prescribed displacement are chosen, so they are sufficiently large to make the redesigned rods buckle. If the force or displacement were made smaller the redesign and the original design would yield nearly identical results.

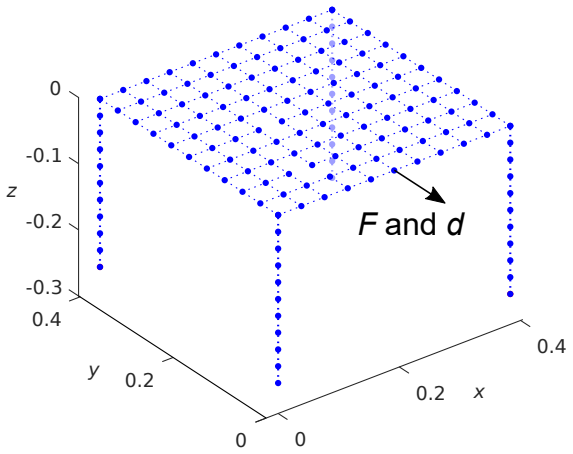

Figure 7.1: The case for the benchmark.

7.2 Implementation of the Redesign in the Net-Rod Model

For the implementation of the redesign in the net-rod model a function called *CustomRodStiffness* is added. This function allows the user to define different bending stiffnesses for each segment of a rod with a fixed discretisation of ten. To activate the function the value *CustomRod* must be equal to one in the input section in *NetRodModel*. The redesign is modelled by setting all the stiffness of all the segments to the default value, except the stiffness of the second segment. The stiffness of the second segment is chosen to model the

non-linear behaviour of the buckling.

The intension was to make the bending stiffness of the second segment dependent on the angle of deflection. The stiffness should drop significantly at a certain angle of deflection, causing the rod to buckle. But it was not possible to do this. When the stiffness was made dependent on the design variables (the displacements), the solver became unstable and the solution useless. The reason why the solver could not handle the non-linear stiffnesses is believed to be due to the calculation of the elastic energy. The elastic energy was calculated with the assumption of linear elasticity and was not updated handle the non-linear stiffness. This meant the elastic energy was calculated for a linear system although it was very non-linear. The non-linear stiffness behaviour modelled in section 4.1.1 did not cause the instability, because it was close to linear. The error was found to late in the project to fix it, but it was still possible to perform the benchmark under given assumptions.

Instead of having the stiffness as a function of the angle of deflection it is made a function of the applied force. This unfortunately limits the net-rod model of the redesign to only work on a single rod loaded or displaced in the x- and/or y-direction. Setting the bending stiffness of the second segment to drop to 45 Nm at forces above 170 N, the force-deflection curve of the net-rod model is nearly coincident with the force-deflection curve from the ANSYS simulation of the chosen redesign. The force-displacement curves are seen in 7.2 and a plot of the deflection at different loads are seen in figure 7.3.

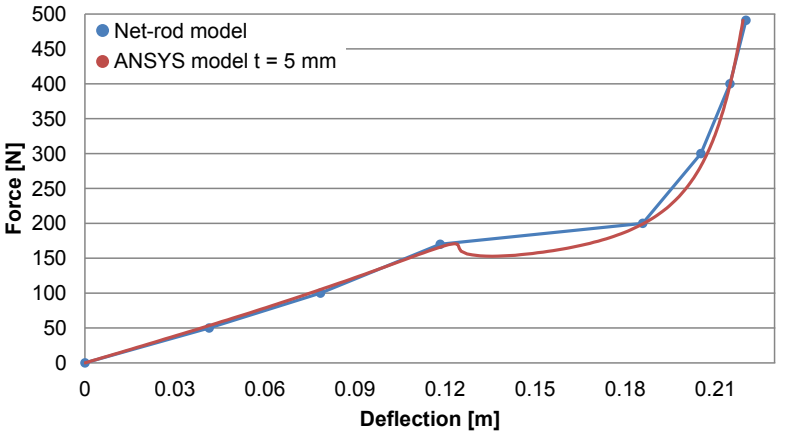

Figure 7.2: The fitted deflection of the net-rod model to the ANSYS simulation.

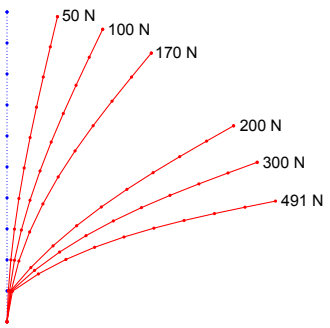

Figure 7.3: Deflection of the fitted rod model.

As stated in section 7.1 the load used in the benchmark is large enough to make the rods buckle. This means that the stiffness of the second segment of the all the rods in the system drops to 45 Nm. Because of this it is not necessary to model the stiffness non-linear. The stiffness of the second segment is just set to 45 Nm from the beginning. This way it is possible to perform the benchmark.

7.3 Benchmark Results

The results from the benchmarks are presented in the following. To measure the improvement of the redesign the elastic energy of the two systems are compared. The load benchmark of the original rod system and the redesigned rod system are seen in figure 7.4 and 7.5 respectively. Comparing the two plots it is clearly seen that the system with the redesigned rod has the largest deflection. The prescribed displacement benchmark of the original rod system and the redesigned rod system are seen in figure 7.6 and 7.7 respectively.

Table 7.1: The energy in the systems in the benchmarks.

Benchmark	Variable	Redesign	Original design
Load	Pi [J]	-351	-286
	U [J]	79	94
	W [J]	430	380
Displacement	Pi [J]	81	167
	U [J]	81	167
	W [J]	0	0

The energy of the models are collected in table 7.1. From the load benchmark the work done by the force is largest for the redesign because it has the largest deformation. The elastic energy is lowest for the redesign, which means the system generally is loaded less than the original design. In the prescribed displacement benchmark it is only the elastic energy which is present since no load is applied. It is seen that the redesign system only obtain half the elastic energy compared to the original design. This shows the advantage the redesign of the rod in a net-rod system.

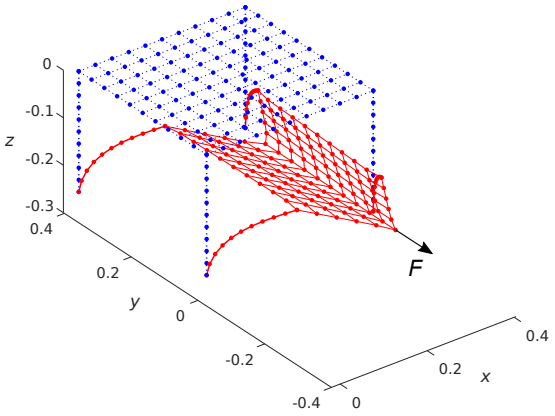

Figure 7.4: Benchmark of the system with the original rod design with applied load.

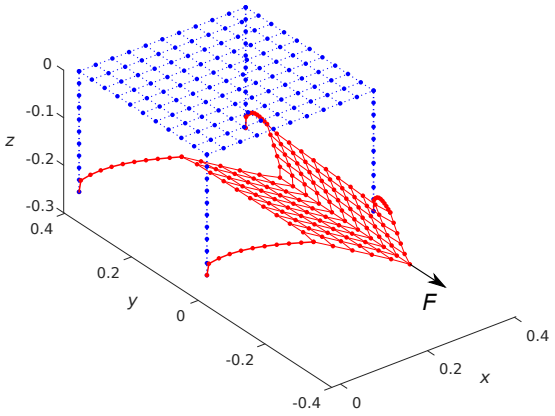

Figure 7.5: Benchmark of the system with the redesigned rod with applied load.

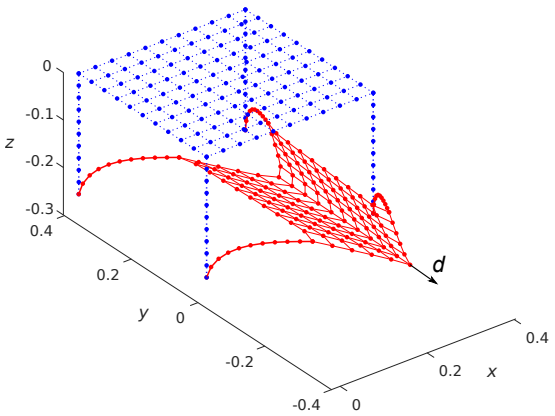

Figure 7.6: Benchmark of the system with the original rod design with prescribed displacement.

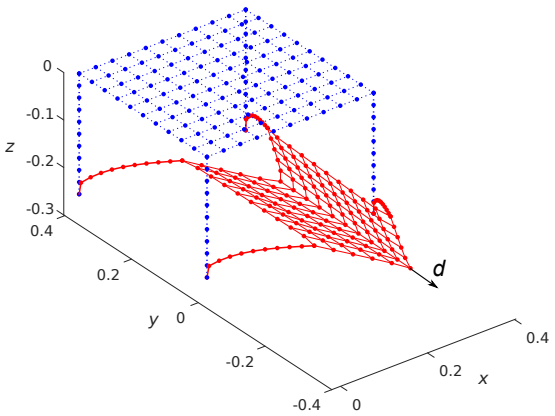

Figure 7.7: Benchmark of the system with the redesigned rod with prescribed displacement.

8 Prototype

This chapter regards a prototype of the redesign developed in chapter 6. The manufacturing of the prototype is described in section 8.1. The chosen design has a thickness of 5 mm, but unfortunately due to a mistake in the data processing, the prototype was made with a thickness of 6 mm. This is elaborated in section 6.4. The prototype is tested to verify the design methodology used for the redesign. The test is described in section 8.2 and a comparison of the prototype and FE simulations are presented in section 8.3.

8.1 Manufacturing

The manufacturing process used to produce the prototype is casting. The prototype is cast in the same thermoset elastomer as the original rod. The thermoset elastomer is produced by mixing two solutions, which then cures to a solid. A mold is to cast the prototype.

8.1.1 Mold Design

The mold is designed using CAD (Computer Aided Design) software. The material used for the mold is HDPE (High Density PolyEthylene). The mold consists of two identical halves. One of the halves can be seen in figure 8.1. The mold halves are joined using six

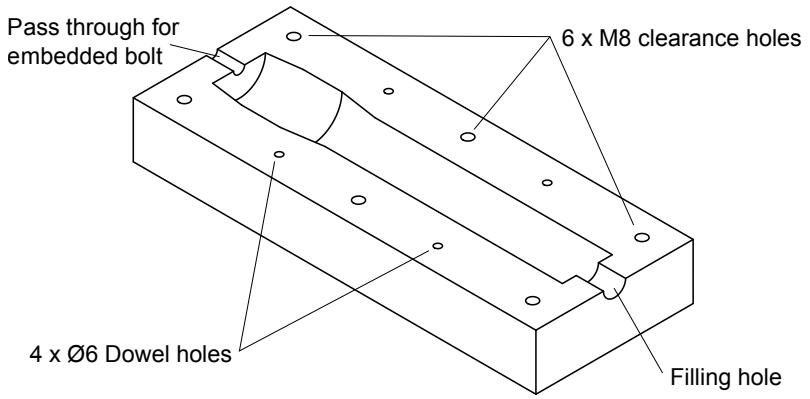

Figure 8.1: CAD drawing of the mold.

M8 bolts for which six clearance holes are made along the edges of the mold. To ensure a correct fit between the two halves four Ø6 dowels are inserted in one of the mold halves and matching holes in the other. A Ø10 hole is made in the top of the mold to allow a M10 bolt to pass through. This is used as a replacement for the thread in the original design. In the bottom of the mold a Ø20 filling hole is made. A technical drawing of the mold can be found in appendix H.

The mold halves are produced in a CNC (Computer Numerical Control) mill. The manufactured mold is seen in figure 8.2. In the top mold half the dowels are seen. In the

bottom half to the left the mentioned M10 bolt insert is seen. As mentioned the purpose

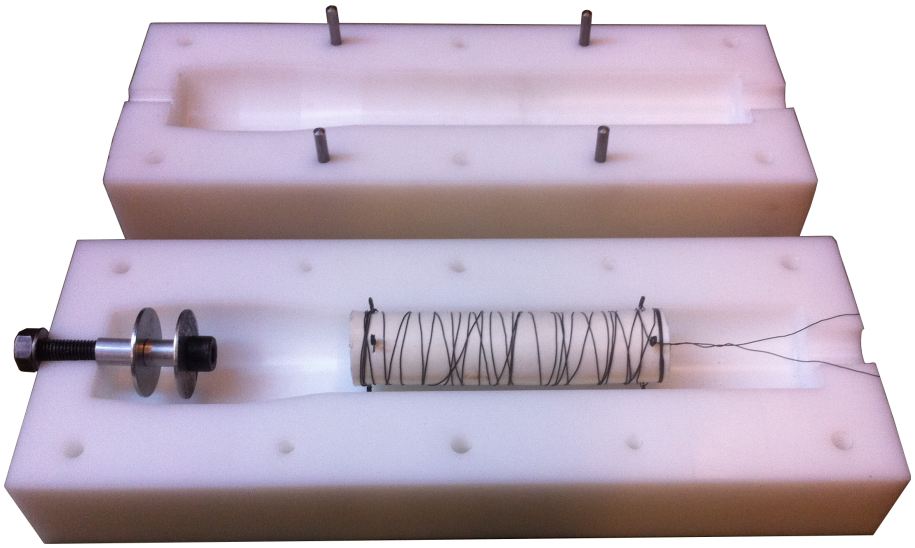

Figure 8.2: Manufactured mold with dowels, embedded bolt and core insert.

of the bolt is to replace the thread of the original design. Beside the M10 bolt, two large M10 washers, two pieces of Ø10 tube and a M10 nut with a small M10 washer is used. The large washers are used to anchor the bolt in the rod and the tube pieces are used as spacers. The nut and the small washer is used to keep the bolt in place and seal the pass through hole. The bolt insert assembly is seen in figure 8.3.

In order to make the rod hollow a core insert is used. This is seen in the middle of the bottom mold half in figure 8.2 and in figure 8.4. The purpose of the core insert is to displace the volume inside the rod without adding any significant stiffness. The tube used for the core is originally Ø40 which is more than the required Ø33 which the design specifies. In order to obtain the correct diameter a section of the tube is cut out and then tightened back into shape using wire. The ends of the tube is sealed with two nylon discs and glue. The core is centered in the mold by using 6 mm feet made of wire. There are four feet at each end distributed with 90 degrees of spacing. The longitudinal position is achieved by hanging the core in wire, which is clamped in between the mold faces, as can be seen in figure 8.2.

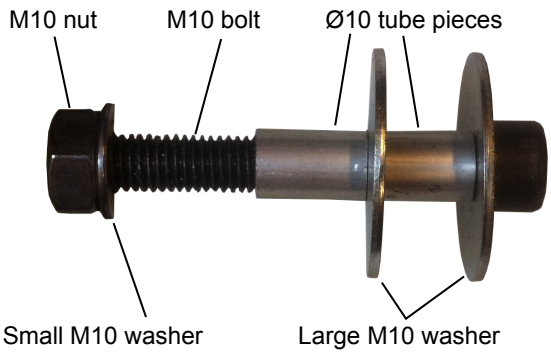

Figure 8.3: The bolt insert assembly.

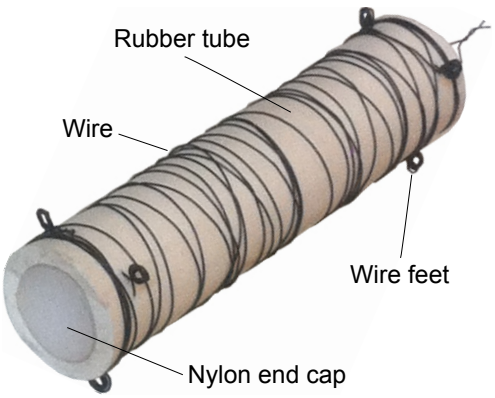

Figure 8.4: The core insert.

8.1.2 The Finished Prototype

The casting process of the prototype was successful and all the functions of the mold worked as expected. The prototype is seen in figure 8.5. The tap in the bottom of the rod is sawed off and a thread cutter is used to remove the excess resin on the thread of the M10 bolt.

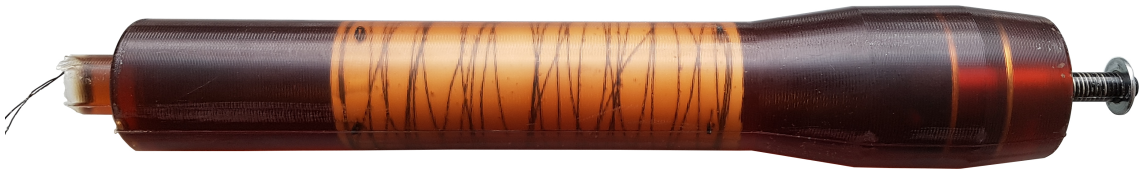

Figure 8.5: The cast prototype.

8.2 Experimental Testing of the Prototype

The prototype is tested to investigate if the developed design behaves as intended. This is done by determining the force-displacement curve of the prototype in bending. The setup for the test is described in section 8.2.1 and the results are presented in section 8.2.2. The journal documenting the test in located in appendix I.

8.2.1 Test Setup

The setup for the test is the same setup used for determining the bending stiffness of the rod. This is described in section 3.3.1. The setup is seen in figure 8.6 which shows some of the deflections obtained during the experiment.

Figure 8.6: The deflection at (from left) 5, 35 and 50 kg. The collapse

8.2.2 Results

The results of the test are seen in figure 8.7 and 8.8 for the x- and y-displacements respectively. Ten weights were applied in the sequence; 5, 10, 15, 20, 25, 30, 35, 40, 45 and 50 kg.

Looking at the x-displacement in figure 8.7, initially the displacement is small as is expected at small rotations. As the load increases the displacements gets larger and show linear behaviour. The transition from bending to tension can not be seen, which is suspected to be due to the buckling. The loss in stiffness due buckling evens out the gained

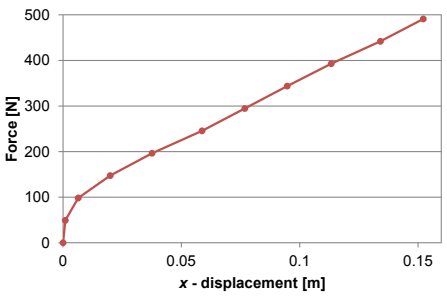

Figure 8.7: The force-displacement curve of the x-direction.

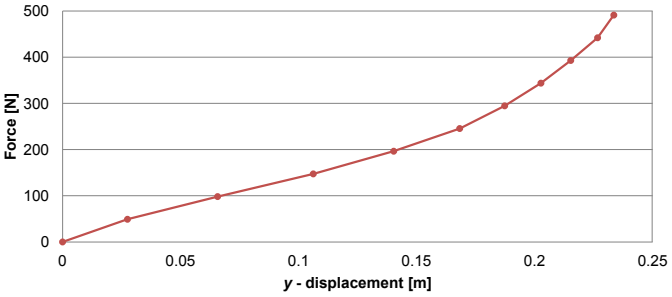

Figure 8.8: The force-displacement curve of the y-direction.

tensile stiffness and results in the linear curve. If the loading were to continue the tension would become visible. The y-displacement in figure 8.8 exhibits linear behaviour until a load of 25 kg. After this point the curve shows non-linear behaviour i.e. stiffening due to the rod starts to be in tension.

The test of the prototype showed the desired behaviour. The collapse of the cross section and ovalisation is seen in figure 8.9. During the experiment the prototype began to take some damage. This was due to the wire feet on the inserted core, which extrude to the surface of the prototype. Due to the small thickness in the areas around the feet the surface began to gash and increased slightly in size during the experiment. This is seen in figure 8.10. The gashes are not believed to have affected the results but further load of the prototype might cause more damage. It was also noticed that the prototype had gotten

Figure 8.9: Collapse of the cross section.

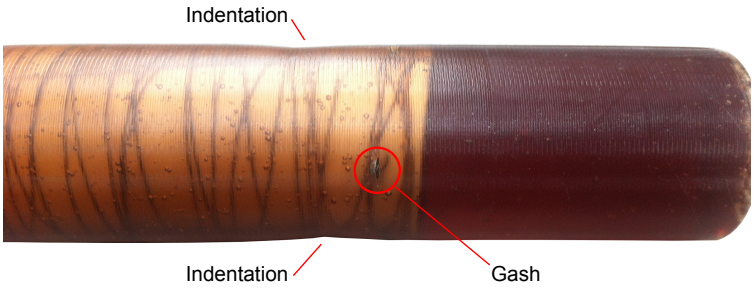

Figure 8.10: The gash around the wire feet is highlighted by the red circle and the indentations are marked.

indentations at the area where it buckles. The indentations are marked in figure 8.10. The cause of the indentations could be plastic deformation of the wire wrapped around the core or simply plastic deformation of the surrounding material.

8.3 Comparison

The prototype is compared with the ANSYS model on which the design is based to see if the desired behaviour is obtained in the prototype. The force-deflection curve of the prototype and the ANSYS solid model with a thickness of 6 mm is seen in figure 8.11. The red curve is the test results and the green curve is the results from the model. The two curves have similar slope below a displacement of 0.1 m. After this point the model is stiffer until it reaches the limit point and buckles. The model approaches the test results, but when the tension becomes dominating the curves deviates.

The deviation between the test results and the model can be explained by two factors.

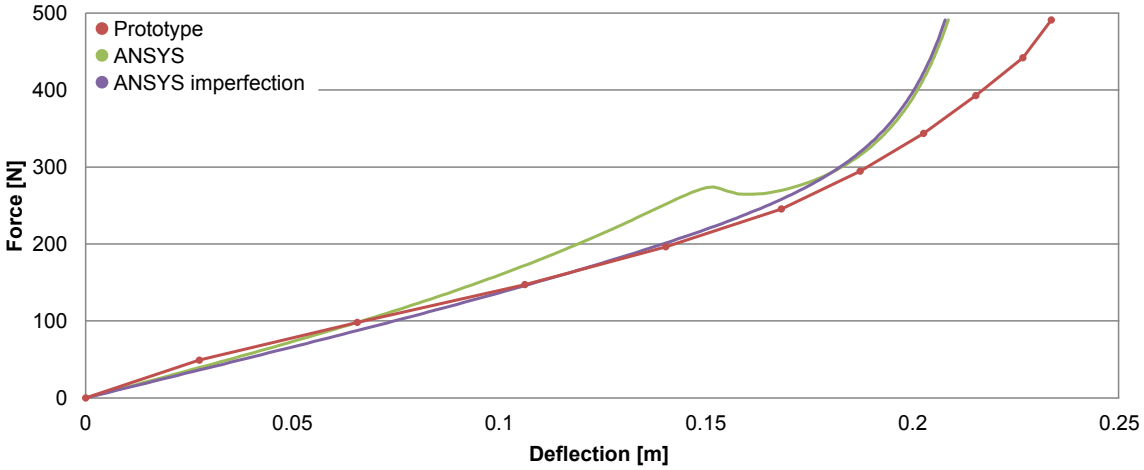

Figure 8.11: Comparison of the prototype, the ANSYS model and a model with imperfection.

One factors is imperfections in the prototype. In appendix I in figure I.4 the prototype showed indentations in the area where it had buckled. Modelling the indentations as imperfections, which was discussed in section 6.5, the resulting deflection approaches the test results. The purple curve in figure 8.11 is the curve of the model with the imperfections. It is seen that the limit point is smoothed out and the curve of the imperfection and the test results are almost coincident. But as tension begins to dominate, the imperfection curve follows the model curve. The cause to deviation in the last part of the curves may be due to material non-linearity. In the ANSYS models a linear modulus of elasticity is used, while the test results softens.

Taking the imperfection and the material non-linearity into account it is assessed that the design method used to develop the redesign is viable.

As a last comparison the prototype is compared to the original design. The force-displacement curves are show in figure 8.12 and 8.13 for the x- and y-displacements respectively. The

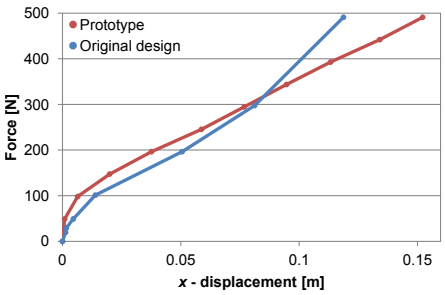

Figure 8.12: The force-displacement curve of the x-direction.

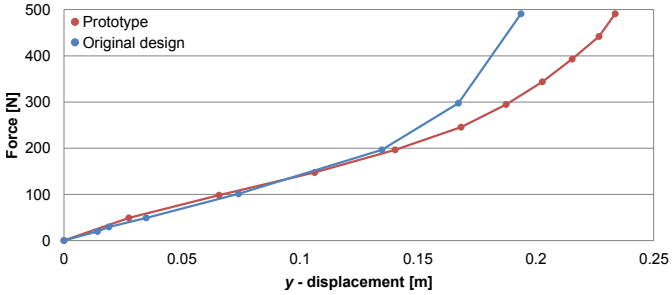

Figure 8.13: The force-displacement curve of the y-direction.

two figures show that the prototype and the original design initially has about the same stiffness. But as the prototype begins to buckle it becomes more compliant than the original design. The buckling is initiated at about 200 N. This shows that the prototype works as intended.

9 | Conclusion

The goal of this master's thesis has been to write a program which establishes a model of a provided mechanical system consisting of a net suspended by flexible rods. In addition the project has also sought to develop a redesign of the rod.

A model of the net-rod system has been programmed in MATLAB. The program utilises the principle of stationary potential energy in a gradient based optimisation routine to solve the system. This method has proved very powerful in solving the geometric non-linear problem. The program is able to model a rectangular net of any size and rods, that can be discretised, can placed at any node in the net. Boundary conditions and loads can also be applied to any node of the system.

The net-rod model uses the tensile stiffness of the net and the tensile and bending stiffness of the rod. These stiffnesses are determined experimentally in order to model the provided net-rod system. Linear stiffnesses has been acquired, although the rod displaced non-linear material behaviour in form of softening.

The modelling of the rods was compared to the results of the bending experiment before validating the entire net-rod model. The bending stiffness was fitted to the results by adding a non-linear softening term and a scaling. The net-rod model was then validated against a physical system. The comparison showed that the knots of the net significantly affected the deformation behaviour. Otherwise there was good agreement between the model and reality.

The redesign of the rod was initialised by a morphological analysis in order to develop a design concept. The morphological analysis was limited to focus on the bending behaviour of the mid section in order to reduce the energy absorbed by the system. The selected concept utilised a tubular cross section to achieve buckling of the rod.

The overall redesign of the rod was determined and a parameter study was used to determine the thickness, which provided the desired behaviour. A thickness of 5 mm was found to give the desired behaviour.

The design concept is benchmarked to determines the performance increase the redesign has provided. The benchmark showed a reduction in the elastic energy of 50% compared to the original system.

A prototype was manufactured with a thickness of 6 mm based on a mistake during data processing. The prototype was then used to validate the design methodology. The prototype displayed the predicted buckling behaviour of the finite element simulations and thereby validated the design methodology.

Many competences have been employed in this project such as: Analytical, numerical, practical. The design process in this project has required the participants to use all of these competences in order to develop an advanced product.

10 | Future Work

In the making of this project some problems and ideas have been noticed. These have not been addressed since it has been out of scope for this project. The problems and ideas are formulated as suggestions for future work on the topics covered by the project. In the following the suggestions as discussed briefly.

10.1 Net-Rod Model

The future work regarding the net-rod model is covered in the following.

10.1.1 Validation Using Another Net

The validation of the net-rod model covered in chapter 4 can be improved by removing the primary deviation factor, the knots. Using a different type of net, where the knots does not affect the deformation, the validation can be improved. Ideally instead of using a net, a system of springs can be used, since this is how the net is modelled.

10.1.2 Modelling the Knots in the Net

It is clear from the validation that by not modelling the knots in the net, the net-rod model deviates significantly from reality. To improve the net-rod model the knots should be taken into account. Figure 10.1 shows the way the net is currently modelled, a piece of the net and the suggestion of how the knots could be modelled. The knots in the figure is

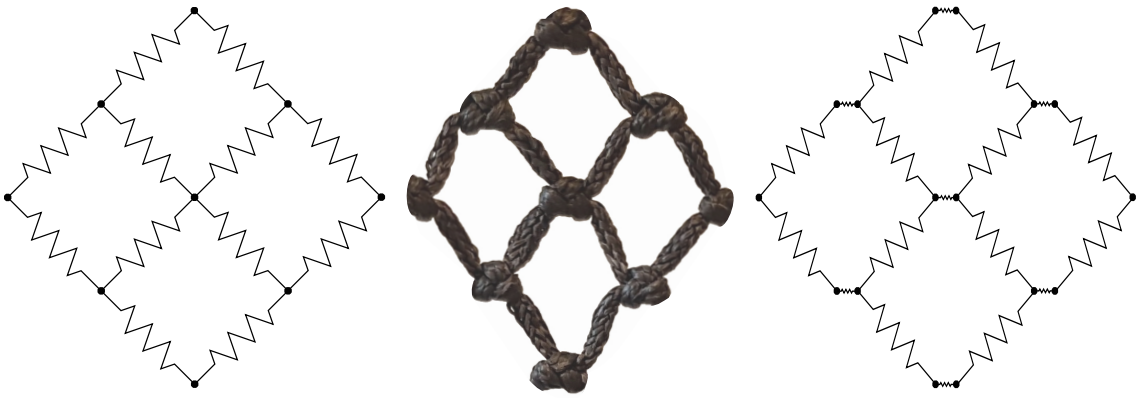

Figure 10.1: Left: current modelling of the net is showed. Middle: The net. Right: Suggested model.

modelled as a short very stiff spring. It could also be made rigid. By adding this to the net-rod model the behaviour should be improved.

10.1.3 Adding Gradients to the Net-Rod Model

In the net-rod model the optimisation routine used to solve the model is gradient based. The default setting (which is used in the net-rod model) is to use finite difference to determine the gradients. If the gradients could be determined analytically, the speed of the optimisation could be increased. The gradients of the objective function, the total elastic potential, are determined as:

$$\frac{\partial \Pi}{\partial d_i} = \frac{\partial U}{\partial d_i} - \frac{\partial W}{\partial d_i} \tag{10.1}$$

Which yields the equilibrium equation.

10.1.4 Elastic Energy of a System with Non-linear Stiffness

As mentioned in section 7.2 the elastic energy of the net-rod model is calculated under the assumption of linear elasticity. In order to properly model non-linear stiffnesses the calculation method for the elastic energy needs to be changed to account for non-linearity.

10.2 Redesign

The future work regarding the redesign is covered in the following.

10.2.1 Mounting Mechanisms for the Rod and Net

In the morphological analysis in chapter 5 the redesign was limited to focus on the stiffness behaviour of the rod, not considering the two other functionalities. For a future study the morphological analysis could be expanded to include the two other functionalities; fixation of the net and mounting of the rod.

10.2.2 Mold Design

The mold designed for the prototype have room for improvements concerning the core insert. The method of using wire to hold the core insert is place was adequate for the prototype, but for a final product another way of placing and manufacturing the core insert should be developed.

Bibliography

ANSYS, (2013). ANSYS Mechanical APDL Element Reference.

Arora, J., (2011). Introduction to Optimum Design. Academic Press.

Brøndsted, P. and Nijssen, R., (2013). Advances in wind turbine blade design and materials. Woodhead Publishing.

Cook, R.D., Malkus, D.S., Plesha, M.E., and Witt, R.J., (2002). Concepts and applications of finite element analysis. Fourth Edition. Wiley.

Lund, E. and Lindgaard, E., (2014). Course on Finite Element Methods 2014.

MathWorks, (2016). MATLAB Documentation. Accessed 8-April-2016.
URL: *www. mathworks. com/ help/*

Rao, S.S. and Fah, Y.F., (2011). Mechanical Vibrations. Fifth Edition. Prentice Hall.

Appendices

A | CD Content

Contents of the appendix CD:

1. Net-Rod model programmed in MATLAB
2. Pictures captured for determining the tensile stiffness of the rod
3. Pictures captured for determining the bending stiffness of the rod
4. Pictures captured during full scale testing
5. Pictures captured during prototype testing
6. .pdf-version of the report with hyperlinks

B | Algorithms

During the development of the net-rod model several algorithms for solving the system has been attempted. In this appendix the basic concept of each of the algorithms are documented.

B.1 Force Equilibrium I

1.	Solve linear system	$\{d\}_0 = [K]_i^{-1}\{F\}$
2.	Determine spring elongation	$\{\Delta\} = \{f(x,y)\}$
3.	Determine non-linear stiffness	$[K_s]$
4.	Update stiffness	$[K]_{i+1} = [K]_i + [K_s]$
5.	Solve system	$\{d\} = [K]_{i+1}^{-1}\{F\}$
6.	Repeat step 2-5 until	$\{d\}_{i+1} - \{d\}_i \approx \{0\}$

B.2 Force Equilibrium II

1.	Solve linear system	$\{d\}_0 = [K]^{-1}\{F\}$
2.	Determine spring elongation	$\{\Delta\} = \{f(x,y)\}$
3.	Determine the force error	$\{\Delta F\} = [K]\{\Delta\}$
4.	Solve system	$\{d\} = [K]^{-1}(\{F\} - \{\Delta F\})$
5.	Repeat step 2-4 until	$\{d\}_{i+1} - \{d\}_i \approx \{0\}$

B.3 Force Equilibrium III

1.	Solve linear system	$\{d\}_0 = [K_1]^{-1}\{F\}$
2.	Determine spring elongation	$\{\Delta\} = \{f(x,y)\}$
3.	Determine the force error	$\{\Delta F\} = [K_2]\{\Delta\}$
4.	Solve system	$\{d\} = [K_1]^{-1}(\{F\} - \{\Delta F\})$
5.	Repeat step 2-4 until	$\{d\}_{i+1} - \{d\}_i \approx \{0\}$

B.4 Energy

1.	Provide initial guess	$\{d\}_0 = \{0\}$
2	Minimise the total elastic potential	$minimise\ \ \Pi(\{d\})$
2.1.	Determine spring elongation	$\{\Delta L\} = \{f(x,y,z)\}$
2.2.	Determine the elastic energy	$U = \frac{1}{2}\sum K_i \Delta_i^2$
2.3.	Determine work done by forces	$W = \{F\} \bullet \{d\}$
2.4.	Determine the total elastic potential	$\Pi = U - W$

C | Determination of the Tensile Stiffness of the Net

This journal describes the experiment made to determine the stiffness of the net. The preliminary measurements mentioned in section 3.1 are not documented in this, but only the four final measurements.

C.1 Purpose

The purpose of the experiment is to determine the tensile stiffness of the net k_{Net}. The stiffness wanted is seen in figure C.1 which is the stiffness between two knots.

C.2 Setup

A Zwick Z100/TL3S tensile testing machine is used to apply tensile force to the net specimen. The net specimen is mounted in the Zwick using specialised mounting equipment. The setup is seen in figure C.2. The knots are blocked by fixtures, which is then blocked by steel plates bolted to the Zwick . An extensometer is used to measure the elongation and is mounted on the specimen. The specimen is unraveled from the net and has a knot in each end.

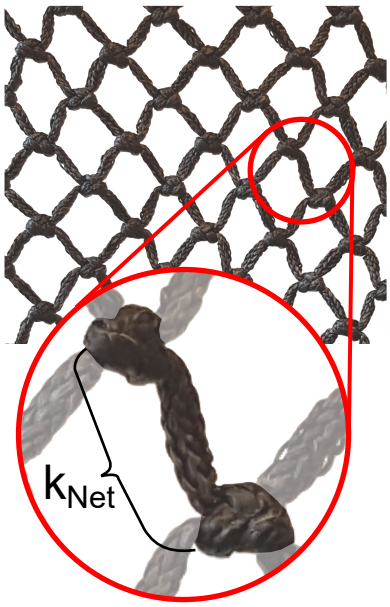

Figure C.1: The net and magnification of the wanted stiffness.

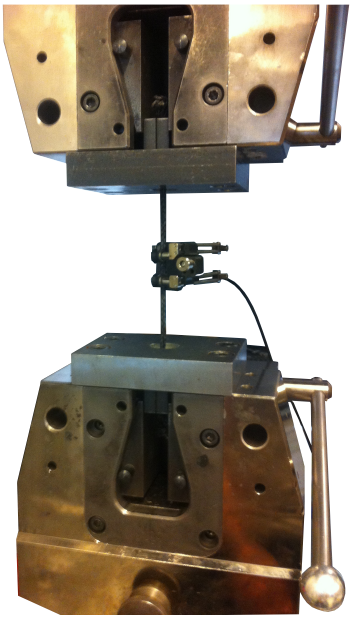

Figure C.2: Setup for the experiment.

C.3 Procedure

The net specimen is mounted in the Zwick and mounted with an extensometer. The specimen is then loaded until the specimen fails. The force is supplied by the Zwick and the displacement by the extensometer.

C.4 Results

The results from the four measurements made are seen in figure C.3. All the measurements were terminated due to a knot being untied.

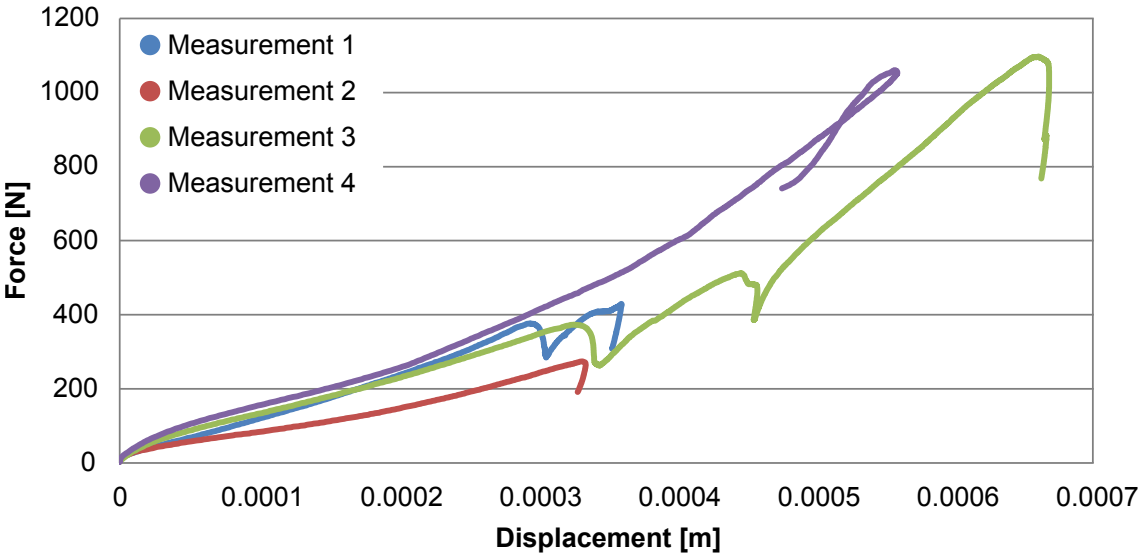

Figure C.3: Results from the experiment.

C.5 Discussion

Looking at the resulting force-displacement curves it can be seen that the second measurement has a lower slope than all the other measurements. This indicates that the specimen used had a lower stiffness than the others. The reason is unknown, but the specimen could have been damaged, when it was cut form the net or the extensometer was not mounted properly. The second measurement is classified as a outlier and should not be used.

Up to a extension of about 0.0003 m the rest of the specimen show a nearly linear behavior with a very slight stiffening observed. This could be due to the structure of the net which is made of braided fibres, where the individual fibre being straighten supplying full stiffness. It could also be non-linear material stiffness behavior.

Each test has a different duration and number of drops. The drops in stiffness seen in the curves are untying of knots. Measurement one and three shows how a knots is being untied and then tightened again regaining and increasing the stiffness.

C.5.1 Uncertainties

The largest source of uncertainty is the knots, since the setup rely on them to fixate the net specimen. Minor uncertainties are found in the precision of the Zwick and the extensometer.

C.6 Conclusion

Through the discussion of the results and the uncertainties it is assessed that a linear stiffness is possible to determine using the results of the experiment. When determining the stiffness the second measurement and data points beyond 0.0003 m should not be used.

D | Determination of the Tensile Stiffness of the Rod

This journal describes the experiment conducted to determine the tensile stiffness of the rod.

D.1 Purpose

The purpose of this experiment is to determine the tensile stiffness ($k_{Rod,t}$) and modulus of elasticity (E_{Rod}) of the rod.

D.2 Setup

The rod is mounted in a Zwick Z100/TL3S tensile testing machine using the mounting cup and locking pin in the bottom and the thread in the top. Both ends are bolted to the steel plates. Since the base of the mounting cup is angled the rod is bend a little in order to be mounted in the top. The setup for the experiment is seen in figure D.1.

Figure D.1: The setup for the determination of the tensile stiffness of the rod.

D.3 Procedure

The displacements are measured using two methods. The total displacement measured by the Zwick and the displacements of two marked points on the rod captured by a camera. The Zwick is controlled via displacements. The rod are displaced and returned to original position before next run. A picture is taken before deformation and after deformation.

D.4 Results

The results of the experiment generated using the Zwick are seen in figure D.2. The rod was elongated 5 mm (First measurement), 7.5 mm (second and third measurement) and 10 mm (fourth measurement). A preload of 100 N was chosen to align and tension the components.

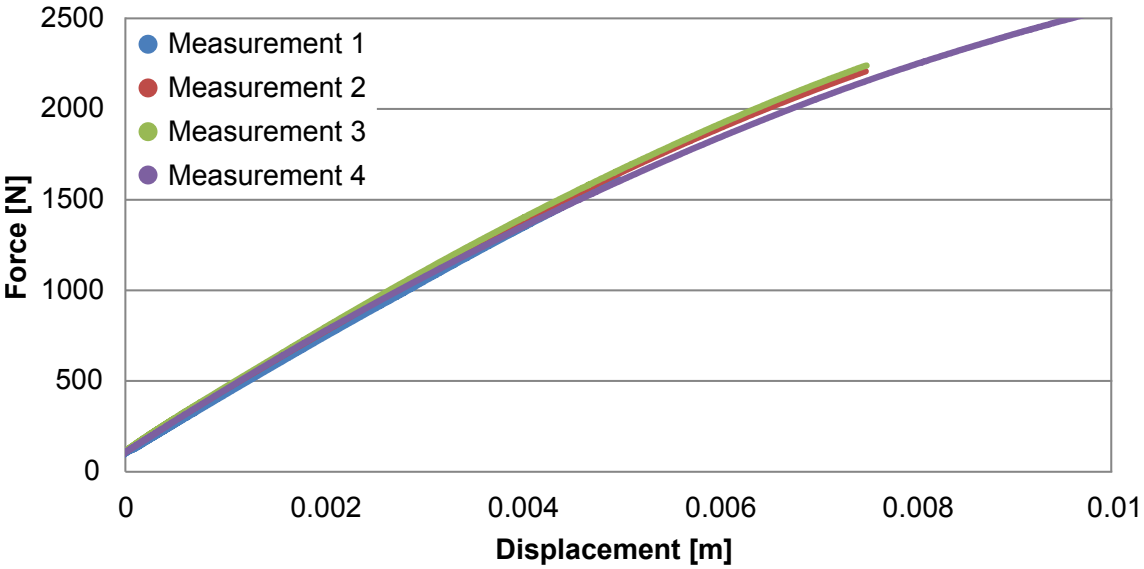

Figure D.2: Results from the experiment.

Beside the force-displacement curves supplied by the Zwick a camera recorded the measurements. Using two frames, one before loading and one at maximum load, the change in distance between the two points is determined. The initial distance between the two points is 0.05 m. The values are collected in table D.1.

Table D.1: Results from the camera measurements.

Measurement	Force [N]	L_{before} [m]	L_{after} [m]	Δ [m]
1	1612.97	0.0500	0.0513	0.0013
2	2207.90	0.0505	0.0522	0.0017
3	2239.56	0.0506	0.0524	0.0018
4	2562.08	0.0509	0.0530	0.0021

D.5 Discussion

Looking at the curves in figure D.2 the results of the four measurements are nearly identical. The repeated accuracy of measurements points towards reliable data. The slight difference which is present may be due to relaxation.

The slope of the curves is slowly declining showing non-linearity. This is probably due to non-linear material behavior.

The results from the camera measurements are very sensitive and subjective requiring a small margin of error in order to obtain good results. This is elaborated in section 3.2.3 where the data is used to determine the modulus of elasticity.

D.5.1 Uncertainties

As mentioned in section D.2 the mounting cup is angled causing the rod to bend in order to be mounted in the top. A preload of 100 N was added to straighten out the rod and to make all components set. The bend is assessed to have insignificant effect on the results and no complications were noticed.

Measurement two and three did not generate the same curves or elongations even though the measurements are identical. Relaxation is likely the cause because the forces and displacements was reset after each run. The curves in figure D.2 indicates the relaxation is minimal, but as the experiment is repeated and if the load is increased one should be aware of the uncertainty.

The displacement measured using the Zwick Z100/TL3S is not only the displacements of rod. The individual components of Zwick Z100/TL3S will deflect, bolts and steel plates will elongate which will be included in the measured displacements. The majority of the parts used in this experiment are steel which is much stiffer than the rod. The elongations and deflections of the Zwick and parts will only be a fraction of the rod and thereby negligible.

The measurements made using the camera can be affected by several uncertainties. The initial distance of the points is measured with a ruler and could be a millimeter off. The results of the processing of images to obtain the elongations are subjective meaning the precision is dependent on person performing the measurements.

D.6 Conclusion

It is assessed that the results form the experiment are usable for further analysis taking the uncertainties into account. The results from images captured by the camera should be used with precaution.

E | Determination of the Bending Stiffness of the Rod

This journal describes the experiment conducted to determine the bending stiffness of the rod.

E.1 Purpose

The purpose of this experiment is to determine the bending stiffness (k_b) of the rod.

E.2 Setup

The setup for the experiment is seen in figure E.1. A steel fixture has been fabricated for the experiment to mount the rod on a steel beam. Instead of using a locking pin to secure the rod, it is clamped in the fixture. Using threaded bars and nuts the fixture is clamped to the steel beam. The rod is mounted on a vertical surface in order to use weights to load the rod. A chain is attached to the head of rod by a bolt to which the weights are applied.

Figure E.1: Setup for determining the bending stiffness

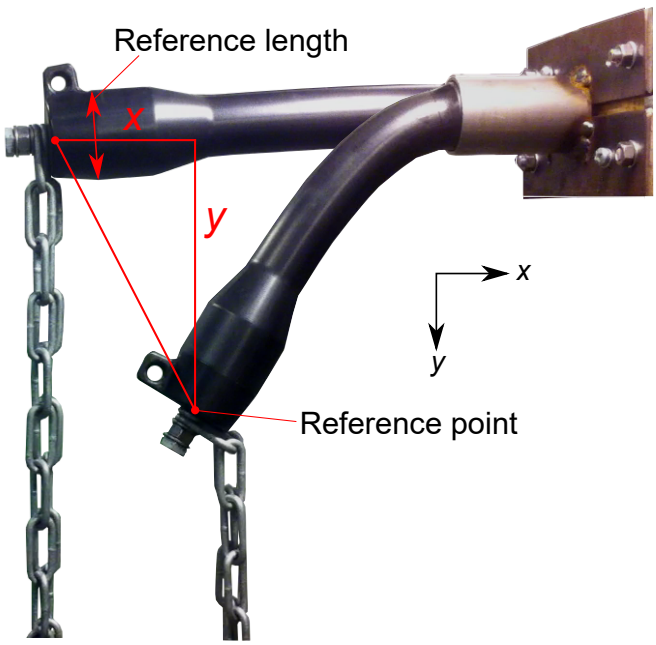

Figure E.2: Illustration of the method used for determining the displacement of the rod.

The experiment is recorded by a camera in order to determine the displacements by image post-processing. The of the rod is used as a reference point and the diameter of the cylindrical part of the rod head is the reference length, as seen in figure E.2. The reference length is used to determine the meter per pixel ratio.

E.3 Procedure

A picture is taken before any weights are applied. The weights are applied and a picture is taken in the deformed state. The weights are removed and the rod is bend in the opposite direction to to compensate for creep. This is an attempt to achieve the same reference position before next load is applied. This is repeated until satisfied results are obtained.

E.4 Results

The results of the experiment is seen in figure E.3 and E.4 for the x- and y-displacements respectively. Eight weights were applied in the sequence; 2, 3, 5, 10.3, 15.3, 20, 30.3 and 50 kg.

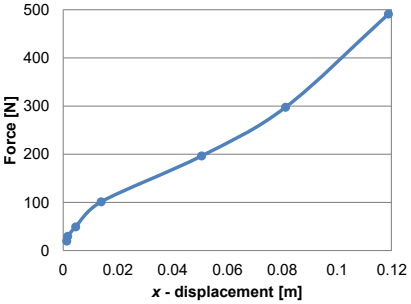

Figure E.3: The force vs. x-displacement curve.

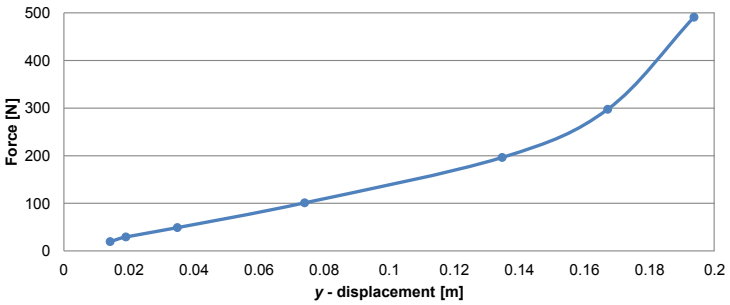

Figure E.4: The force vs. y-displacement curve.

The x-displacement is not used to determine the bending stiffness, but has been measured to determine the full deflection behavior of the rod. The y-displacement or deflection is used to determine the bending stiffness. Some of the deflections obtained during the experiment are seen in figure E.5. All the pictures processed are found on the attached CD in appendix A.

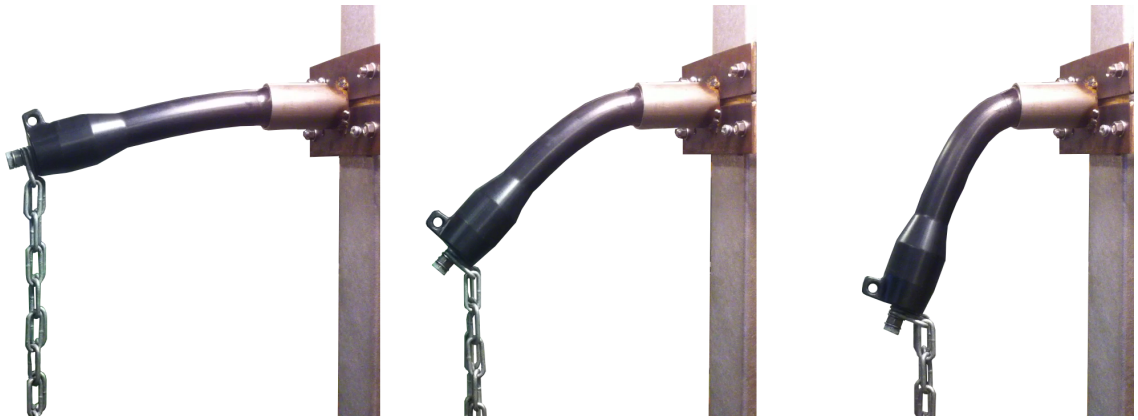

Figure E.5: The deflection at (from left) 5, 20 and 50 kg.

E.5 Discussion

Looking at the x-displacement in figure E.3, it is seen that in the beginning there is little displacement, which is expected at small rotations. As the load increases the displacement gets larger until it begins to be in tension, as seen in figure E.5. The deflection (y-displacement) in figure E.4 exhibits linear behaviour until a load of 20 kg. After this point the curve shows non-linear behaviour i.e. stiffening due to the rod starting to being in tension.

In appendix D it was clear that the rod exhibited non-linear material behaviour. This cannot be seen in this experiment since the material non-linearity is mixed with the geometrical non-linearity.

E.6 Uncertainties

The measurement done using image post-processing seems to provide decent results as there is no questionable behaviour in the results, but there will still lie a small uncertainty in the measurement.

The weights used for the experiment were not tested to see the deviation from the labeled weight. It is possible that the actual weight has small deviations. The weights were applied to a chain which was bolted to the thread in the top of the rod. But as it can be seen in figure E.5 the first link does not rotate causing the weights to be shifted resulting in a smaller moment arm. It is assessed that the deviation caused by the shift of the weights is insignificant.

E.7 Conclusion

Based on the discussion it is assessed that the uncertainties will not affect the results significantly and that the results are usable for determining the bending stiffness.

F | Test of the Physical System

The content of this chapter is a journal the experiment made to determine the displacements of the physical system used to validate the net-rod model.

F.1 Purpose

The purpose of this experiment is to determine the displacements of the flexible rods and a knot of the net for a given load case.

F.2 Setup

The setup for the experiment is seen in figure F.1. The setup consists of a 7x7 net and four rods, one mounted in each corner of the net. Four fixtures are made for the rods. The fixtures fit around the base of the rods and a bolt is used to lock the rods in place. The fixtures are mounted on a board of MDF and positioned so the rods stretch out the net, applying a bit of tension. The board is hung on a concrete wall with two U-shaped steel bars.

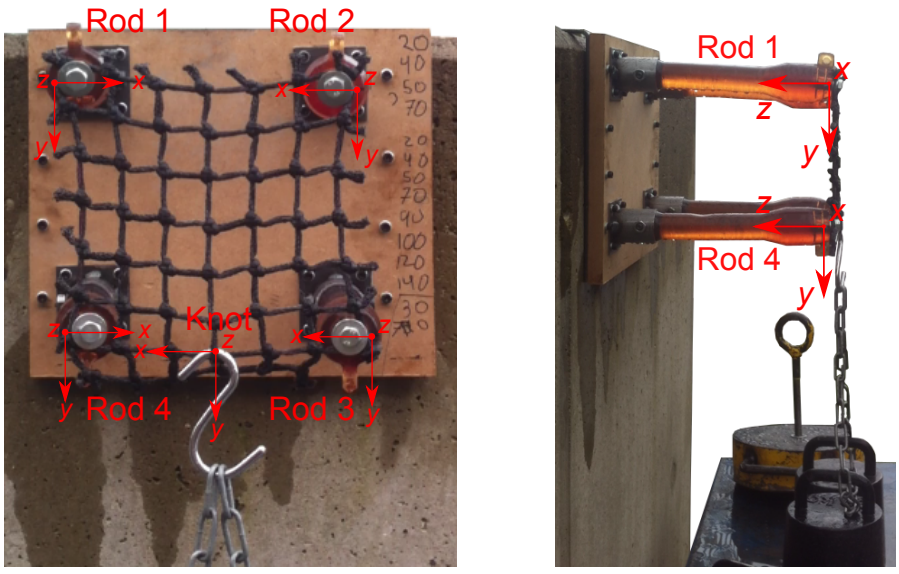

(a) Front view. **(b)** Side view.

Figure F.1: Setup of the physical system.

The net is connected to the end of each rod with two washers and a bolt as seen in figure F.2. The washers are used to apply the pressure to the knot surface and prevent the knots to slip when the rods experience large displacements as seen in figure F.3.

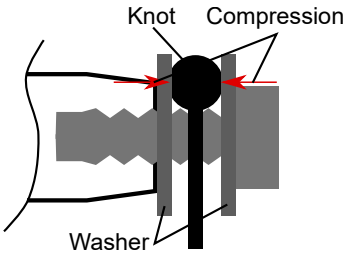

Figure F.2: Securing the net.

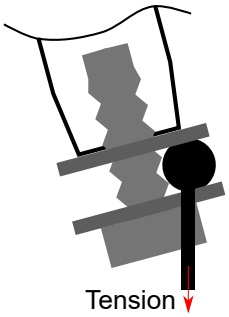

Figure F.3: The washer keeps the knots from slipping out.

The load is applied to the net on the center bottom knot with a hook, as seen in figure F.1a. The displacements of the system is captured by using two cameras. One in front of the setup and one beside the setup.

F.3 Procedure

In order to reduce the amount of data for the experiment, only three loads are used; 40, 70, and 100 kg. The two cameras record videos of the displacements. Pictures are taken form the video at the different loads and the displacements can be determined by analysing the pictures. The displacement of the tip of the four rods and the knot to which the load is applied are determined.

F.4 Results

The physical system loaded with 100 kg is seen in figure F.4. The displacements w.r.t. the local coordinate systems (shown in figure F.1) are seen in figure F.5 to F.8. The front camera is used to capture the x- and y-displacements and the side camera is used to

(a) Front view at 100 kg.

(b) Side view at 100 kg.

Figure F.4: The physical system under load.

capture the y- and z-displacement of rod 1 and rod 4. The y-displacement of rod 1 and rod 4 is captured twice and are found to be coincident, so the y-displacements from the side camera are omitted to reduce the number of curves in figure F.6.

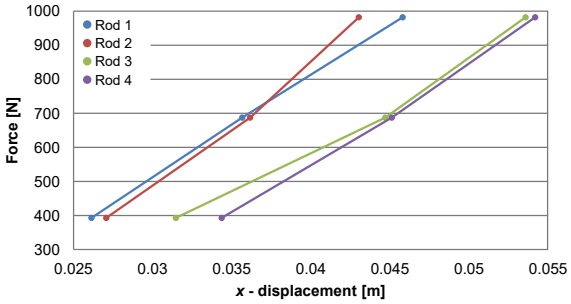

Figure F.5: x-displacements.

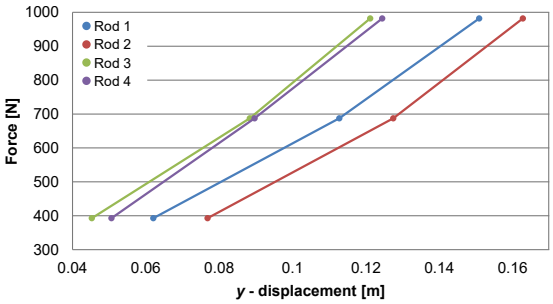

Figure F.6: y-displacements.

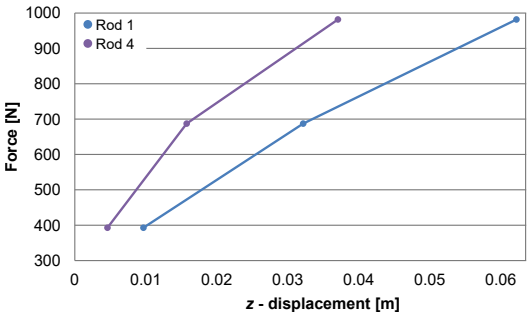

Figure F.7: z-displacements.

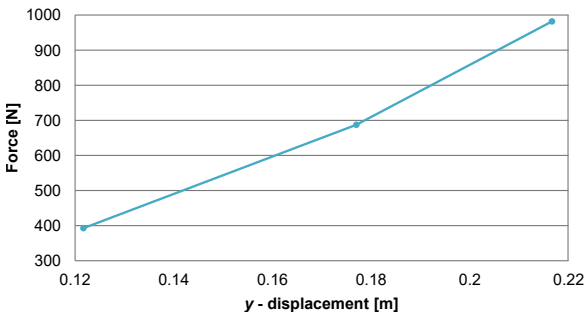

Figure F.8: y-displacement of the knot.

F.5 Discussion

The displacements of rod 1 compared to rod 2 are not the same though the load is applied on the vertical symmetry line. This also applies for rod 3 compared to rod 4. The vertical symmetry line is parallel and coinciding with the local y-axis of the knot in figure F.1a. The reason for the large difference in displacements of rod 1 and 2 or 3 and 4 is due to the

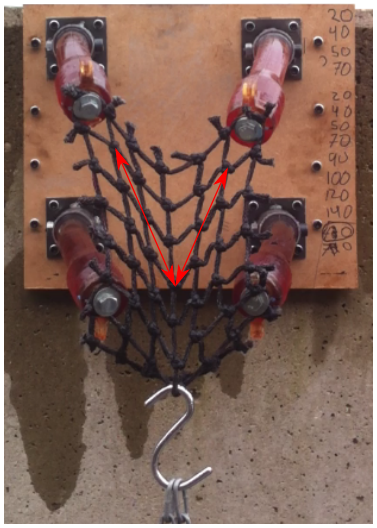

Figure F.9: Front view at 50 kg.

knots in the net. The knots makes the stiffness dependent on the orientation as described back in section 1.1. Investigating the deformed configuration in figure F.9 the left side of the net collapses more than the right side indicated by the red arrows. This shows the stiffness dependency of orientation.

The lower rods (3 and 4) has a smaller y-displacement than the upper rods (1 and 2). This is because the net has slipped from the washers. Instead of being pulled down due to the intended clamped knots, the net is pulled down by the knot above.

F.5.1 Uncertainties

The following uncertainties has been noticed:

- The bottom rods (1 and 2) did not manage to hold on to the intended knot. This lead to a larger deflection of the top rods (1 and 2) compared to the lower ones (3 and 4).
- The loads used for the experiment were not weighed to test if the labeled weight was correct.
- The pretension of the net is not known, but is small compared to the loads applied.
- The position of the net is based on applying the pretension and are not in line with each other.

F.6 Conclusion

The knots have significant influence on the behaviour of the system as explained. This influence is expected result deviations in the validation with the net-rod model. The uncertainties listed should be remained in the validation but most are insignificant compare to the effect of the knots.

G | Shell Model

This chapter explain how the shell model is setup w.r.t. geoemtry, boundary conditions, load and mesh.

Geometry

The rod geometry and boundary conditions are simplified in ANSYS as can be seen in figure G.1. The rod is fixed where the cup ends as seen in figure G.1a. Prescribed y-displacement is used instead of applied forces. The prescribed displacement will be applied to one node. When using the arc-length method it does not matter if force or displacement is applied as both are incremented.

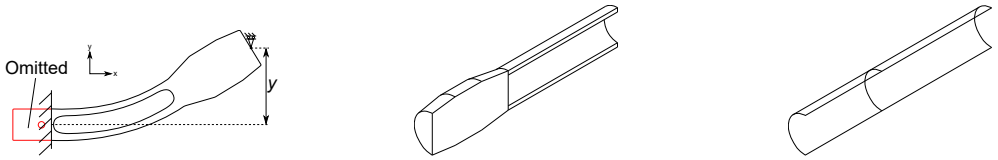

(a) Fixation and prescribed displacement will be used.

(b) Symmetry is utilized.

(c) Shell model.

Figure G.1: The first part of the rod is omitted to simplify the boundary conditions and half of the rod is modelled. These simplifications greatly reduced the computation time.

Symmetry has been applied as seen in figure G.1b to greatly reduce the number of elements and thereby computational time. The head of the rod has been simplified to a tube as seen in figure G.1c. Symmetry should be performed with care since asymmetric mode shapes will not be permitted. The first mode shape from the shell model are seen in figure G.2 which is compared with the mode shape from a full solid model seen in figure 6.12a. Both mode shapes are from a linear buckling analysis. The mode shapes are as expected i.e. bucking occurs in the wall near the fixation. In figure 6.12a the model is loaded in the x-direction which explains why the mode is not in the top. Both models yields the same mode shape so the symmetry is acceptable.

G.0.1 Material Properties

The same material properties have been used in as in section 6.3.1 but with $\nu = 0.21$.

Elements

The shell model can be seen in figure G.3. Shell281 has been used in this model. The geometry is divided into sections to control the mesh size throughout the rod. A small mesh size are used where buckling will take place in order to accurate represent the buckling event. The mesh size is gradually increased away from the buckling area to reduced the number of elements and to minimise distorted elements. The shell elements are preferred because

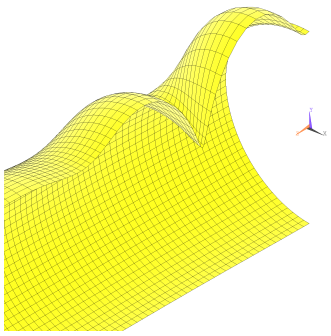

Figure G.2: First mode shape from a linear buckling analysis.

they have less nodes than the solid elements and thereby less computational demanding. Solid186 tetrahedral element have 10 nodes with three D.O.F. per node, translation in x, y and z where as Shell281 have 8 nodes with the same three D.O.F. per node.

Key Options

The key options used is:

KEYOPT(1) Bending and membrane (default).

KEYOPT(8) Store data for bottom of bottom layer and top of top layer (multi-layer elements) (default)

KEYOPT(9) No user subroutine to provide initial thickness (default)

KEYOPT(8) is relevant when working with composites where many layers are used. We have one layer with uniform material properties. KEYOPT(9) is used if the user has made a subroutine to define the thickness. The thickness has been defined in ANSYS so this key option is irrelevant for us (ANSYS, 2013). The shells will be offset such that the top

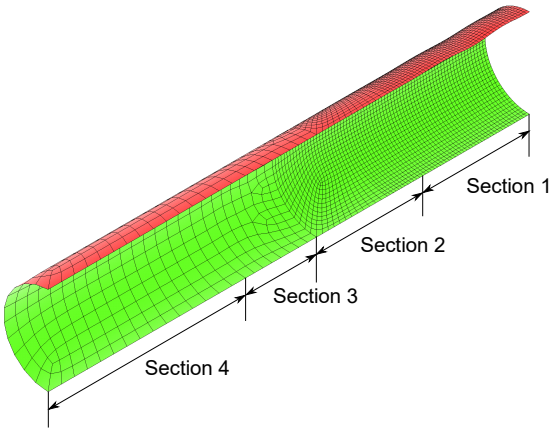

Figure G.3: Meshed shell model.

surface is parallel to the outer geometry as seen in figure G.4. This way the thickness can be changed easily without changing the outer geometry. Section three and four in figure G.3 corresponds to the solid section in G.1b. This part has to be included in the model

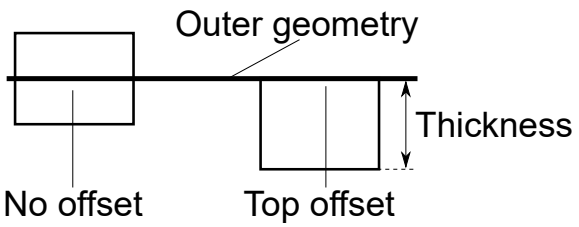

Figure G.4: Offset of shell to easier change the thickness.

is to get the same internal forces as the solid model. To compensate for solid geometry simplification the tube will be 10 times stiffer.

G.0.2 Results

The results from the shell model is presented in section 6.4.2.

H | Technical Drawing of the Mold

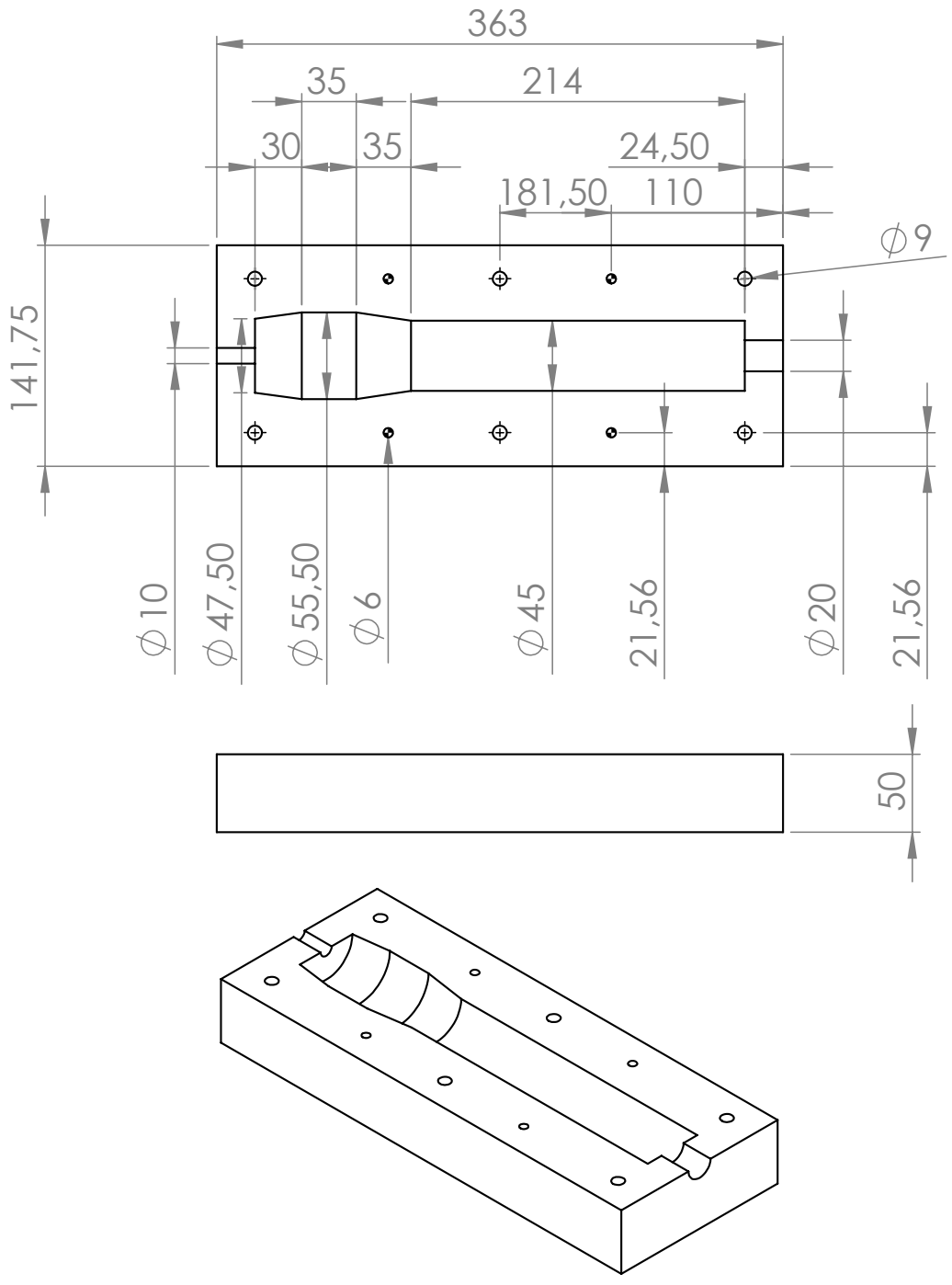

I Test of the Prototype

This journal describes the experiment conducted to investigate the behaviour of the prototype in bending.

I.1 Purpose

The purpose of this experiment is to determine the force-displacement curve of the prototype.

I.2 Setup

The setup for the experiment is the same as was used in appendix E, where the setup can be seen in figure E.1.

I.3 Procedure

A video is recorded through the duration of the experiment. Form the video, pictures are taken at each load and the displacements are determined through image post-processing.

I.4 Results

The results of the experiment is seen in figure I.1 and I.2 for the x- and y-displacements respectively. Ten weights were applied in the sequence; 5, 10, 15, 20, 25, 30, 35 , 40, 45 and 50 kg.

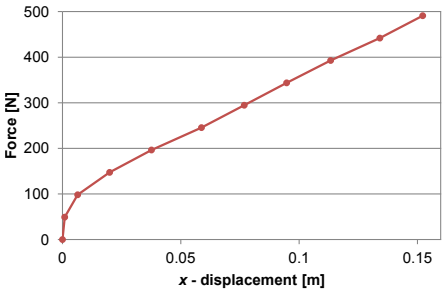

Figure I.1: The force vs. x-displacement curve.

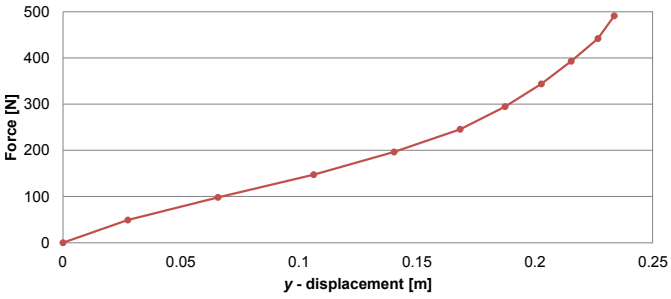

Figure I.2: The force vs. y-displacement curve.

Some of the deflections obtained during the experiment are seen in figure I.3. All the pictures processed are found on the attached CD in appendix A.

Figure I.3: The deflection at (from left) 5, 35 and 50 kg.

I.5 Discussion

Looking at the x-displacement in figure I.1, initially the displacement is small as is expected at small rotations. As the load increases the displacements gets larger and show linear behaviour. The transition from bending to tension can not be seen, which is suspected to be due to the buckling. The loss in stiffness due buckling evens out the tension and results in the linear curve. If the loading were to continue the tension would become visible.

The y-displacement in figure I.2 exhibits linear behaviour until a load of 25 kg. After this point the curve shows non-linear behaviour i.e. stiffening due to the rod starting to being in tension.

During the experiment the prototype began to take some damage. This was due to the wire feet on the inserted core, which extrude to the surface of the prototype. Due to the small thickness in the areas around the feet the surface began to gash and increased slightly in size during the experiment. This is seen in figure I.4. The gashes are not believed to have affected the results but further load of the prototype might cause more damage.

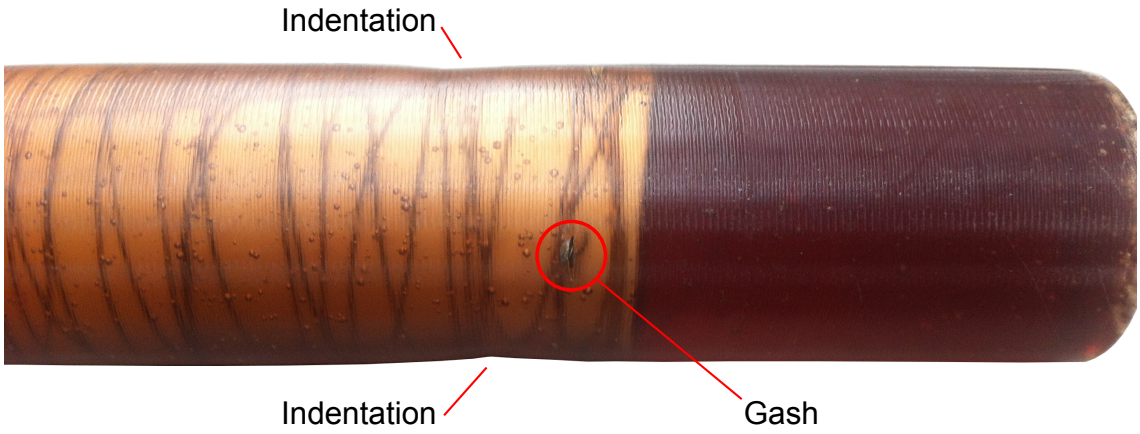

Figure I.4: The gash around the wire feet is highlighted by the red circle and the indentations are marked.

It was also noticed that the prototype had gotten indentations at the area where it buckles. The indentations are marked in figure I.4. The cause of the indentations could be plastic deformation of the wire wrapped around the core or simply plastic deformation of the surrounding material.

I.6 Uncertainties

The uncertainties are the same as in E.

I.7 Conclusion

It is concluded based on the discussion and the uncertainties that the resulting force-displacement curve represent the behaviour of the prototype.